EXPLORING EXCITON AND TRAP STATE RECOMBINATION DYNAMICS IN CADMIUM SULFIDE QUANTUM DOTS

by

Danielle Louise Woodall

A dissertation submitted to the faculty of
The University of North Carolina at Charlotte
in partial fulfillment of the requirements
for the degree of Doctor of Philosophy in
Nanoscale Science

Charlotte

2015

Approved by:

_____
Dr. Marcus Jones

_____
Dr. Michael Fiddy

_____
Dr. Thomas Schmedake

_____
Dr. Yong Zhang

_____
Dr. Amy Ringwood

ABSTRACT

DANIELLE LOUISE WOODALL. Exploring exciton and trap state recombination dynamics in cadmium sulfide quantum dots. (Under the direction of DR. MARCUS JONES)

Colloidal semiconducting quantum dots (QDs) are ideal candidates for optoelectronic devices such as solar cells and LEDs because of their high photoluminescence (PL) quantum yields and photostability. In order to improve device efficiencies, we must understand how QD surfaces affect charge dynamics within the QD. In this work we demonstrate that CdS is an excellent model system for studying QD carrier dynamics for two principle reasons: (i) they produce both exciton and surface-localized trap state emission and (ii) their surface chemistry is simplified by the presence of only one ligand species.

First we, use temperature-dependent time-resolved photoluminescence (TRPL) to measure both exciton and trap recombination dynamics and find that an activated trapping process influences exciton dynamics while trap dynamics are dominated by non-radiative recombination. We propose a model to explain the exciton dynamics in which electron transfer from the exciton state to the deep emissive trap state occurs via a temperature-dependent multi-step process requiring multiple non-emissive trap state distributions. Second, we identify the nature of the trap state using excitation-dependent TRPL, and demonstrate for the first time that trap excited state lifetimes are up to four times longer when influenced by the exciton state compared to direct excitation. Finally, we attempt to control trap emission by altering the amount of native ligand, oleic acid on the QD surface. We present evidence that the ligand coverage on the QD surface and in

solution affects not only trap emission but also exciton emission, and suggest that oleic acid plays a more complicated role in QD emission than previously expected. By developing CdS as a model system for trapping dynamics, we further our understanding of these dynamics and enable the development of new technologies that take advantage of the trap state benefits such as broad emission and long-lived charge separated states.

DEDICATION

This dissertation is dedicated to my father, Bryan Kevin Woodall for teaching me to never give up no matter what.

ACKNOWLEDGMENTS

I would like to thank many individuals who without them, this dissertation would not have been possible. Firstly, I would like to thank my parents, Bryan and Teresa, and my godparents, Craig and Nini. You have been my cheering squad since day 1 and I knew I could always count on you. Secondly, I would like to thank my adviser, Dr. Marcus Jones for giving me the opportunity to earn my Ph.D. and continuously pushing me beyond what I thought were my limits. It wasn't always pleasant, but I feel more capable as I take the next step. I also want to acknowledge the rest of my committee, Dr. Fiddy, Dr. Zhang, Dr. Schmedake, and Dr. Ringwood for reviewing my dissertation and being with me through this process.

I also need to acknowledge the Chemistry department and Nanoscale Science Ph.D. program for their funding and support. Thanks especially to Robin, Caroline, Linda, and Lisa. Without you ladies, nothing would ever get done. I also need to thank Dr. Carlin and Dr. Merkert. Your help was invaluable when it came to fixing instruments and learning new experimental techniques. Additionally, I wish to thank the Graduate school for providing financial support from the GASP funding as well as the Wayland H. Cato Jr. Fellowship. Further funding was provided by EPIC and I thank them as well.

Finally, I want to acknowledge past and current members of the Jones Research Group. You guys and ladies listened to me about my research and helped me when I was stuck. You also made me laugh while aggravating me at the same time. You now have permission to move things on my desk. Have at it.

TABLE OF CONTENTS

LIST OF TABLES x

LIST OF FIGURES xi

LIST OF ABBREVIATIONS xvi

CHAPTER 1: INTRODUCTION 18

1.1. Motivation 18

1.2. Quantum Dots 20

1.3. Optical Processes in QDs 22

1.4. Electron Transfer in QDs 24

1.4.1. Regions of classical ET 26

1.4.2. Modeling Exciton and Trap Dynamics 30

1.5. Aim of Research 32

CHAPTER 2: DISCUSSION ON SPECTROSCOPIC TECHNIQUES 36

2.1. Absorption Spectroscopy 36

2.2. Photoluminescence Spectroscopy 37

2.3. Steady-State PL 38

2.3.1. Correcting PL and PLE Spectra 39

2.3.2. Quantum Yields 41

2.3.3. Homogenous and Inhomogeneous Broadening of Spectra 45

2.3.4. Extracting ET Parameters from Steady State PL 48

2.4. Time-Resolved PL 53

2.4.1. Time-Correlated Single Photon Counting 53

2.4.2. Considerations 54

2.4.3. Collecting PL Decays 56

2.4.4. Analyzing PL Decays 57

CHAPTER 3: EXPERIMENTAL 62

3.1. CdS QD Synthesis 62

3.2. QD Purification 62

3.3. Temperature-dependent TRPL 63

3.4. Excitation-dependent TRPL 65

3.5. CdS QDs and Oleic Acid 65

3.5.1. Oleic Acid Purification 65

3.5.1.1. Oleic Acid Characterization 67

3.5.2. CdS-Oleic Acid Sample Preparation 68

3.5.3. CdS-Oleic Acid Sample Characterization 69

CHAPTER 4: RESULTS 72

4.1. Comparing CdSe and CdS QDs 72

4.1.1. Nature of Emitting Trap State 73

4.1.2. Comparing Trap Energetics for CdS and CdSe QDs 74

4.1.3. Concluding Remarks 76

4.2. Solvent Effects on Trap State Energetics 77

4.2.1. Absorption Spectra 77

4.2.2. Emission Spectra 78

4.2.3. Concluding Remarks 80

4.3. Exciton and Trap PLE 80

4.4. Spectroscopic Characterization of CdS QDs 86

4.4.1. Quantum Yield Spectra 88

4.4.2. ET Parameters for CdS Samples 1, 2, and 3 92

4.5. Comparing Temperature-dependent Exciton and Trap TRPL 94

4.5.1. Temperature-dependent Exciton and Trap Average PL Lifetimes 98

4.5.2. Calculating Relative Quantum Yields From PL Decays 108

4.5.3. Modeling Temperature-Dependent Exciton TRPL 114

4.6. Understanding Trap Dynamics with Excitation-Dependent TRPL 123

4.6.1. Excitation Energies Above the Band-edge 130

4.6.2. Excitation Energies Below the Band-Edge 132

4.6.3. Relative Quantum Yields 139

4.7. Controlling Trap Emission with Oleic Acid 141

4.7.1. Changes in Trap Emission Using 90% Oleic Acid 143

4.7.2. Effects of Purified Oleic Acid on Trap Emission 146

4.7.3. Concluding Remarks 151

CHAPTER 5: FINAL REMARKS 152

REFERENCES 155

LIST OF TABLES

TABLE 2.1: ET parameters extracted from the multi-peak fit of the PLE and PL spectra for CdS in dichloromethane 51

TABLE 4.1: Size and quantum yields calculated for the three CdS samples shown in Figure 4.15 87

TABLE 4.2: ET parameters calculated from the multi-peak fits from the absorption and emission lineshape spectra for samples shown in Figure 4.15 92

TABLE 4.3: ET parameters extracted from modeling with the kinetic scheme for K_1 (above) and K_2 (below) 122

TABLE 4.4: Excitation energies and wavelengths used for excitation-dependent TRPL study 129

LIST OF FIGURES

FIGURE 1.1: Cartoon describing how the electronic levels within the conduction band (CB) and valence band (VB) change as the QD radius changes 21

FIGURE 1.2: Diagram defining classical ET parameters 25

FIGURE 1.3: Graphical representation of the three different regimes of classical ET 27

FIGURE 1.4: Generalized kinetic scheme for the exciton and graphical representation of the free energy curves for the exciton state and a single trap state 29

FIGURE 1.5: Schematic showing different surface trapping models (left column) and their predicted emission spectra (right column) 30

FIGURE 2.1: CdS QD absorption spectrum 37

FIGURE 2.2: Block diagram of a typical fluorimeter 38

FIGURE 2.3: Schematic showing data points in wavelength units and energy units 41

FIGURE 2.4: Representative absorption (black) and PLE (red) spectra for CdS in toluene 43

FIGURE 2.5: Schematic showing how the free energy curves affect the emission linewidth for the exciton (a) and trap (b) 48

FIGURE 2.6: Trap PLE (blue) and PL (red) lineshape spectrum for CdS in dichloromethane 49

FIGURE 2.7: Multi-peak fit to the trap PLE (blue) spectrum 50

FIGURE 2.8: Multi-peak fit of the PL lineshape spectrum using a series of Gaussian peak (black and grey) 50

FIGURE 2.9: Free energy curves for the exciton (blue) and trap (red) constructed using the values listed in Table 2.1 52

FIGURE 2.10: TCSPC setup in forward mode 54

FIGURE 2.11: Representative trap state PL decay in CdS collected with two TACs 58

FIGURE 2.12: Exciton average PL lifetimes at various temperatures calculated using an infinite time window 59

FIGURE 2.13: Exciton average PL lifetimes at various temperatures as a function of the time window of the experiment 60

FIGURE 2.14: Exciton average PL lifetime within 100 ns (left), 1 μs (center), and 10 μs (right) 61

FIGURE 3.1: Recrystallization vessel used for oleic acid purification 66

FIGURE 3.2: UV-Vis absorption spectrum collected during the recrystallization of oleic acid 68

FIGURE 3.3: UV-Vis spectrum of 90% oleic acid and purified oleic acid 69

FIGURE 4.1: Absorption (black) and emission (red) spectra for CdSe (left) and CdS (right) QDs 72

FIGURE 4.2: Absorption (black) and emission (red) for core/shell CdSe/CdS QDs 73

FIGURE 4.3: Schematic showing core/shell QD (left) and its band structure (right) 73

FIGURE 4.4: CdS emission spectrum for QDs synthesized with excess sulfur 74

FIGURE 4.5: Free energy curves for 2 nm CdS (blue) and 4 nm CdS (red) 75

FIGURE 4.6: Free energy curves for CdS (blue) and CdSe (red) 76

FIGURE 4.7: CdS UV-Vis absorption spectra in various organic solvents 77

FIGURE 4.8: Same spectrum as Figure 4.7 plotted on a log scale to make the trap absorption more visible 78

FIGURE 4.9: CdS PL lineshape spectra in various organic solvents 79

FIGURE 4.10: CdS trap emission energy for varying solvent dielectric constants 80

FIGURE 4.11: Representative PLE spectra for exciton (blue) and trap (red) states 81

FIGURE 4.12: Schematic for different ways traps are formed 82

FIGURE 4.13: Trap PLE collected at different emission wavelengths 84

FIGURE 4.14: Schematic showing how large QDs may exhibit trap emission at longer wavelengths 85

FIGURE 4.15: Absorption and emission lineshape spectra for three different sized CdS QDs 87

FIGURE 4.16: Exciton PLE (blue) and absorption spectra (black) for CdS QDs 88

FIGURE 4.17: Relative QY spectra for three CdS samples shown in Figure 4.15 90

FIGURE 4.18: Schematic showing the possible recombination pathways 91

FIGURE 4.19: Free energy curves constructed using ET parameters in Table 4.2 92

FIGURE 4.20: Possible mechanisms for ET in the inverted region 93

FIGURE 4.21: Representative PL decays at various temperatures for the exciton state (a) and trap state (b) 95

FIGURE 4.22: Average emission lifetimes for the exciton (left) and trap state (right) in three different CdS samples 99

FIGURE 4.23: Schematic explaining the temperature-dependent average lifetime 100

FIGURE 4.24: Exciton average PL lifetime 2D plot for sample 1 102

FIGURE 4.25: Exciton average PL lifetimes within 10 ns (red), 1 μs (black), and infinite time (blue) for sample 1 102

FIGURE 4.26: Exciton average PL lifetime 2D plot for sample 2 103

FIGURE 4.27: Exciton average PL lifetime 2D plot for sample 3 103

FIGURE 4.28: Trap average PL lifetime 2D plot for sample 1 105

FIGURE 4.29: Trap average PL lifetimes for sample 1 within specific time windows 105

FIGURE 4.30: Trap average PL lifetime 2D plot for sample 2 107

FIGURE 4.31: Trap average PL lifetime 2D plot for sample 3 107

FIGURE 4.32: Schematic showing a trapped hole recombining with a delocalized electron in the conduction band (CB) or a trapped electron 108

FIGURE 4.33: Exciton relative QYs calculated from the PL decays 110

FIGURE 4.34: Trap relative QYs calculated from the PL decays 112

FIGURE 4.35: Screenshot of the software used to construct the kinetic schemes for TRPL analysis 119

FIGURE 4.36: General three state model consisting of an exciton state, a distribution of non-emissive trap states, and a ground state used to build the kinetic scheme 120

FIGURE 4.37: Comparison of model exciton PL decays (black) with experimental exciton PL decays (red) for temperatures ranging from 80K to 305 K 121

FIGURE 4.38: Non-emissive trap state distributions needed to adequately model the exciton PL decays 122

FIGURE 4.39: Trap PL decays at 110 K collected with 3.26 eV excitation (blue) and 2.64 eV excitation (red) 124

FIGURE 4.40: Trap PL decays at 110 K collected with 3.26 eV excitation (blue) and 2.64 eV excitation (red) 124

FIGURE 4.41: Trap PL decays recorded using 2.64 eV excitation for temperatures ranging from 80 K to 305 K 126

FIGURE 4.42: Trap PL decay (red) at 110 K and IRF (black) recorded using a 500 ns TAC 126

FIGURE 4.43: Temperature-dependent trap average PL lifetimes for 3.26 eV excitation energy (blue) and 2.64 eV excitation (red) 127

FIGURE 4.44: Absorption lineshape spectrum for CdS QDs 128

FIGURE 4.45: Trap average PL lifetime 2D plots for three different excitation energies above the QD band-edge 130

FIGURE 4.46: Excitation and temperature-dependent trap average PL lifetimes extracted from Figure 4.45 at specific time windows 131

FIGURE 4.47: Trap average PL lifetime 2D plots for three different excitation energies below the QD band-edge 133

FIGURE 4.48: Excitation and temperature-dependent trap average PL lifetimes extracted from Figure 4.47 at specific time windows 134

FIGURE 4.49: Cartoon showing how trap states are formed with different excitation energies 135

FIGURE 4.50: Trap state relative QY calculated from the PL decays for above band-gap excitation (left) and below band-gap excitation (right) energies 139

FIGURE 4.51: CdS absorption spectra with varying amounts of 90% oleic acid added 143

FIGURE 4.52: Normalized CdS PL spectra with increasing amounts of 90% oleic acid (left) 144

FIGURE 4.53: Change in exciton emission energy with additional oleic acid 146

FIGURE 4.54: Normalized CdS PL spectra with increasing amounts of purified oleic acid 147

FIGURE 4.55: Normalized PLE spectra recorded at the exciton emission (left) and maximum trap emission (right) 148

FIGURE 4.56: Normalized CdS absorption spectra for varying additions of purified oleic acid 149

LIST OF ABBREVIATIONS

ACN	acetonitrile
CB	conduction band
CdS	cadmium sulfide
CdSe	cadmium selenide
DOE	Department of Energy
ET	electron transfer
eV	electron volt
HOMO	highest occupied molecular orbital
IR	infrared
IRF	instrument response function
LED	light emitting diode
LUMO	lowest unoccupied molecular orbital
NMR	nuclear magnetic resonance
ODE	octadecene
PbSe	lead selenide
PL	photoluminescence
PLE	photoluminescence excitation
PMT	photomultiplier tube
QD	quantum dot
QY	quantum yield
TAC	time to amplitude converter
TCSPC	time-correlated single photon counting

TRPL	time-resolved photoluminescence
UV-Vis	ultraviolet visible
VB	valence band

CHAPTER 1: INTRODUCTION

1.1. Motivation

Fossil fuels are finite. As a result, we must find new energy sources that are renewable and less harmful to the environment. Solar energy offers a potentially promising solution because, according to the Department of Energy (DOE) website, the amount of solar energy that reaches the Earth's surface in one hour is greater than the total amount of energy needed for an entire year. The DOE has initiated numerous programs such as Energy Frontier Research Centers and the Sunshot Initiative to further solar energy research and to reduce the cost of solar power by 75% by 2020.[1] Current commercial cells have efficiencies less than 25%[2] but high production and installation costs mean that the price of electricity produced from solar cells is still higher compared to when it is produced from fossil fuels.[2]

National research laboratories such as the National Renewable Energy Laboratory have been investigating new materials for solar cells like colloidal semiconducting nanocrystal quantum dots (QDs). QDs are excellent candidates for solar cells and other optoelectronic devices because of their size tunable optical properties.[3-6] Since colloidal QDs are made in solution, it is relatively straightforward to incorporate them into devices using techniques such as spin coating or electrophoretic deposition. These methods do not require the use of a clean room or a controlled atmosphere, meaning QD based solar cells are theoretically less expensive to make than traditional silicon solar cells.[7] Additionally, QDs, particularly Pb chalcogenide QDs, exhibit a phenomenon known as

multiple exciton generation (MEG) where one photon of light of sufficiently high energy can generate two or more electron hole pairs also known as excitons.[8] This allows QD solar cells to have external quantum efficiencies greater than 100% when absorbing short wavelengths of the solar spectrum.[8-12] QD based solar cell efficiencies have increased over the last several years, and are now comparable to dye-sensitized solar cells as well as bulk heterojunction photovoltaics.[13-16]

Even though QD based solar cells are gaining in efficiency, they still have not met their full potential. This is because fundamental processes such as charge transfer through the interface between the QDs and the local environment remain poorly understood. Additionally, the surface effects on charge carrier recombination dynamics remain unclear. Surfaces are more important in QDs compared to bulk materials because QDs have a large surface to volume ratio, meaning that many of the atoms are on the surface.[17,18] For example, a 3.2nm CdSe QD has approximately 800 atoms, with 1/3 of those atoms on the surface.[19]

Furthermore, the quality of the surface has been shown to create surface states such as trap states where either the electron or hole becomes localized rather than moving freely through either the conduction or valence bands. These trap states enable additional recombination pathways for photogenerated carriers, affecting both exciton dynamics[20] and decreasing photoluminescence quantum yields,[21,22] hindering device performance. By understanding how the surface impacts photophysical behavior of the QDs, we can engineer more efficient solar cells and other optoelectronic devices.

1.2. Quantum Dots

QDs are generally near spherical particles with diameters ranging from 2-10 nm. They are a class of material with a size regime existing between molecular systems and bulk systems, giving them unique electronic properties. In molecules, the electronic energy levels are well separated. Transitions from the ground to excited state are defined by the energy separation between the highest occupied molecular orbital (HOMO) and the lowest unoccupied molecular orbital (LUMO).

As the size of the material increases, the electronic energy spacings become closer and eventually form bands, which are used to define bulk materials. In bulk materials, the electrons occupy the valence band while in the ground state. When the material is excited, an electron is excited into the conduction band, leaving an absence of charge referred to as a hole. The energy spacing between the valence band and conduction band is referred to as the bandgap, and this spacing also determines the amount of energy needed to excite the material.

The formation of a correlated electron hole pair is called an exciton. The electron and hole are correlated because they are charged particles, and there is a Coulombic or attractive force between the particles. The distance between the electron-hole pair is referred to as the Bohr exciton radius. The Bohr exciton radius is material specific and can be calculated using the following equation:

$$r = \frac{\epsilon \hbar^2}{\mu e^2}$$

where ϵ is the dielectric constant of the material, $\hbar$ is the reduced Planck's constant, μ is the reduced electron hole mass where $\frac{1}{\mu} = \frac{1}{m_e} + \frac{1}{m_h}$ and e is the electron charge. The Bohr exciton radius is 4.9 nm in CdSe and 2.8 nm in CdS.[23]

When the physical size of the material decreases from the bulk to the nanoscale regime, the physical size modifies the electronic structure of the material, which is referred to as quantum confinement. Quantum confinement causes the continuous electronic band structure of a bulk material to become discrete or quantized electronic levels. The electronic levels within a QD can be modeled using the "particle in a sphere" formalism from quantum mechanics. We assume that the particle is confined to a sphere and is surrounded by an infinite potential. The energy of the quantized electronic levels for either the electron or hole can be written as:

$$E_{l,n} = \frac{\hbar^2 \phi_{l,n}^2}{2ma^2}$$

where l is the angular quantum number, $\hbar$ is the reduced Planck's constant, $\phi$is the n^{th}

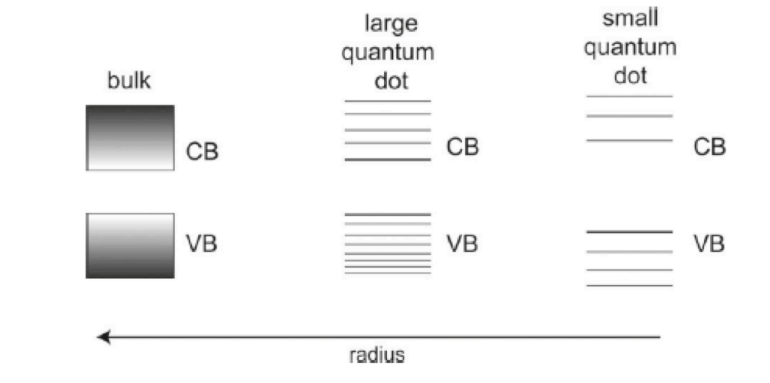

Figure 1.1: Cartoon describing how the electronic levels within the conduction band (CB) and valence (VB) change as the QD radius changes. When the radius increases (right to left), the electronic levels become closer together and eventually form bands as in the bulk material. Reproduced from Kambhamptai.[24]

root of the spherical Bessel function, *m* is the effective mass of either the electron or hole, and *a* is the crystal radius. As the crystal radius decreases, the energy of the electron and hole electronic states also increases.

If the crystal radius becomes smaller than the Bohr exciton radius, the system is strongly confined because energy spacings between the electronic levels are greater than the exciton binding energy or the Coulomb interaction between the electron and hole. The strong confinement regime is responsible for the size-depend bandgap exhibited by most QDs. For strongly confined QDs, a decrease in the QD size causes the bandgap to become larger and shifts the optical transitions to higher energies as shown in Figure 1.1 Being able to control QD emission and other optical properties simply by changing their size is what makes QDs attractive for applications ranging from photovoltaics[2,7,8,12,16,25-29] and other optoelectronic devices[30-34] to biological imaging.[35-38]

1.3. Optical Processes in QDs

In order to utilize QDs in optoelectronic devices such as solar cells, we must understand how light produces charge carriers and the fate of those carriers after an excitation event. QDs interact with light by absorbing a photon as long as the photon energy matches the transition energy. In QDs where the only electron and hole states are within the conduction and valence band respectively, the QD bandgap dictates the minimum photon energy needed to excite an electron from the valence band to the conduction band and generate an exciton. QDs may also absorb photons with energy less than the bandgap if there are states such as trap states within the bandgap. These states are not referred to as exciton states, because these charges are localized rather than delocalized over the entire particle.

After an excitation event produces an exciton, it recombines either radiatively by emitting a photon or non-radiatively by coupling to phonon modes or Auger recombination. Auger recombination occurs when the electron and hole recombine and the energy produced from this event is transmitted to a third particle. If exciton emission does occur, it generally occurs at a lower energy than the absorption energy. This shift in the absorption and emission energy is referred to as a Stoke's shift. The Stoke's shift is a result of excitation into high-energy states within the conduction and valence bands. The electron and hole then immediately relax to their respective band-edges before radiatively recombining.

If states exist within the QD bandgap, then the electron and hole can relax past the conduction and valence band-edges and into these states. In some species of QDs like CdS, these trapped charges can radiatively recombine, and this emission is referred to as trap emission. Since trap emission involves states within the QD bandgap, trap emission primarily occurs at emission energies less than the exciton emission peak.

Trap states also form in other species of QDs such as CdSe, but they are primarily non-emissive. If they are non-emissive, then how do we know that they exist? Evidence for non-emissive trap states comes primarily from time-resolved photoluminescence spectroscopy (TRPL) conducted on exciton states. TRPL is a techniques that measures excited state recombination dynamics and is discussed in more detail in Section 2.4.

Temperature studies using TRPL showed that exciton average lifetimes, or the average time it takes for the exciton to emit a photon, are temperature-dependent. The quantum yield (QY) or the efficiency in which the QD emits a photon also showed a similar temperature-dependence. QYs are described further in Section 2.3.2. The trends

in the temperature-dependent exciton average lifetimes and QY were successfully modeled using an activated trapping process where one charge carrier becomes localized in a surface state or trap state at low temperatures. As the temperature is raised, the charge carrier gains enough thermal energy to be released from the trap state and becomes delocalized, increasing the likelihood of radiative recombination with the other charge carrier.

Because trap states are charge-separated states, we theorize that these states are formed through a charge transfer process, and therefore can be modeled using classical electron transfer (ET) theory, which is sometimes referred to as "Marcus theory" after its creator. Classical ET theory describes the process in which an electron is transferred from one entity, referred to as the donor, to another entity, referred to as the product. It was originally developed for molecular systems,[39] but has been more recently applied to describe ET in QD-metal oxide junctions[40] as well trapping dynamics in core/shell QDs[41-43] and nanorod heterostructures.[44,45] In the case of QDs, the exciton state acts as the donor and the trap state behaves as the acceptor.

1.4. Electron Transfer in QDs

Classical ET theory uses parabolas to describe each state of the system. The parabolas are potential energy surfaces representing all possible configurations including nuclear and solvent coordinates for that state. The potential energy surfaces are parabolas because the system is described in terms of harmonic oscillators, and the potential energy of a harmonic oscillator is a parabola. However, the potential energy surfaces are generally described in terms of Gibb's free energy ($\Delta G°$) surfaces because low frequency vibrations modes from the solvent cannot be accurately modeled as harmonic oscillators.

In the classical theory we assume that the curvature of the parabolas for the donor and acceptor along a common reaction coordinate are the same. The electronic coupling or mixing between the donor and the acceptor free energy surfaces determines if ET is adiabatic or non-adiabatic. Adiabatic classical ET occurs when the electronic coupling is strong, and the donor and acceptor form one free energy surface. Non-adiabatic classical ET occurs when the electronic coupling is weak, and the donor and acceptor free energy surfaces form two distinct surfaces.

Non-adiabatic ET can only occur when the donor and acceptor free energy surfaces intersect, primarily because of the Franck-Condon principle. The Franck-Condon principle is an approximation that says electronic transitions happen before the nuclei have a chance to move. The only place where the donor and acceptor have the

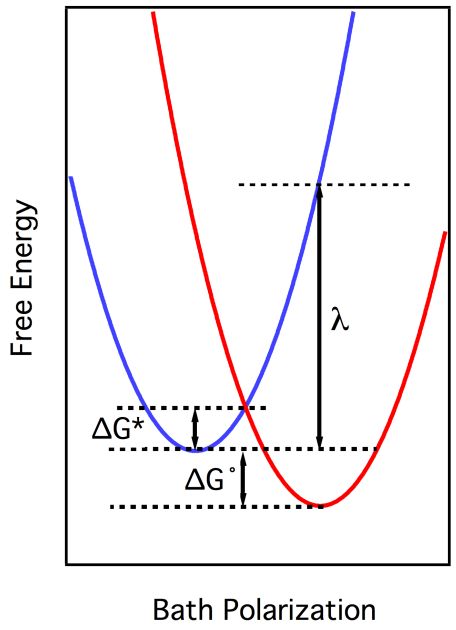

Figure 1.2: Diagram defining classical ET parameters. ΔG° is the change in free energy, λ is the reorganization energy, and ΔG* is the activation barrier. The blue parabola represents the donor state, and the red parabola represents the acceptor state.

same nuclear configuration is where the free energy surfaces intersect. In addition to intersection point or transition state, two more parameters are needed before discussing ET rates. The difference in Gibb's free energy (ΔG°) is the difference in energy between the equilibrium position of the donor and the equilibrium position of the acceptor. These equilibrium positions occur at the bottom of the parabolas. The reorganization energy (λ) is defined as the change in Gibb's energy if the donor were to adopt the equilibrium configuration of the acceptor state without transferring the electron.[46] Finally, the activation barrier (ΔG*) is defined as the amount of energy needed for the system to reach the transition state where ET can occur. These variables are shown schematically in Figure 1.2.

1.4.1. Regions of classical ET

Once ΔG°_{CT} and λ_{CT} are defined, the ET rate (k_{ET}) can be calculated using the classical ET equation shown below:

$$k_{ET} = \frac{2\pi}{\hbar}\,\mathcal{H}_{rp}^{2}\,\frac{1}{\sqrt{4\pi\lambda k_B T}}\,exp\left[-\frac{(\lambda + \Delta G^{\circ})^2}{4\lambda k_B T}\right]$$

where $\mathcal{H}_{rp}$ represents the electronic coupling between the two states, k_B is Boltzmann's constant, and T is temperature. If the ET is non-adiabatic, then $\mathcal{H}_{rp}$ is << 1 and the ET process can be separated into three different regions, which are shown in Figure 1.3. The first region is the normal region where $-\Delta G^{\circ} \ll \lambda$ and k_{ET} increases as ΔG° becomes more negative. The second region is the barrierless region where $-\Delta G^{\circ} \approx \lambda$ and k_{ET} is the fastest. The third region is the inverted region where $-\Delta G^{\circ} \gg \lambda$ and k_{ET} is expected to decrease as $-\Delta G^{\circ}$ becomes more negative because the activation barrier is increasing.

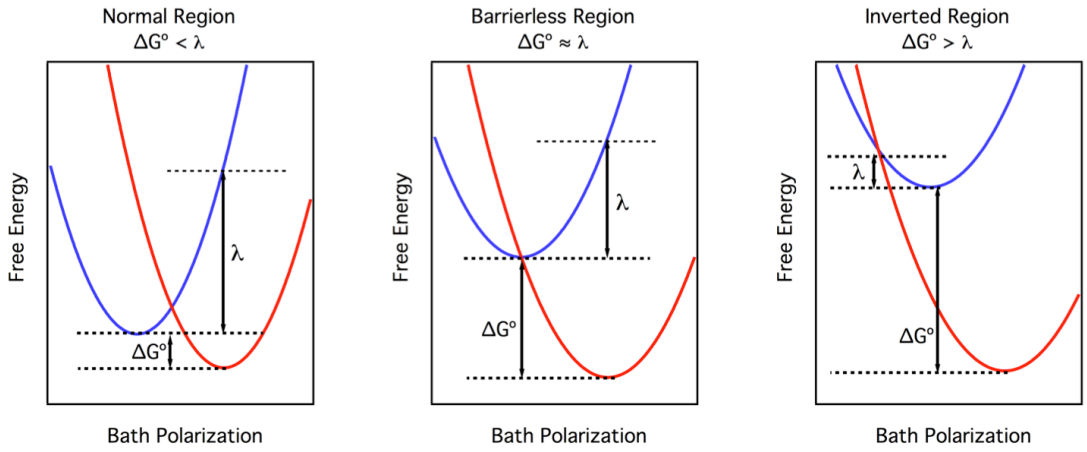

Figure 1.3: Graphical representation of the three different regimes of classical ET. The blue parabola represents the donor, and the red parabola represents the acceptor. ΔG° and λ are defined in the text.

The inverted region is not commonly encountered in intermolecular reactions due to limits of diffusion between donor and acceptor.[47,48] In order for ET to occur in intermolecular reactions, the donor and acceptor must come together to form the transition state complex. When ET occurs in the normal region, the electron transfer rate is slower than the diffusion rate of the donor and acceptor. As we increase -ΔG°, or the driving force of the reaction, the electron transfer rate increases. Eventually, it becomes faster than the diffusion rate of the two reactants, and the rate of diffusion becomes the rate-determining step. The inverted region is therefore seen in primarily intramolecular reactions such as bridged systems and QDs because diffusion is no longer needed to bring the donor and acceptor together.

Non-adiabatic ET can also occur at points slightly below the transition state if nuclear and electron tunneling occurs. Nuclear tunneling is temperature-independent, and therefore allows ET to occur at very low temperatures. However, nuclear tunneling requires the displacement between donor and acceptor free energy surfaces to be quite

small. Electron tunneling is possible if there is significant vibrational overlap between the donor and acceptor states. Electron tunneling is temperature-dependent because thermal energy is required to reach the donor vibrational state which has the greatest overlap with acceptor vibrational state.

High frequency vibrational modes can be incorporated into the ET rates using a semi-classical ET theory that was first developed by Marcus and Jortner.[49] This ET theory is considered semi-classical because the solvent modes, which are low frequency, are treated classically while the internal high frequency vibration modes of the donor and acceptor are treated quantum mechanically. In both classical and semi-classical ET theory, the reorganization energy is split into the outer reorganization energy (λ_{out}) and the inner reorganization energy (λ_{in}). The outer reorganization energy is also known as the solvent reorganization energy and refers to the energy needed for the solvent molecules around the donor to reorient to the configuration around the acceptor without the electron transfer occurring. The inner reorganization energy is solvent independent and includes all intramolecular vibrations. The classical ET equation is extended to include the vibrational modes and becomes the Marcus-Jortner equation:

$$k_{ET} = \frac{2\pi}{\hbar}\,\mathcal{H}_{rp}^2\,\frac{1}{\sqrt{4\pi\lambda_{out}k_BT}}exp(-S)\sum_{m=0}^{\infty}\frac{S^m}{m!}exp\left[-\frac{(\lambda_{out}+\Delta G°+mhv)^2}{4\lambda_{out}k_BT}\right]$$

where m is an integer and S is the Huang-Rhys parameter. The Huang-Rhys parameter is the electron-phonon coupling constant and is defined as

$$S = \frac{\lambda_{in}}{hv}$$

The Marcus-Jortner equation assumes that all high frequency vibrations in the donor can be represented by a single average vibrational mode with frequency v.

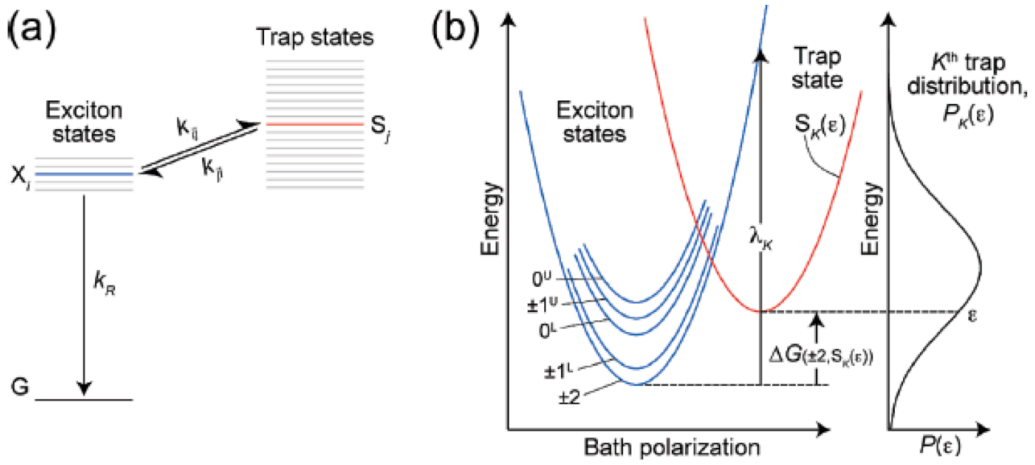

Figure 1.4: Generalized kinectic scheme for the exciton (a). Graphical representation of the free energy curves for the exciton state and a single trap state from chosen from the K^{th} trap distribution. Further details are provided in the text. Reproduced from Jones et al.[43]

As previously mentioned classical ET was used to model trapping in core/shell QDs as a way to explain the temperature-dependence of the exciton's average PL lifetime. The model consisted of an exciton and a distribution of trap states within a few k_BT of the exciton as shown in Figure 1.4 (a). The exciton (X_i) had a radiative recombination rate (k_R) as well as a charge transfer rate (k_{ij}) to a trap state (S_j) within the distribution $P_K(\varepsilon)$. Each trap state distribution was assigned a single reorganization energy (λ_K) shown in Figure 1.4 (b). The driving force of the reaction ($\Delta G°$) was calculated as the energy difference between the exciton state and a trap state with energy ε. Figure 1.4 (b) displays $\Delta G°$ for the lowest state within the exciton fine structure and an arbitrarily chosen trap state within the distribution. Even though Figure 1.4 (b) presents ET as an endergonic process, it does not have to be endergonic. ET can also be an exergonic process if the trap state energy is less than the exciton state. Once λ_K and $\Delta G°$ were defined for each trap state, then the trapping rate (k_{ij}) and detrapping rate (k_{ji}) were calculated using the classical ET equation and detailed balance respectively.

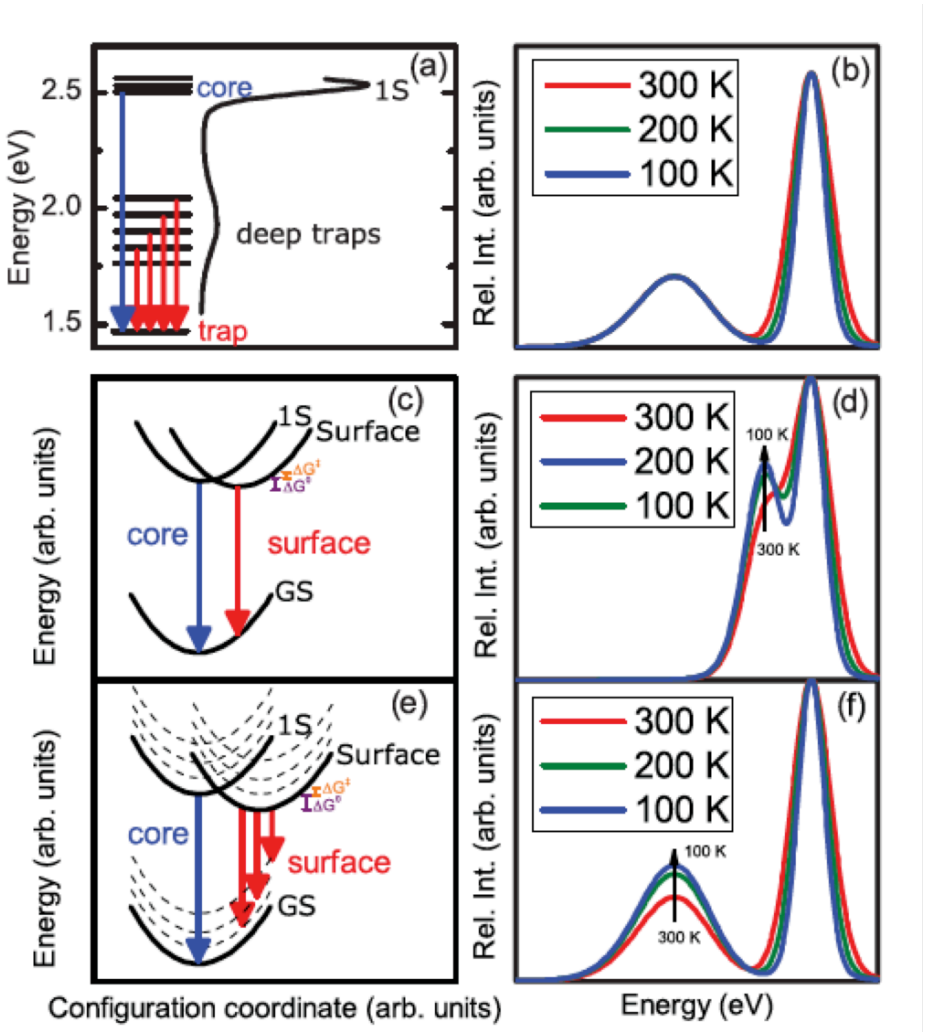

Figure 1.5: Schematic showing different surface trapping models (left column) and their predicted emission spectra (right column). Reproduced from Mooney et al.[51]

1.4.2. Modeling Exciton and Trap Dynamics

However, Mooney et al showed that classical ET fails to describe the temperature-dependent PL of QDs of small CdSe and CdS QDs where the PL emission consists of one narrow high energy peak and one broad low energy peak.[50,51] They reviewed the current models for surface (trap) emission and presented a new one based on semi-classical ET. The models and their predicted steady-state emission spectra are presented in Figure 1.5.

The first model (Figure 1.5 (a)) developed for surface emission stated that trap emission arose from states lying deep within the bandgap, causing the red-shift in trap emission.[52,53] The broadness of the trap emission was then attributed to a broad distribution of states. However, this model cannot explain the temperature-dependent relationship between exciton and surface emission observed by Mooney et al because thermal population exchange is not feasible between the two states. The energy difference between the exciton and trap state is greater than 500 meV. Once a trap state is populated, it is not energetically capable of returning to the exciton state.

Therefore, a second model was proposed where the exciton is coupled to a surface state that is relatively close in energy, and population exchange occurs through classical ET (Figure 1.5 (c)). The charge transfer would occur in the normal region because ΔG° is small, and therefore an activation barrier exists. The temperature-dependence of the exciton average lifetimes is then explained by the probability of overcoming the barrier. Since the surface state is relatively close to the exciton state, its emission energy would only be a few meV less than the exciton emission (Figure 1.5 (d)), which is not the case.

Furthermore, the ΔG° values extracted from the small CdSe and CdS spectra, assuming classical ET, indicate charge transfer is occurring in the inverted region where ET rates decrease as $-\Delta G^\circ$ increases. This is discussed in more detail in Section 2.3.4 and Section 4.1.2. Because the charge transfer rates decrease in the inverted region, they will not effectively compete with exciton radiative recombination, and trap emission is unlikely to occur. Obviously trap emission is taking place, so the trap state must be populated in a manner other than classical ET.

Because classical ET cannot explain the red-shift of trap emission seen in small CdSe and CdS, Mooney et al used semi-classical ET between the exciton to a single surface state to explain both the temperature relationship between exciton and trap emission and the observed red-shift (Figure 1.5 (e)).[50,51,54] Semi-classical ET is useful because it incorporates internal high-frequency vibrational quantum modes for donor (exciton) and acceptor (trap). It also includes a measure of the electron-phonon coupling defined as the Huang-Rhys parameter.

The minimum of the surface free energy curve is close in energy to the minimum of the exciton free energy, and ET to occur through the overlap of the high frequency vibrational modes between the exciton and trap state. This is still an activated process because thermal energy is required to reach the vibrational state in the exciton with the optimal overlap with the trap vibrational state. The large reorganization energy and strong electron-phonon coupling for the trap state indicates a large displacement from the exciton state. Displacement refers to the shift of the parabola representing the trap free energy surface along the x-axis. The minimum of the trap state free energy curve now lies above the side of the ground state parabola rather than its minimum. Since emission occurs as a vertical transition, the transition occurs from the lowest vibration state within the trap state into a high frequency vibration in the ground state. As a result, the trap emission energy is red-shifted compared to the exciton.

1.5. Aim of Research

The goal of this research is to develop CdS QDs as a model system for understanding trap recombination dynamics and their impact on exciton lifetimes. Most QD studies on photogenerated charge carrier dynamics focus primarily on CdSe QD

systems, particularly on core/shell systems because of their high fluorescent quantum yield (>80%)[55,56] and long term photostability. However, CdSe QDs exhibit primarily exciton emission, making it difficult to optically probe trap states and determine their effects on exciton dynamics. In contrast to CdSe, CdS QDs have exciton emission as well as a broad, red-shifted band attributed to trap emission.[57-63] This feature enables us to measure trap state dynamics directly with optical techniques such as steady state photoluminescence (PL) and time-resolved photoluminescence (TRPL). Furthermore, the conventional CdS QD synthesis uses only one ligand, oleic acid,[64] making it a simpler system than CdSe, which is often synthesized using three ligands[65,66] thus complicating the surface characterization and making it difficult to determine how each ligand influences exciton and trap state dynamics.

Even though CdS is a potentially a better model system for studying trap recombination dynamics, little research has been conducted on CdS QDs compared to the CdSe system. Research on QDs began in the 1980's and both CdSe and CdS were the primary systems for study. However, research efforts soon shifted to CdSe, probably because of the negative connotation associated with trap emission. Researchers originally saw trap emission as an indicator of poor surface quality for CdS, and discontinued their investigation into its fundamental behavior.

Therefore, the first aim of this dissertation is to further our understanding of photogenerated charge carrier recombination dynamics in CdS and compare them to the more heavily studied CdSe. The recombination dynamics in CdS are more complex than CdSe because there are two emissive states, the exciton and trap state, which may be

correlated in some manner. However, before we start to untangle the exciton dynamics from the trap dynamics, we first must determine what are those dynamics.

We accomplish this by performing temperature-dependent time-resolved photoluminescence (TRPL) on the exciton and trap state. TRPL is an excellent tool for this study because it allows us to monitor excited state dynamics on timescales ranging from nanoseconds to microseconds. Furthermore, the temperature aspect to the TRPL allows us to determine if activated processes are occurring within each state. Temperature-dependent TRPL has previously been used to study exciton dynamics in CdSe (discussed in more detail in Section 4.5), and we wish to see if the models developed for CdSe are applicable to CdS.

The second aim of this dissertation is to answer the fundamental question of how are trap states populated? Are they formed directly or are they influenced by the exciton state in some manner? To answer these questions, we conducted both temperature-dependent and excitation-dependent TRPL to monitor the trap state recombination dynamics. Since we believe the trap state is formed through ET from the exciton state, we use temperature-dependent TRPL to change the transfer rates in a predictable manner (classical ET is an activated process). We can then extract the relevant ET parameters from careful analysis of the PL decays.

Excitation-dependent TRPL is advantageous because it enables us to spectrally separate the exciton dynamics from the trap dynamics. CdS QDs exhibit trap emission that is up to 1 eV less in energy compared to the exciton state. This large separation makes it relatively easy to excite the trap state directly without the possibility of exciting the exciton states. Temperature-dependent TRPL has previously been conducted on

CdS,[58,67] but excitation-dependent TRPL has never been reported for this system. Furthermore, we found that excitation-dependent TRPL was vital for unraveling the trap state recombination dynamics.

The final aim of this dissertation is to understand the cause of trap states. The most prevailing theory for trap emission is incomplete ligand coverage, but little research has been done to confirm this hypothesis. Consequently, we performed experiments where the ligand coverage on the CdS QDs was altered in a systematic way. We then monitored the changes in the exciton and trap state using steady-state spectroscopy such as photoluminescence (PL) and photoluminescence excitation (PLE). We established that ligands affect the exciton and trap state in unexpected ways, and we propose future experiments to decipher the mechanism by which ligands are affecting the recombination dynamics.

CHAPTER 2: DISCUSSION ON SPECTROSCOPIC TECHNIQUES

2.1. Absorption Spectroscopy

Absorption spectroscopy is primarily used in this research to determine the optical band-gap, and therefore the size of the QD as well as its concentration.[65] Absorption spectroscopy measures the transmittance of a sample for various wavelengths of light. Transmittance is then converted to absorbance using the following equation:

$$A(\lambda) = -\log T(\lambda)$$

where $A(\lambda)$ is the absorbance of a sample at a given wavelength, λ, and $T(\lambda)$ is the transmittance at the same wavelength. A typical CdS absorption spectrum is shown in Figure 2.1. The peak at 432 nm is the first exciton absorption peak, which corresponds to the QD band-gap energy. Because the band-gap energy is size-dependent, the size of the CdS QD can be calculated using an empirical fitting function developed by Yu et al shown below[65]:

$$D = (-6.6521\times10^{-8})\lambda^3 + (1.9557\times10^{-4})\lambda^2 - (9.2352\times10^{-2})\lambda + 13.29$$

where λ is the first exciton absorption wavelength. The size of the CdS QDs is then used to calculate the extinction coefficient (ε), which is a measure of how strongly the QD absorbs light. For CdS QDs, ε is calculated using the relationship developed by Yu et al[65]:

$$\varepsilon = 21536\times D^{2.3}$$

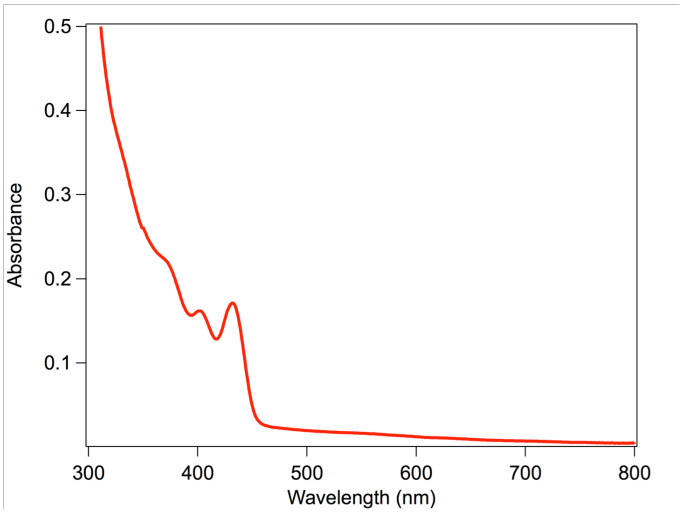

Figure 2.1: CdS QD absorption spectrum.

where D is the size of the QD in nm. Once ε is known, the QD concentration is determined by rearranging the Beer-Lambert's Law to yield the following equation:

$$C = \frac{A}{\varepsilon \ell}$$

where C is the concentration in molarity and ℓ is the path length of the cuvette. The size calculated for the sample shown in Figure 2.1 is 4.5 nm and the concentration is 2.5×10^{-7} M. The QD concentrations are kept low, on the order of 10^{-7} M to ensure the absorption is less than 0.1. By using dilute samples, we can neglect self-absorption and ensure that the photoluminescence (PL) intensity of a sample is linearly proportional to the QD concentration.

2.2. Photoluminescence Spectroscopy

Photoluminescence spectroscopy measures the light produced by the QD as it relaxes back down to the ground state. In these studies we consider only spontaneous decay because the excitation sources are too weak to induce much stimulated emission. PL spectroscopy can be divided into to separate regimes referred to as steady-state PL

and time-resolved PL (TRPL). In a steady-state PL experiment, we measure the fluorescence intensity of an illuminated sample under (quasi) equilibrium conditions where the proportion of emitting fluorophores remains constant.[68] Conversely, in a TRPL experiment we measure the time taken for a fluorophore to emit a photon after being excited by a short burst of light. Steady-state PL provides information on the energies and relative emission quantum yields of states in a fluorophore, while TRPL provides information on the recombination dynamics of those states.

2.3. Steady-State PL

Steady-state PL intensities are typically recorded as a function of the wavelength of the emitted light or the absorbed light. The former are known as photoluminescence (PL) spectra and the latter are photoluminescence excitation (PLE) spectra. Both PL and PLE are collected using a spectrophotometer, which consists of three main components: a light source, a sample chamber, and a detector shown schematically in Figure 2.2. The light source is usually continuous: in the fluorimeter used in this study, it was a xenon arc

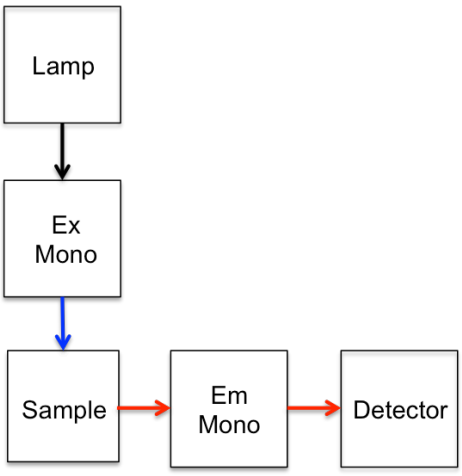

Figure 2.2: Block diagram of a typical fluorimeter. Ex mono and em mono refer to the excitation and emission monochromators respectively.

lamp. Xenon arc lamps are preferred because they have a spectral range of approximately 250 nm across the visible spectrum to the near infrared, which is usable for most applications.

The sample holder is located in line with the excitation source, and the detector is positioned at a right angle to the sample holder. This configuration minimizes the probability of stray excitation light hitting the detector and possibly damaging it. Spectrophotometers also contain an excitation monochromator and an emission monochromator. The monochromator allows the user to select specific wavelengths of light, either excitation or emission, when collecting spectra.

In order to collect a PLE spectrum, the emission wavelength is set constant and the excitation wavelengths are scanned using the excitation monochromator. A PLE spectrum, once corrected, should resemble the absorption spectrum because, according to Kasha's rule, the emission of a chromophore occurs in appreciable yield only from the lowest excited state of a given multiplicity. Therefore, any variation in emission intensity arises from changes in absorption at the excitation wavelengths as long as the concentration of fluorophores is kept low. PL spectra are collected by choosing a single excitation wavelength and scanning the emission monochromator.

2.3.1. Correcting PL and PLE Spectra

In both PL and PLE, the spectra need to be corrected before they can be analyzed. This is because the components of the spectrophotometer distort the spectra. For example, the lamp causes distortions because the lamp does not emit at constant intensity at all wavelengths. A photodiode is used to record the reference signal in addition to the sample signal, which monitors changes in the lamp. The sample signal is divided by the

reference signal while the spectrum is collected to correct for the lamp. The detector causes distortions because its quantum efficiency or the ability to convert photons into electrons to measure signal intensity is wavelength dependent and less than 100%. For example, the detector used in the fluorimeter for this study consists of a Hamamatsu R928 photomultiplier tube with a peak quantum efficiency of 25.4% at 260 nm. The quantum efficiency drops rapidly as the wavelength increases and is only 2-3% at 800 nm. This means that the detector does not easily seen photons with wavelengths longer than 800 nm, resulting in artificially low signal intensity at long wavelengths. The monochromators also cause distortions because their transmission efficiencies are wavelength dependent. Therefore, correction factors need to be applied to all spectra before analysis. Correction factors are generated by recording a spectrum with a calibrated light source. The recorded spectrum is then compared to the true spectrum of the light source to calculate the correction factors. These correction factors are applied when the spectra are imported into the analysis software.

Further corrections are necessary when the recorded spectra are converted from wavelength units into energy units. Wavelength is easily converted into energy using the following equation:

$$E = \frac{hc}{\lambda}$$

Because of the inverse relationship between wavelength and energy, data points that are evenly spaced in wavelength units are not evenly spaced in energy units. This is shown pictorially in Figure 2.3. Spectra are recorded as signal intensity per unit wavelength. Since the data points in the energy scale are no longer uniformly spaced, the signal intensity must also be scaled in order to maintain the same signal intensity when in

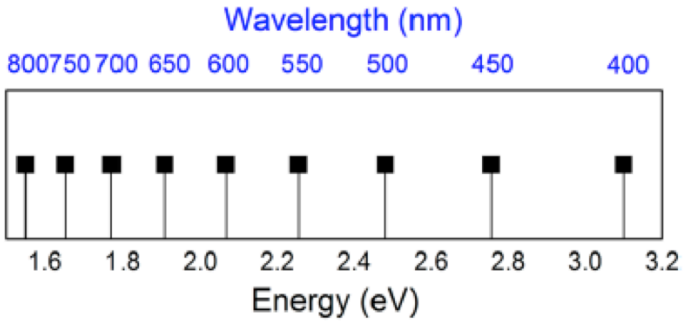

Figure 2.3: Schematic showing data points in wavelength units and energy units. Notice that data points are not evenly spaced when the scale is converted into energy. Reproduced from Mooney et al.[69]

wavelength units. When we convert the spectrum into energy units, the signal intensity is multiplied by the wavelength squared in addition to changing the wavelength scale into energy scale.

We also convert the steady-state PL or PLE spectra into lineshape spectra in addition to changing it from wavelength units to energy units. The lineshape spectra allow us to gain insights into different populations of emitting states based on the relative areas of the emission peaks. Lineshape spectra furthermore allow us to calculate reorganization energies and Gibb's free energies, which are needed to construct the free energy curves for each state. The free energy curves enable us to determine the electron transfer regions. We produce lineshape spectra following the guidelines from Scholes et al.[45] If we represent the absorption or PLE spectrum as $a(\nu)$, then its lineshape spectrum is merely $a(\nu)/\nu$, where ν is the frequency. The PL spectrum, $f(\nu)$, is converted into a lineshape spectrum using the equation $f(\nu)/\nu^3$. The divisions are necessary in order to remove the frequency dependence of either spontaneous absorption or emission.

2.3.2. Quantum Yields

Steady-state PL is also used to measure the emission quantum yield (QY) of the samples. Here, QY is defined as the ratio of photons emitted to photons absorbed. In

other words, a QY is a measure of the PL efficiency. In an ideal system, all the absorbed photons are emitted resulting in a 100% QY. However, real systems exhibit non-radiative recombination caused by a multitude of factors such as trapping at defect sites within the QD lattice, thermalization through phonon modes, or excess charge on the QD surface leading to Auger recombination, and therefore QYs are generally less than 100%.

We typically calculate QYs by taking a QD PL spectrum and comparing it to a spectrum of a reference dye such as rhodamine 6G that was collected using the same experimental conditions. This method uses only one excitation energy, which may not accurately reflect the QY because QDs have been shown to exhibit a QY spectrum where the QY changes with excitation energy.[70-74]More specifically, these studies showed QDs have higher QYs when excited near the band-edge compared to excitation energies much greater than the band-edge.

In order to check if a QY spectrum exists, we collect a PLE spectrum and compare it to the absorption spectrum. If the PLE does not line up with the absorption spectrum, then the QY is excitation-dependent. An example of an excitation-dependent QY is presented in Figure 2.4. Both the absorption and PLE spectra have been normalized to the first exciton peak. This normalization assumes that the first exciton peak has a 100% QY, which is not realistic. However, we are primarily interested in whether the QY changes, rather than its absolute value, and the normalization allows us to determine if a changing QY is present.

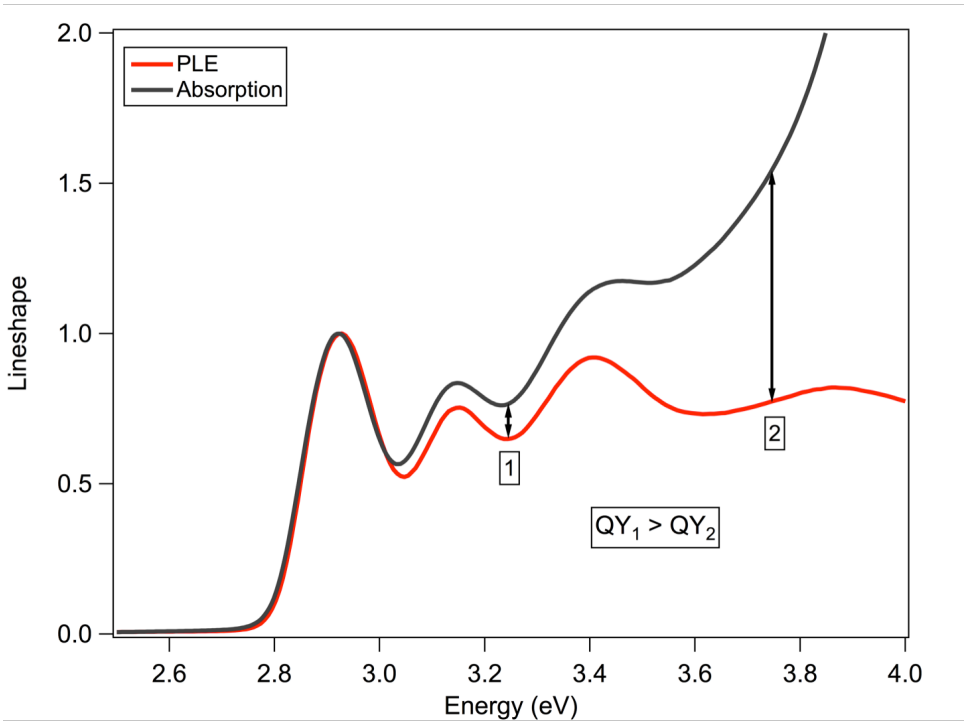

Figure 2.4: Representative absorption (black) and PLE (red) spectra for CdS in toluene. The arrows labeled 1 and 2 have been included to show how the deviation of the PLE spectrum from the absorption spectrum is not constant with excitation energy.

As Figure 2.4 shows, the PLE and absorption spectra are similar for excitation energies below 3.0 eV, meaning that the QY is constant. The same percentage of absorbed photons is emitted with the same efficiency regardless of excitation energy. In contrast, the PLE spectrum intensity is less than the absorption spectrum for excitation energies greater than 3.0 eV. Since the PLE is collected by measuring changes in emission, this difference indicates a diminished QY because the number of absorbed photons remains constant while the number of emitted photons is less.

Furthermore, the decrease in the PLE spectrum is not constant for excitation energies above 3.0 eV as evidenced by the two arrows labeled 1 and 2. Arrow 2 exhibits a much larger difference between the absorption and PLE spectrum compared to arrow 1, implying that emission efficiencies at excitation energies greater than 3.5 eV are less. In

other words, the fraction of photogenerated charge carriers relaxing to the band-edge, and then emitting is less when excited above 3.5 eV compared to 3.0 eV or less.

Hoheisel et al reported the first excitation-dependent QY for CdSe QDs, and theorized the decrease in the QY with excitation energies greater than 300 meV above the band-edge was a result of transitions involving different types of states.[71] Excitation energies within 300 meV of the band-edge excited discrete states that immediately relaxed down to the lowest excited state, resulting in identical QYs for these excitation energies. In contrast, excitation energies greater than 300 meV above the band-edge excited a different manifold of closely spaced states that relaxed to the lowest excited state with less than 100% efficiency, causing a reduction in the QY at high excitation energies.

Hoy et al confirmed the results produced by Hoheisel using CdSe QDs and CdSe/ZnS core/shell QDs, and suggested the new non-radiative pathways accessible with the higher excitation energies was caused by interactions with surface ligands. Higher excitation energies enable charge transfer to the ligands, which compete with relaxation to the band-edge and decrease the QY. In contrast to the previous two studies on CdSe, Tonti et al reported that CdSe QDs do not exhibit a QY spectrum, and scatter from QD aggregates causes the deviations observed in the PLE from the absorption spectrum.[74]

Excitation-dependent QYs have also been reported for InP QDs, but there is some controversy in the possible explanation.[72,73] For example, Rumbles et al reported an excitation-dependent QY, but no excitation dependence to the carrier cooling rates using transient bleaching spectroscopy.[72] In order to explain this discrepancy, the authors proposed that the QY is size-dependent rather than excitation-dependent. Higher

excitation energies excite smaller QDs that have a lower emitting efficiency because of more trapping. The smaller QDs would have the same relaxation pathways as the larger QDs, but would not contribute to the PL, resulting in a reduction of the overall PL at higher excitation energies.

In contrast to the study by Rumbles et al, Ellingson et al used femtosecond transient absorption on InP QDs to show that the carrier cooling rates are excitation-dependent, and there is a reduced efficiency for carriers to relax to the band-edge for excitation energies greater than the first exciton transition.[73] They speculated that surface states or capping molecules caused new relaxation pathways at higher excitation energies in agreement with the previously mentioned studies on CdSe.

2.3.3. Homogenous and Inhomogeneous Broadening of Spectra

The CdS QD absorption and emission spectra show transitions for the exciton and trap state that are not infinitely narrow. Each transition has a width that includes both homogenous broadening and inhomogeneous broadening. Homogenous broadening refers to broadening caused by mechanisms that affect the emitting particles equally. The mechanisms for homogenous broadening include vibrational coupling to the surrounding medium and lattice vibrations[75]as well as lifetime broadening.

There is always a line width to the transition even at 0 K. This line width is called the natural line width or lifetime broadening, and is a result of the energy-time uncertainty relationship where the uncertainty in the state energy (ΔE_i) is defined by:

$$\Delta E_i = \frac{h}{4\pi\tau_i}$$

where τ_i refers to the lifetime of the excited state and h is Planck's constant. The energy-time uncertainty relationship states that any state with a finite excited state lifetime

cannot have a well-defined energy. The ground state is precisely defined in energy because it has an infinite lifetime.

The energy-time uncertainty relationship shows that as the excited state lifetime increases, the natural line width for the transition decreases. Therefore, transitions that are long such as nuclear spin relaxation (~ms) have much narrower peaks while optical transitions such as radiative recombination (~ns) have broader peaks. For example, the lifetime broadening for a 1 ms lifetime is approximately 0.33 peV, while a 1 ns lifetime has a broadening of 0.33 μeV.

Because exciton average lifetimes are shorter than trap average lifetimes, the exciton natural line width is expected to be broader than the trap natural line width. However, natural line widths are only a small fraction of the overall homogenous line width. The rest of the homogeneous line width arises from interactions with the surrounding medium. Trap states are expected to have larger homogenous broadening compared to the exciton state. Trap states are located on the QD surface, and will interact more strongly with the environment compared to exciton states, which are formed in the QD core.

Inhomogeneous broadening occurs from mechanisms that do not affect the emitting particles equally. The primary inhomogeneous broadening mechanism for QDs is caused by the particle size. A QD synthesis always produces a size distribution. Since the exciton emission energy is size dependent, variations in the size causes a distribution of emission energies. As the size distribution broadens, the width of exciton emission energies also increases. Therefore, the width of the exciton emission peak can be a qualitative indicator of the size distribution within the sample. The effect of size

distribution on trap states is unknown, because it is unclear how the QD size affects the trap state energies, and therefore their emission..

The degree of homogenous and inhomogeneous broadening can be calculated from the absorption and emission spectra following a procedure developed by Scholes et. al.[45] First the absorption and emission spectra are converted into lineshape spectra. This removes the frequency dependence of spontaneous emission, and therefore the transitions are now represented by total linewidth. The lineshape absorption and emission spectra are fitted with Gaussian peaks to determine the state energies. The width of the Gaussian peak includes both homogenous and inhomogeneous broadening components and can be represented mathematically as:

$$\sum\nolimits_T = \sqrt{\sigma_H^2 + \sigma_I^2}$$

where σ_H^2 represents the homogenous broadening and σ_I^2 represents the inhomogenous broadening. The homogenous broadening can be determined from the reorganization energies used to generate the free energy curves for each state as shown in Figure 2.5. The reorganization is calculated as half the Stokes shift. The exciton reorganization energy is small, and therefore, the displacement from the ground state is also small. This results in a narrow line shape because transitions from the excited state occur to few vibrational states in the ground state. But on the other hand, the trap state reorganization energy is large, and therefore the displacement from the ground state is also large. This means that the trap state transitions to a steeper portion of the ground state free energy curve where more states are possible, leading to broader line shape.

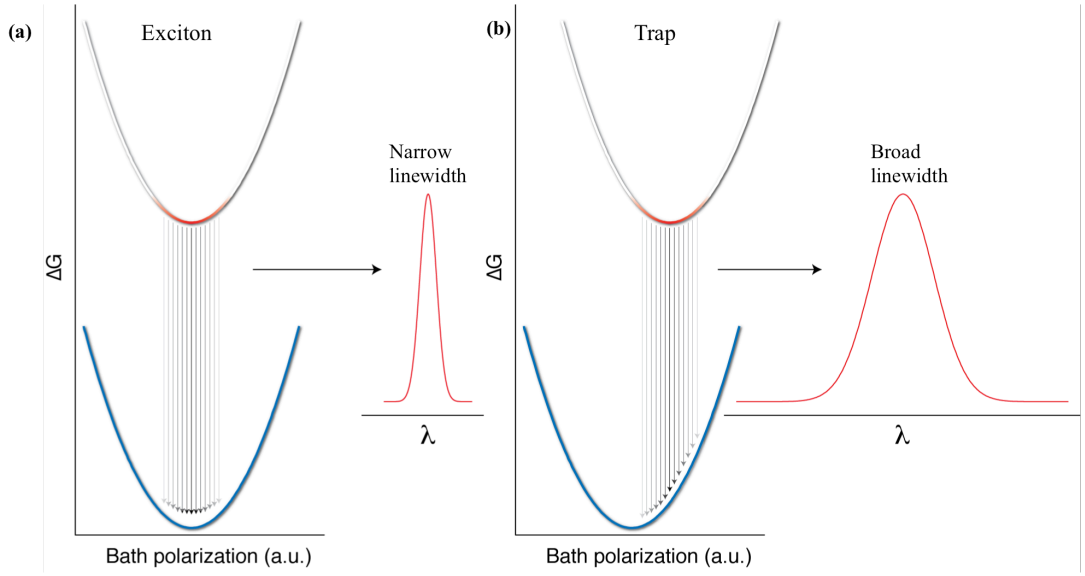

Figure 2.5: Schematic showing how the free energy curves affects the emission linewidth for the exciton (a) and trap (b).

The differences in exciton and trap homogenous broadening based on the reorganization energies are shown schematically in Figure 2.5. Because the total width and homogenous broadening are known, the inhomogeneous broadening is calculated by rearranging the previous equation to obtain:

$$\sigma_I = \sqrt{\sum_T^2 - \sigma_H^2}$$

2.3.4. Extracting ET Parameters from Steady State PL

The parameters needed to define ET can be extracted from the photoluminescence excitation (PLE) and photoluminescence (PL) spectra using the procedure developed by Scholes et al.[45] The PLE spectrum is used instead of the absorption spectrum because it provides better signal to noise for determining the trap state absorption energy. The PLE and PL spectra are first converted into line shape spectra to remove the frequency dependence of spontaneous absorption and emission. The PLE and PL lineshape spectrum for CdS in dichloromethane are shown in Figure 2.6.

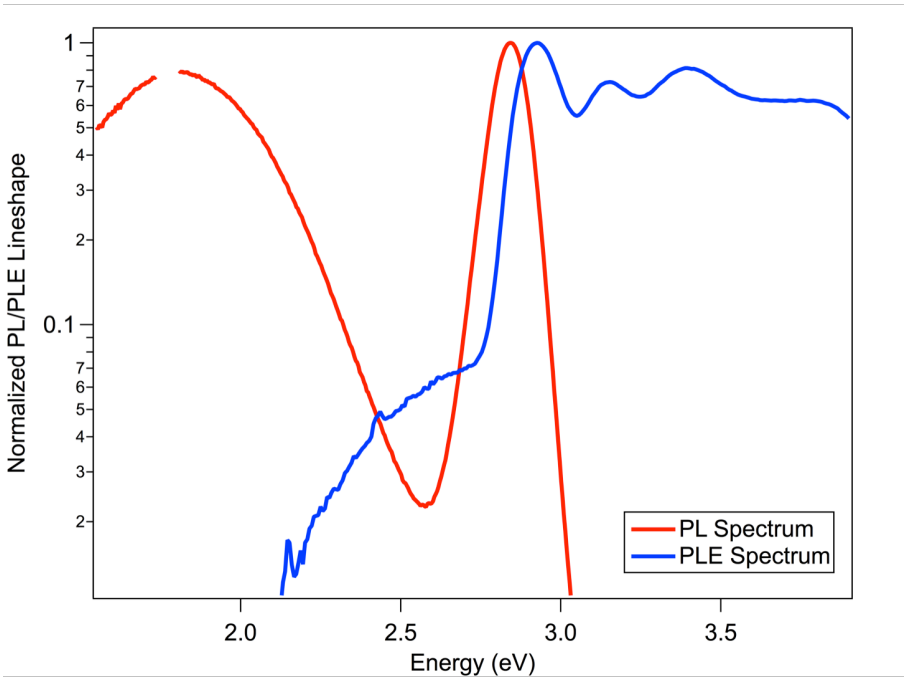

Figure 2.6: Trap PLE (blue) and PL (red) lineshape spectrum for CdS in dichloromethane.

The line shape spectra are then fit with a series of Gaussian peaks to determine the absorption and emission energies of each state. The PLE spectrum is used to determine the absorption energies as shown in Figure 2.7, and the PL spectrum is used to determine the emission energies as shown in Figure 2.8.

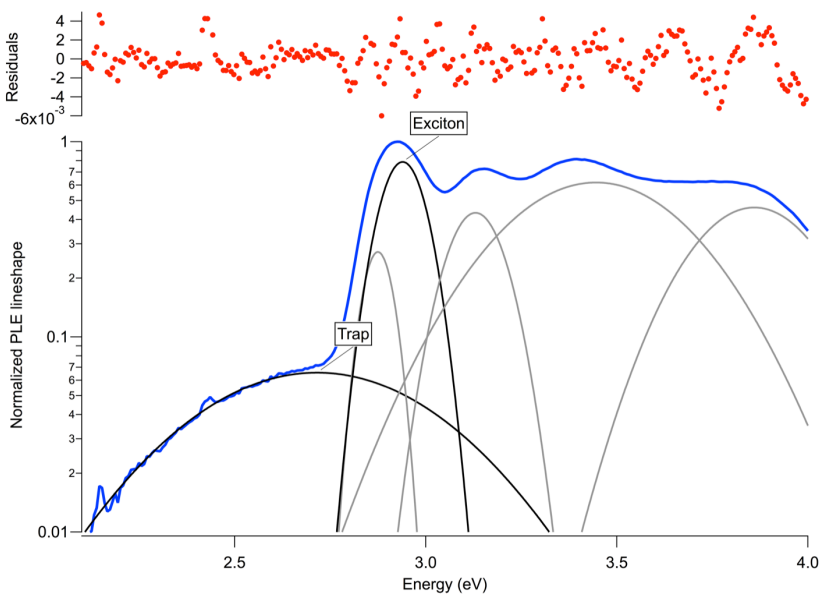

Figure 2.7: Multi-peak fit to the trap PLE (blue) spectrum. The spectrum was fit using a series of Gaussian peaks (black and grey). Only the black peaks were used to calculate the exciton and trap absorption energies. The red dots are the residuals from fitting the spectrum.

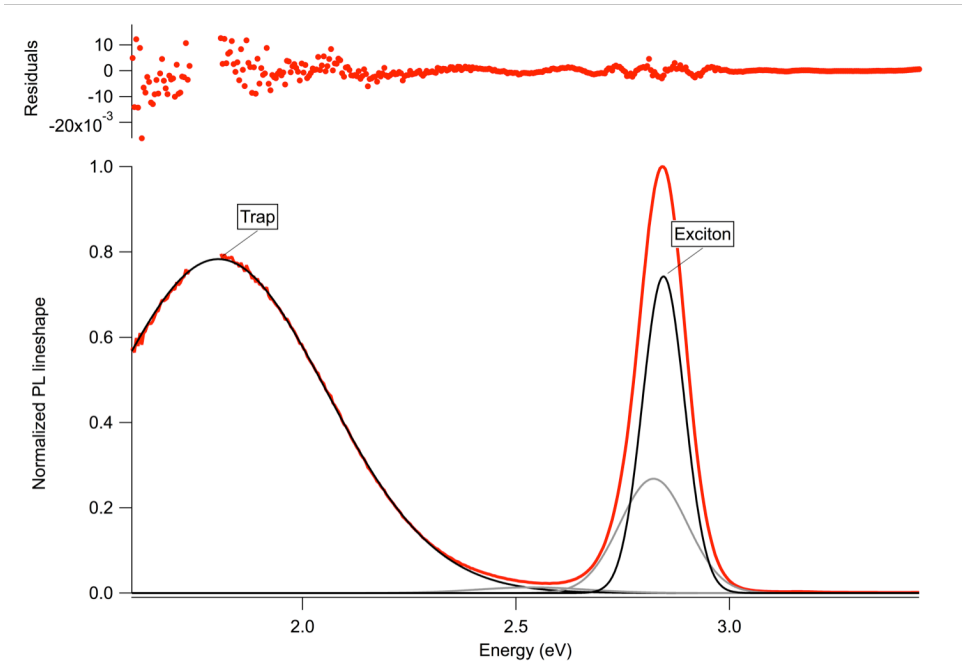

Figure 2.8: Multi-peak fit of the PL lineshape spectrum using a series of Gaussian peaks (black and grey). Only the black peaks were used to calculate the exciton and trap emission energies.

The free energy curves for each state are then determined using the following function:

$$\Delta G_i = \frac{1}{2}(x-a)^2 + \Delta G_i^\circ$$

where ΔG_i° represents the free energy between state i and the ground state, and a is the displacement of state i relative to the ground state. ΔG_i° is calculated as

$$\Delta G_i^\circ = \alpha_i - \lambda_i$$

where α_i represents the absorption maximum from the fitted spectrum and λ_i is the reorganization energy of state i relative to the ground state. The reorganization energy for each state is calculated as half the Stokes shift where the Stokes shift is defined as the difference between the absorption and emission energies. The displacement, a, is calculated as

$$a_i = \sqrt{\text{Stokes shift}}$$

The absorption and emission energies as well as the calculated ET parameters needed to construct the free energy curves are shown in Table 2.1.

The reorganization energy (λ_{CT}) and change in free energy (ΔG_{CT}°) for the charge transfer

Table 2.1: ET parameters extracted from the multi-peak fits of the PLE and PL spectra for CdS in dichloromethane.

Parameter	**Exciton**	**Trap**
Absorption (α_i)	2.9396 eV	2.7156 eV
Emission (ε_i)	2.8455 eV	1.8027 eV
Stokes Shift	0.0941 eV	0.9129 eV
Displacement (a_i)	0.307	0.955
Reorganization (λ_i)	0.0471 eV	0.456 eV
Free Energy ($\Delta G°_i$)	2.4691 eV	2.2592 eV

are calculated using the following equations:

$$\lambda_{CT} = \frac{1}{2}(a_T - a_E)^2$$

$$\Delta G^{\circ}_{CT} = \Delta G^{\circ}_{T} - \Delta G^{\circ}_{E}$$

where a_T and a_E represent the displacements of the trap and exciton states, and ΔG°_{T} and ΔG°_{E} represent the free energy of the trap and exciton states. Using the parameters listed

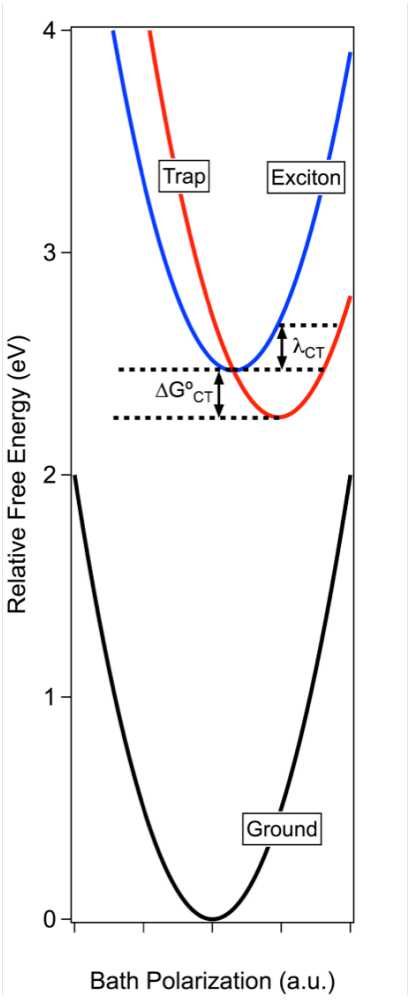

Figure 2.9: Free energy curves for the exciton (blue) and trap (red) constructed using the values listed in Table 2.1. The displacements are relative to the ground state (black).

in Table 2.1 in the preceding equations, λ_{CT} is 210 meV and ΔG°_{CT} is -210 meV. Finally, the activation barrier for the charge transfer is calculated as

$$\Delta G^{*} = \frac{\left(\lambda_{CT} + \Delta G^{\circ}_{CT}\right)^{2}}{4\lambda_{CT}}$$

Because λ_{CT} and ΔG°_{CT} are equal, the activation barrier for ET is zero, and the reaction is in the barrierless region. This is more clearly seen in Figure 2.9, where the free energy curves of each state calculated from the values listed in Table 2.1.

2.4. Time-Resolved PL

Time-resolved photoluminescence (TRPL) can be used to measure exciton and trap state recombination dynamics because it is sensitive to small changes on the QD surface.[76] Additionally, TRPL allows the dynamics of QD emission to be studied over a wide range of time scales, from picoseconds to microseconds. This is necessary because various mechanisms such as trapping and detrapping within the QD occur on these time-scales.[27,77-80]

2.4.1. Time-Correlated Single Photon Counting

TRPL decays were recorded on CdS QDs using the method of time-correlating single photon (TCSPC). TCSPC relies on the principle that the probability of detecting a single photon at a set time after an excitation pulse is proportional to the fluorescence intensity at that time. By recording the times of detected photons after a large quantity of excitation pulses, the fluorescence intensity decay is reconstructed.[68] A general schematic of a TCSPC experiment is shown in Figure 2.10. In a typical measurement, a pulsed light source generates an optical pulse at the same time as an electronic pulse. The optical pulse excites the sample while the electronic pulse travels to the input of the time-to-amplitude converter (TAC), which initiates the charging of a capacitor. The sample

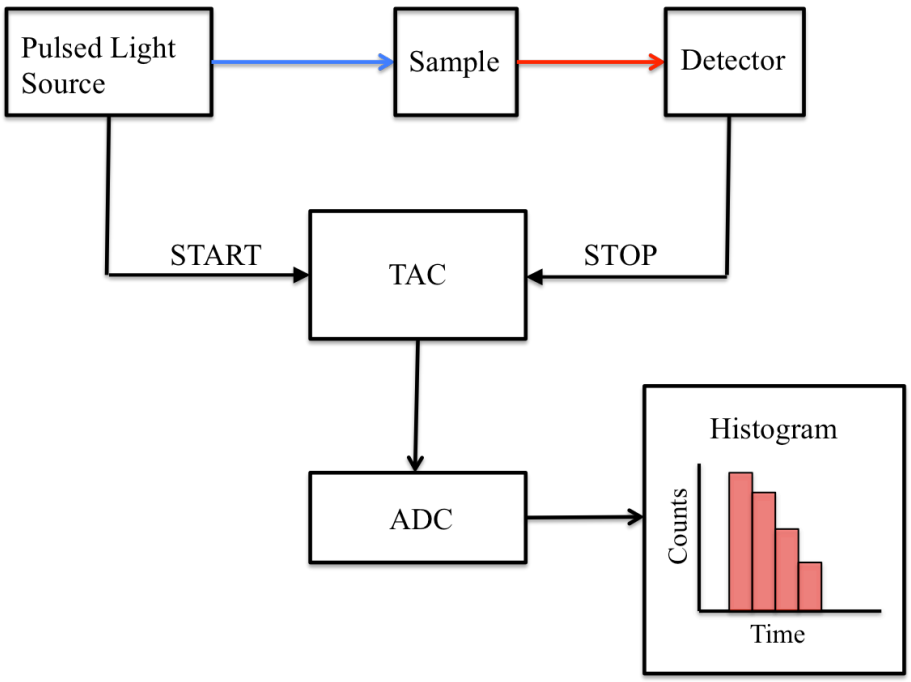

Figure 2.10: TCSPC setup in forward mode. TAC is the time to amplitude converter and ADC is the analogue to digital converter.

fluoresces which is detected by a photon counting detector. The detector generates an electronic signal that passes onto the TAC and stops the charging of the capacitor. Because the voltage ramp of the TAC is proportional to the time between the start and stop pulses, the time of the emitted photon can be determined. The counted photons are then binned into channels with a set time width and a histogram is generated. After a large number of excitation events, the histogram represents the fluorescence decay curve.

2.4.2. Considerations

TCSPC measurements require a pulsed light source, and early TCSPC experiments utilized either ps dye lasers or flashlamps. Ps dye lasers can be challenging to operate and maintain, and they have been replaced with titanium sapphire (Ti:sapphire) lasers. Ti:sapphire lasers are advantageous for TCSPC measurements because their pulse width is on the order of 100 fs. Another advantage to Ti:sapphire lasers is their long term

stability because they are solid state devices. One disadvantage to Ti:sapphire lasers is their high repetition rate (~80 MHz), which is too fast for most TCSPC experiments.

When conducting TCSPC experiments, the time between pulses needs to be longer than the sample's relaxation time in order to prevent the sample from excited multiple times before it has fully relaxed. For a Ti:sapphire laser with a 80 MHz pulse rate, the time between pulses is 12.5 ns. In order to prevent multiple excitations of the QDs, we reduce the 80 MHz pulse rate of the laser using electro-optical modulators.

An electro-optical modulator acts as a shutter where it passes one pulse then blocks a select number of subsequent pulses in order to achieve the desired repetition rate. The modulator consists of non-linear crystals in which changing the electric field switches the polarization of the crystal from horizontal to vertical. In order for laser light to pass through the modulator, the crystals must be horizontally polarized since our laser consists of horizontally polarized light. When the crystal is vertically polarized, the laser light is blocked.

In our experiments, the pulse rate is generally 100 kHz or slower. Furthermore, the photon count rate of the detector needs to be less than 1% of the repetition rate of the laser to ensure accurate counting of the photons because the TAC only detects the first photon. The TAC relies on the charging of a capacitor. The start signal charges the capacitor while the stop pulse discharges it. If the TAC receives two stop pulses in a row, only the first is counted because there was not a second start pulse to initiate the voltage ramp. When the count rate of the detector is more than 1%, the probability of receiving two stop pulses after one start pulse increases. . Because only the first photon is seen, only the first photon is counted, and the PL decay becomes biased to shorter times. This

effect is called pulse pile up. The photon count rate is controlled by the concentration of the sample, as well as using neutral density filters to reduce excitation and emission light intensities.

2.4.3. Collecting PL Decays

PL decays can be collected in either forward mode or reverse mode. In forward mode, the light source acts as the start for the TAC and the detector acts as the stop for the TAC. Forward mode is the easiest to understand conceptually, but it is rarely used in practice because it can be inefficient. When running in forward mode, the TAC may not always receive a stop pulse from the detector since the photon count rate is less than 1%. In reverse mode, the detector acts as the start pulse and the light source becomes the stop pulse. This ensures that the TAC will always have a stop signal and the voltage ramp will not begin unless the detector sees a photon.

The length of the TAC is also important for measuring PL decays because any photons, which arrive outside of the TAC window, will not be counted. For example, if the TAC is 500 ns, then any photons emitted after 500 ns will not be counted. Therefore, the TAC needs to be at least as long as the PL decay. For trap states in CdS, the PL decays are microseconds long and require at minimum, a 10 μs TAC. However, long TACs suffer from poor resolution because the number of channels available for binning photons is the same regardless of the TAC length.

On our system, a 10 μs TAC has a resolution of 2.5 ns per channel while a 500 ns TAC has a resolution of 122 ps per channel. To address the low resolution of long TAC windows, two PL decays are collected for each measurement. One PL decay is collected with a long TAC, and another is collected using a short TAC that is approximately 5% of

the long TAC. For example, trap state PL decays were collected using a 10 μs TAC as well as a 500 ns TAC. By collecting two PL decays, the full decay is measured and high resolution is maintained at the early parts of the decay where the most change is occurring.

2.4.4. Analyzing PL Decays

Once the long and short PL decays are collected, they are analyzed simultaneously using least squares iterative reconvolution of a multi-exponential decay function with a recorded instrument response function (IRF) shown in Figure 2.11.[81]

An IRF measures the response of the detection system to an instantaneous process such as scattering. IRFs are necessary because the detection system does not have an infinitely fast response time, and therefore will contribute to the measured PL decay. The IRF is convoluted with a multi-exponential decay function of the form:

$$y = \sum_{i=1}^{N} A_i e^{-t/\tau_i}$$

where N is equal to the number of exponentials used in the decay function, A is the pre-exponential factor, and τ is the decay component. We use multi-exponential functions (rather than single exponential decays) because QD recombination dynamics are typically complex and inhomogeneously broadened with a distribution of non-radiative processes.[76] When fitting the PL decay, I use a minimum number of exponentials. The first step is to choose initial values of A and τ to generate a PL decay, which are then compared to the observed PL decay. The values of A and τ are then adjusted until the residuals are minimized and are randomly scattered around zero. The PL decays analyzed in this work were fitted with N ranging from 4 to 7.

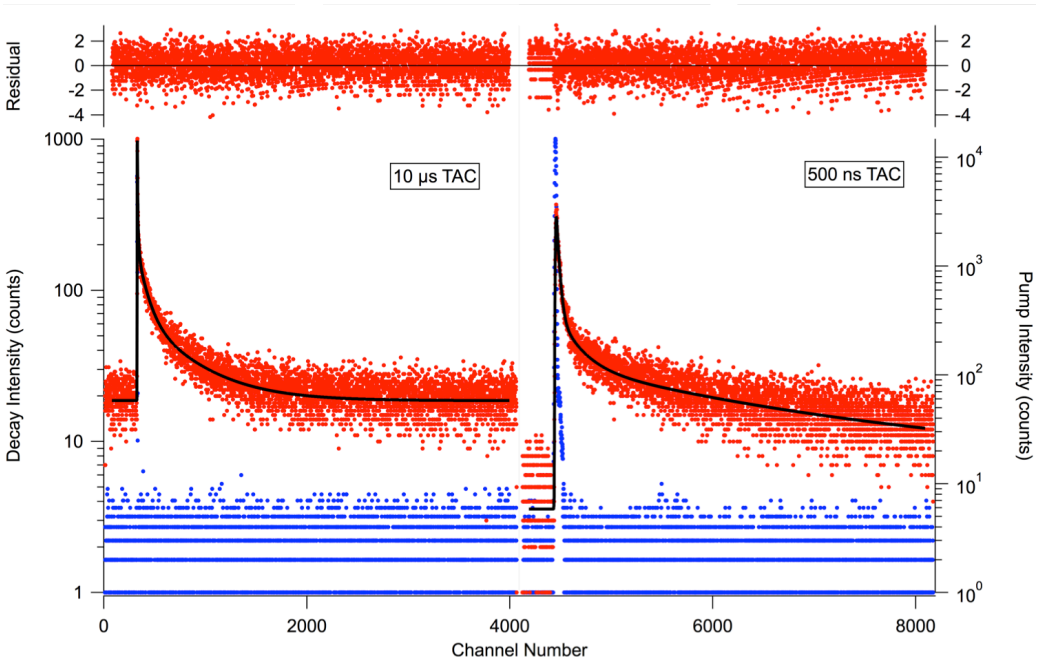

Figure 2.11: Representative trap state PL decay in CdS collected with two TACs. Blue dots are the IRFs and black lines represent the multi-exponential fit, which is the same for both decays. This decay required 4 exponentials to successfully fit the PL decay.

The quality of the fit is described by the reduced chi-square (χ^2) and the Durbin-Watson parameters. The reduced χ^2 is simply the χ^2 divided by the degrees of freedom. χ^2 is a statistical test in which the observed values are compared to the expected values to determine whether the differences between the observed and expected values are significant. For a good fit, reduced χ^2 should have values reasonably close to 1. Values much larger than 1 indicate significant errors between the measured decay and the theoretical decay, and more decay components may be necessary. If χ^2 is less than 1, then the number of counts in the PL decay is not large enough for statistical analysis (over fitting). The Durbin-Watson parameter is a statistical test to see if there is any correlation in the residuals from the fits. If no correlations exist in the residuals, then the Durbin-Watson parameter should be 2.

The fit function is then used to calculate the average PL lifetime, or the average time it takes the QD to emit a photon after an excitation event. The average PL lifetime is calculated using the following equation:

$$\langle \tau \rangle = \sum_n \frac{\int_0^{t_{exp}} A_n \tau_n \exp(-t'/\tau_n)\, dt'}{\sum_m \int_0^{t_{exp}} A_m \tau_m exp(-t''/\tau_m) dt''}$$

where t_{exp} represents the time window of the experiment. When the time window becomes much longer than any measured component, then $t_{exp} = \infty$ and previous equation becomes

$$\langle \tau \rangle = \sum_n \frac{A_n \tau_n^2}{\sum_m A_m \tau_m}$$

When we analyze a series of exciton PL decays recorded at different temperatures using the second equation presented in Figure 2.12, we see that the exciton average lifetimes are temperature-dependent and increase from 40 ns to 120 ns and then decreases

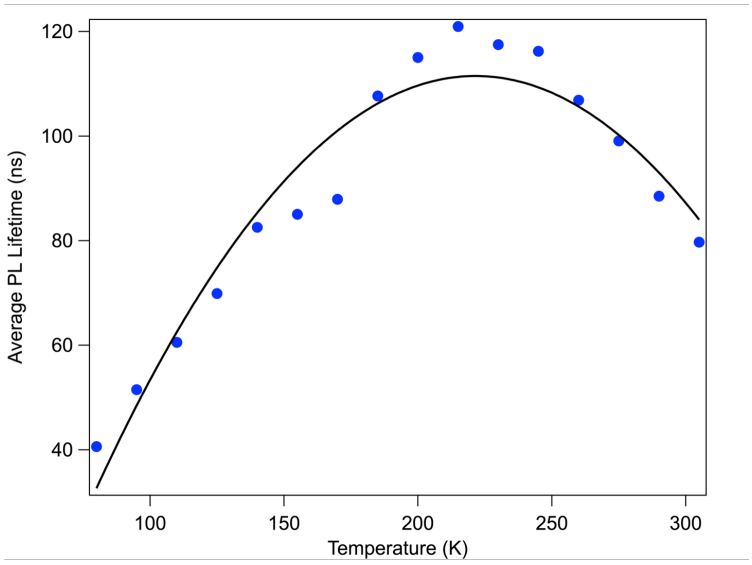

Figure 2.12: Exciton average PL lifetime at various temperature calculated using an infinite time window. The black line is a trend line fitted to the data using a polynomial function.

to 80 ns as the temperature is raised from 80 to 305 K. However, Figure 2.12 provides no information on how the shape of the decay changes with temperature. We do not know if the fast components or the long components are responsible for the variation in the exciton average lifetimes.

Therefore, we analyze PL decays using the first equation, and we generate a 2D plot of the average lifetime as shown in Figure 2.13. This allows us to see how the decay shape changes with temperature because short time windows emphasize the fast decay components while long time windows focus on long time components. Each horizontal slice of the 2D plot represents how the average lifetime changes with temperature at a particular time window. For example, the temperature-dependent average lifetimes within 100 ns, 1 µs, and 10 µs are shown in Figure 2.14. The 10 µs time window resembles Figure 2.12 because all of the decay components used to fit the PL decays are much less

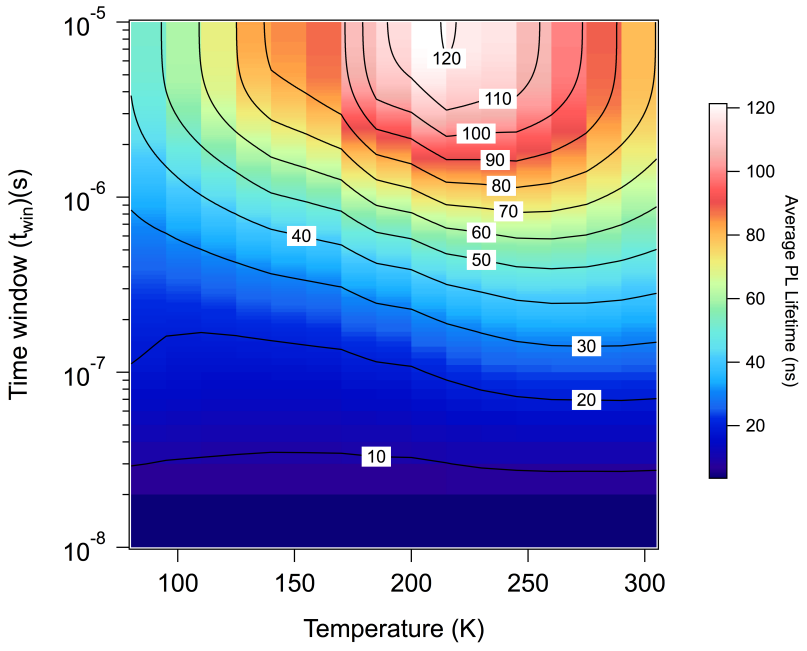

Figure 2.13: Exciton average PL lifetimes at various temperatures as a function of the time window of the experiment. The colors represent the average lifetime magnitude.

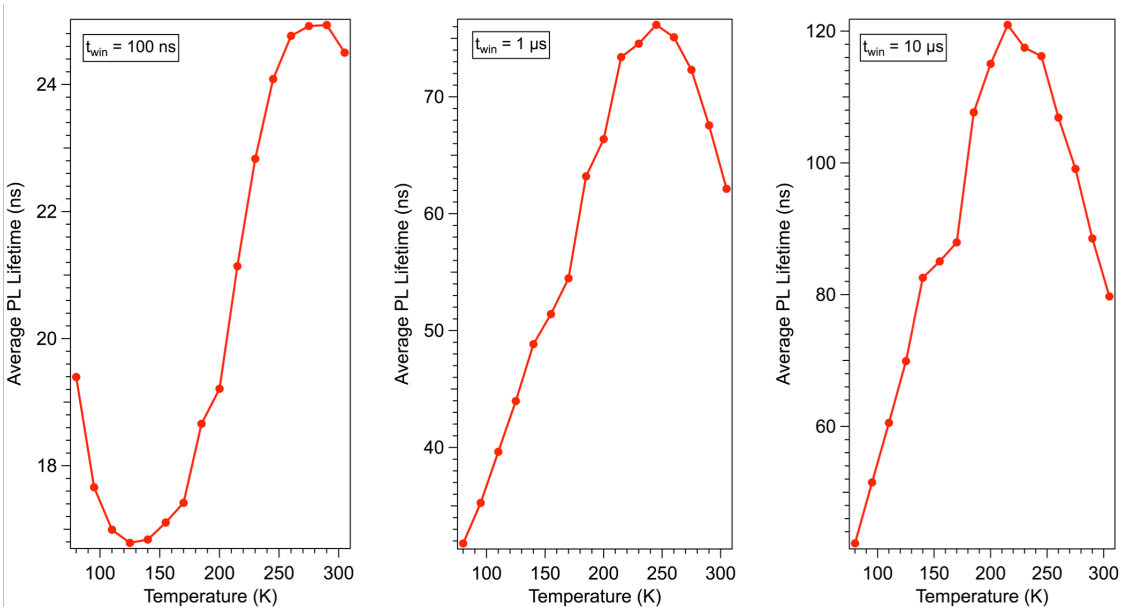

Figure 2.14: Exciton average PL lifetime within 100 ns (left), 1 µs (center), and 10 µs (right).

than 10 µs.

The 2D plot indicates that components longer than 1 µs are responsible for the temperature-dependent average lifetime. We also see that at short times, the average PL lifetime actually decreases as the temperature is raised from 80 to 140 K before increasing for temperatures greater than 140 K. Possible explanations for these trends are discussed in more detail in Section 4.5.1. Analyzing the PL decays using plots such as Figure 2.13 enables us to observe how the shape of the decay changes in response to a perturbation and to associate those changes to physical processes that may be occurring.

CHAPTER 3: EXPERIMENTAL

3.1. CdS QD Synthesis

CdS QDs were synthesized following the procedure from Battaglia et al.[82]. In general, the cadmium precursor was prepared by dissolving 0.3 g of cadmium acetyl acetonate and 1.0 g of oleic acid into 25 mL of 1-octadecene (ODE) in a 100 mL round bottom flask. The sulfur precursor was prepared by dissolving 0.014 g of elemental sulfur in 25 mL of ODE. The cadmium precursor was degassed at room temperature until bubbles were no longer present before heating to 100° C under vacuum for 30 minutes. The sulfur precursor was degassed at room temperature for 30 minutes then heated to 100° C under nitrogen. The cadmium precursor was heated to 300° C under nitrogen. Once the cadmium precursor reached temperature, the sulfur precursor was quickly injected into the cadmium precursor to promote QD nucleation and growth. The QDs were allowed to grow for 10 minutes. Rapidly cooling the flask by removing it from heat and blowing N_2 gas over the flask stopped QD growth.

3.2. QD Purification

QDs were purified by adding a non-solvent such as acetone or methanol in a 1.5:1 ratio. For example, 7.5 mL of methanol was added to 5 mL of raw QD solution before centrifuging at 6500 rpm for 15 minutes. After centrifugation, the supernatant was discarded and the precipitated QDs were redispersed into 95% anhydrous hexane. The purification process was repeated a minimum of three times. After the final

centrifugation, the QDs were redispersed into the solvent for spectroscopic measurements. Spectroscopic measurements were conducted using 2 different solvents. All temperature-dependent experiments used a glass-forming solvent, which was a 6:1 mixture of isopentane to methylcyclohexane. All other experiments used 95% anhydrous hexane.

3.3. Temperature-dependent TRPL

Three different sizes of CdS QDs were synthesized and dispersed into the glass forming solvent. Absorption measurements were collected using a Cary 5000 UV-Vis-NIR spectrometer set to a double beam configuration. Spectra were collected from 900-300 nm in 1 nm intervals with a 0.5 s averaging time. Steady state PL and PLE were collected using a Jobin-Yvon Flurolog 3 with a Hamamatsu R928 PMT detector. For PL experiments, excitation and emission monochromators were set to 2 nm bandpass. Samples were excited at 340 nm and emission spectra were collected from 360-800 nm in 1 nm intervals with a 1 s integration time.

For PLE measurements, the excitation monochromator was set to 2 nm bandpass. The emission monochromator was set to 5 nm for measuring the exciton PLE and 10 nm for measuring the trap PLE. Exciton PLE and trap PLE were measured at the maximum emission wavelength of each state. For example, the exciton PLE was collected at 443 nm and the trap PLE was collected at 600 nm for one sample. Exciton PLE spectra were recorded from 300-500 nm in 1 nm intervals with a 2 s integration time. Trap PLE spectra were recorded from 300 nm until 5 nm less than the chosen emission wavelength to prevent excitation light from saturating the detector. Trap PLEs were also recorded

with a 2 s integration time. All spectra were corrected for PMT sensitivity and for fluctuations in excitation intensity by using a diode reference detector.

Samples were mounted into a modified cryostat (Janis ST-500) by placing one sapphire window into the sample holder followed by a 1 mm Teflon spacer. The sample was injected into the opening of the spacer while sliding the second sapphire window over the sample until a small bubble remained. The small bubble allowed monitoring of the sample when the cryostat was placed under vacuum. The sample chamber was sealed by slowly lowering the gold sample cover (with all four screws already inserted) on top of the sample chamber. The screws were alternatively tightened to lower the sample cover fully into place. This procedure minimized the risk of cracking a window and prevented more bubbles from forming in the sample. The front plate was placed onto the cryostat, and it was evacuated for 10-15 minutes before being mounted vertically on the laser table. Once mounted on the table, the cryostat was connected to the vacuum pump and the liquid N_2 transfer line was also connected. The cryostat remained under continuous vacuum while all measurements were being conducted. A Lakeshore temperature controller (Model 331) was used to control the temperature.

Temperature-dependent TRPL was collected using TCSPC in reverse mode using a home-built laser set-up. Samples were excited using a Ti:sapphire Mai-Tai HP laser (Spectra-Physics) frequency doubled using a SpectraPhysics Inspire Auto 100 optical parametric oscillator (OPO). The 80 MHz pulse rate of the Mai-Tai was reduced to 80 kHz using two electro-optic modulators (Con-Optics 350-105) in series. Emission was collected in a front face configuration using a double monochromator (Spectral Products CM 112) coupled to a hybrid PMT (HPM-100). Exciton and trap PL decays were

measured at the maximum emission peak for each state. The exciton emission wavelength was adjusted as needed to account for the temperature-dependent band-gap of the QDs.

Exciton and trap PL decays were collected from 80 K to 305 K in 15 K increments. Both exciton and trap PL decays were recorded using a 10 μs TAC using DPC-230 16 channel photon correlator (Becker&Hickl GmbH) and a 50 ns TAC using a SPC-130 photon correlator (Becker&Hickl GmbH) for two samples. The third sample used a 100 kHz repetition rate. Exciton PL decays were recorded using a 3 μs TAC and a 50 ns TAC. The trap PL decays were recorded with a 10 μs TAC and a 500 ns TAC.

3.4. Excitation-dependent TRPL

In order to separate the exciton dynamics from the trap state dynamics, one CdS sample was excited using six different excitation energies. Trap PL decays were recorded using the same temperature series as mentioned before. The sample was excited using the Mai-Tai laser. The Mai-Tai emission wavelength was changed as needed to ensure the doubled light was at the correct wavelength. The doubling crystal within the OPO was rotated to ensure maximum power at each excitation wavelength. Trap PL decays were recorded with a 10 μs TAC using a DPC-230 16 channel photon correlator (Becker&Hickl GmbH), as well as a 500 ns TAC using a SPC-130 photon correlator (Becker&Hickl GmbH).

3.5. CdS QDs and Oleic Acid

3.5.1. Oleic Acid Purification

Because pure oleic acid is rather expensive, technical grade (90%) oleic acid was purified following the procedure from Arudi et al.[83] The key component of the

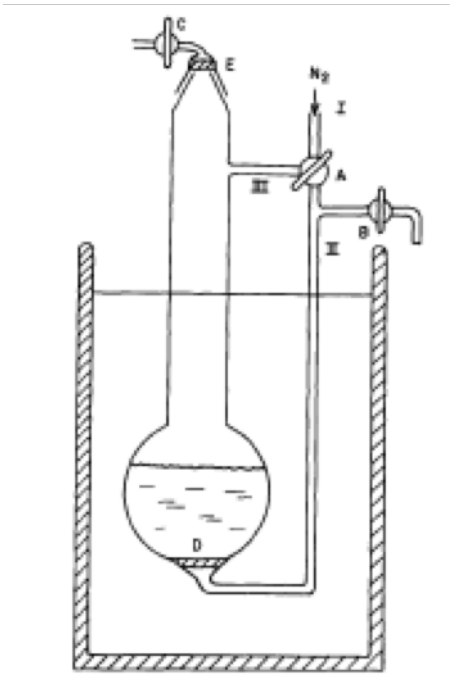

Figure 3.1: Recrystallization vessel used for oleic acid purification. Reproduced from Arudi et. al.[83]

purification was the custom made piece of glassware made by Palmetto Scientific shown in Figure 3.1. The vessel consists of a three-way stopcock labeled A and a two-way stopcock labeled B, which are used to control the direction of N_2 flow. Approximately 20 mL of 90% oleic acid was added to the vessel using a glass funnel followed by 180 mL of ACS reagent grade acetonitrile (ACN). N_2 gas was forced through the bottom of the flask (I→II) to physically mix the ACN and oleic acid since the two liquids are not miscible. The solution was bubbled violently at room temperature for a minimum of 10 minutes. The vessel was slowly lowered into a dewar containing a dry ice/acetone bath at -20° C and continued to bubble for approximately 30 minutes. The dry ice/acetone bath froze the oleic acid since the melting point is 13-14° C, while the ACN and any impurities remained in liquid form.

After 30 minutes, stopcock A was used to change the N_2 flow to I→III and stopcock B was opened. The vessel was sealed at the top to build up pressure within the flask and force the ACN containing the impurities through the coarse glass frit at the bottom of the vessel and out the valve labeled B. The filtrate was collected in a beaker and characterized using UV-Vis absorption. This process took approximately several hours to remove all the ACN. After the ACN was removed, 50 mL of chilled ACN was added to wash the frozen oleic acid. The N_2 flow was changed to I→II and the vessel was unsealed to bubble the chilled ACN within the dewar for another 30 minutes. The wash was removed from the frozen oleic acid and also characterized using UV-Vis absorption.

After the wash was removed, the vessel was removed from the dewar to thaw the frozen oleic acid. The vessel was covered with aluminum foil to minimize exposure to light. N_2 continued to flow through the vessel (I→II) to minimize exposure to oxygen. Once the oleic acid thawed, the recrystallization procedure was repeated with additional ACN being added under continuous flow of N_2. The second recrystallization took less time and was monitored using UV-Vis absorption. After 3 recrystallizations, the oleic acid was transferred to a 100 mL Schlenk flask containing a stir bar using a double-edged cannula needle. The recrystallized oleic acid was slightly heated under vacuum to remove any remaining ACN. The oleic acid was removed from the vessel after three recrystallizations to check the purity as well as to clean the coarse glass frit within the vessel. Once the oleic acid was sufficiently pure, it was stored in a Schlenk flask under nitrogen and covered with aluminum foil in a −70°C freezer.

3.5.1.1. Oleic Acid Characterization

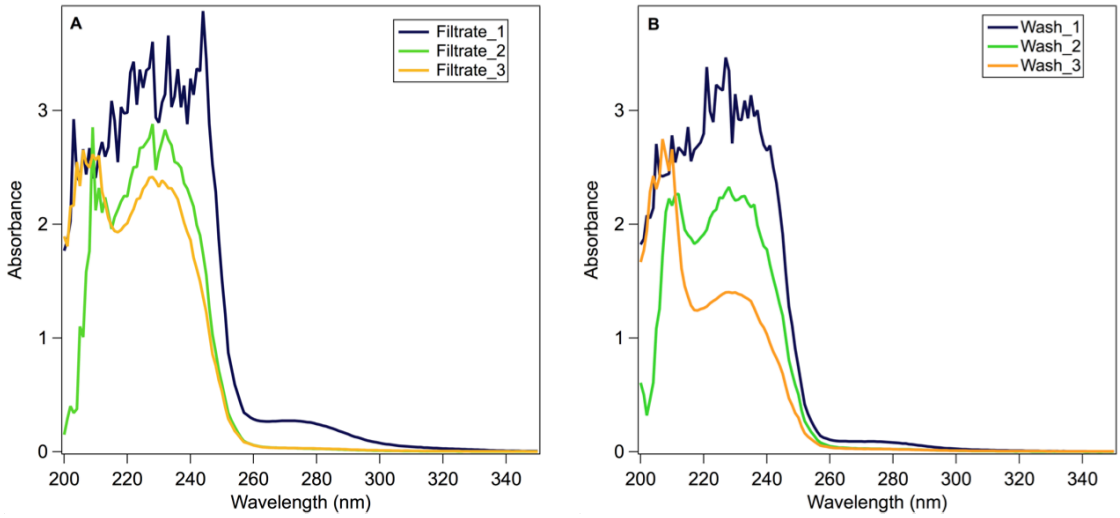

Figure 3.2: UV-Vis absorption spectrum collected during the recrystallization of oleic acid. A is the filtrate removed from the vessel, and B is the wash removed from the vessel.

The purification of oleic acid was monitored using UV-Vis absorption. After each recrystallization, an aliquot of the filtrate or wash was using analyzed using a Cary 50 UV-Vis spectrophotometer set to "fast" corresponding to 0.0125 s integration for every 1 nm with a scan range from 200-400 nm. Necessary baseline corrections were made using ACN. The purity of the filtrates and washes was determined by the disappearance of the peak at approximately 270 nm as well as a decrease in the overall absorption as seen in Figure 3.2.

To determine the purity of the oleic acid, 2.5 µL of oleic acid was dispersed in 3 mL of methanol. UV-Vis spectra were collected using the same settings as the filtrate. The peak at 230 nm is attributed to the impurities. As the purity of oleic acid increases, this peak decreases as shown in Figure 3.3.

3.5.2. CdS-Oleic Acid Sample Preparation

A stock solution of 4.8 nm diameter CdS (2.0×10^{-7} M) in 95% anhydrous hexane and a stock solution of the purified oleic acid (0.01 M) in 95% anhydrous hexane were used to prepare the samples for spectroscopic measurements. Each sample contained 0.5

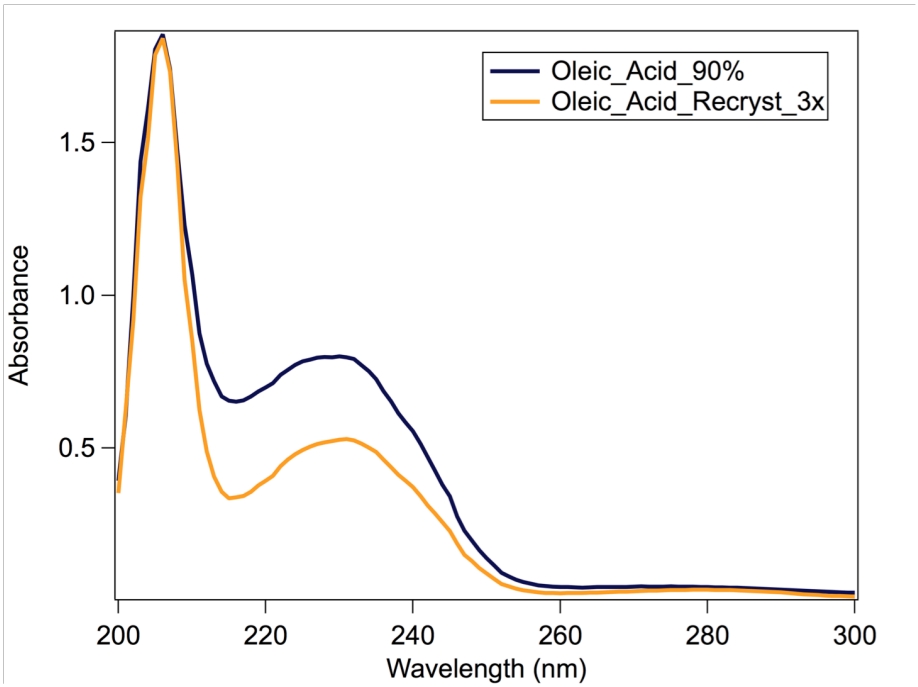

Figure 3.3: UV-Vis spectrum of 90% oleic acid and purified oleic acid. The decrease at 230 nm indicates the impurities are being removed.

mL of QD and varying amounts of oleic acid (10-1000 μL). The samples were then adjusted to a total volume of 5.0 mL using 95% anhydrous hexane. This allowed the concentration of QD to remain constant for each sample while only the oleic acid concentration was varied. After preparation, the samples were placed on a shaker for overnight. All samples were allowed to equilibrate for at least one day before any spectra were collected.

3.5.3. CdS-Oleic Acid Sample Characterization

Absorption spectra of the CdS-oleic acid samples were collected using a Cary 50 UV-Vis spectrophotometer set to “slow” corresponding to 0.1s integration time every 0.5 nm. The scan range was set to 800-300 nm, and necessary baseline corrections were made using 95% anhydrous hexane.

Steady state and TRPL measurements were made using a Jobin-Yvon Flurolog 3 with a Hamamatsu R928 PMT detector. PL measurements were collected at 420 nm and 389 nm excitation from a xenon-arc lamp with the excitation and emission monochromator slit widths set to 2 nm bandpass. Emission spectra were collected from 430-800 nm when exciting at 420 nm and from 400-800 nm when exciting at 389 nm. The integration time for all emission spectra was 2 s. Excitation spectra were collected at both the exciton and trap emission wavelengths. Because the trap emission is broad, excitation spectra were collected at a range of trap emission wavelengths from 500-800 nm in 20 nm intervals. Each excitation spectrum was collected from 300-500 nm in 1 nm intervals with 2 s integration. The excitation monochromator was set to 2 nm bandpass while the emission monochromator was set to 5 nm bandpass. Both emission and excitation spectra were corrected for PMT sensitivity and for lamp fluctuations by using a diode reference detector.

TRPL measurements were collected TCSPC utilizing a 389 nm pulsed LED (IBH) set to a 100 kHz repetition rate. IRFs were collected before each sample measurement by recording a PL decay using the scattered light from the LED. Exciton PL decays were measured in forward mode for the 2 μs time TAC and in reverse mode for the 100 ns TAC. All exciton PL decays were recorded at 454 nm with a 5 nm bandpass. Neutral density filters were placed before the detector for some of the samples to prevent the count rate of photons being greater than 1% of the repetition rate of the LED.

Trap PL decays were measured in forward mode for the 10 μs TAC and reverse mode for the 500 ns TAC. Because of the limited delay times included in the TCSPC

collection software, a delay generator (Stanford Research Systems Model DG535) was necessary for collecting the trap PL decays. Trap PL decays were measured from 500-800 nm in 20 nm intervals with the emission monochromator set to 7 nm bandpass. A 450 nm longpass filter was placed on the emission side to prevent scatter from the LED from dominating the trap PL decays. Neutral density filters were used for some of the samples to prevent the photon counting rate being greater than 1% of the repetition rate of the LED.

CHAPTER 4: RESULTS

4.1. Comparing CdSe and CdS QDs

An absorption and emission spectrum for CdSe and CdS are presented in Figure 4.1. Both types of QDs exhibit sharp features in the absorption spectra, which are indicative of exciton absorption and absorption into higher energy states. The QD absorption for both types of QDs are blue-shifted from the bulk absorption because of quantum confinement. The CdS absorption is blue-shifted compared to the CdSe absorption because CdS has a wider band-gap (2.4 eV) compared to CdSe (1.74 eV).[23] Even though CdSe and CdS have similar absorption spectra, their emission spectra are quite different. CdSe has a single emission peak that is centered at approximately 550 nm. This emission is caused by exciton radiative recombination. CdS has a similar

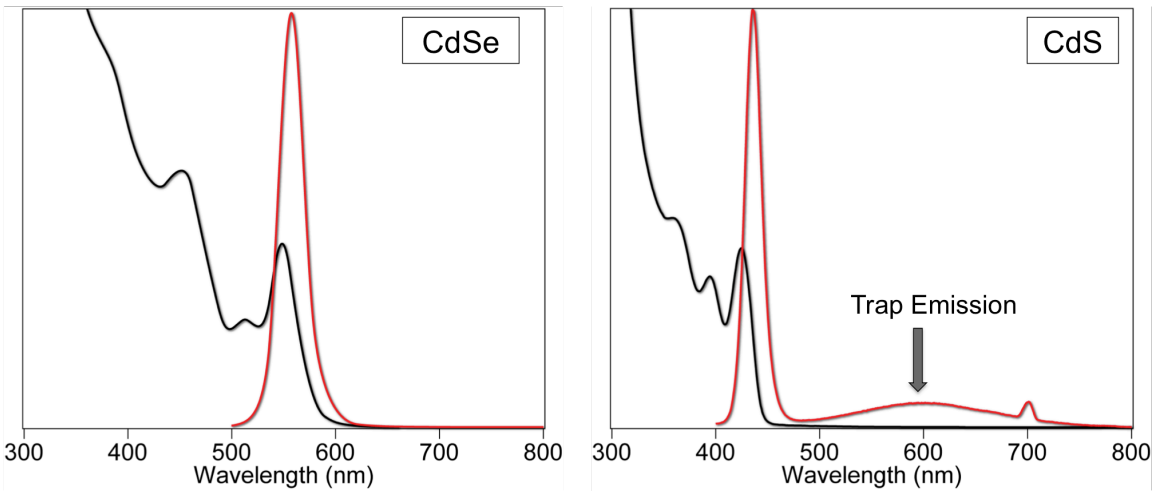

Figure 4.1: Absorption (black) and emission (red) spectra for CdSe (left) and CdS (right) QDs.

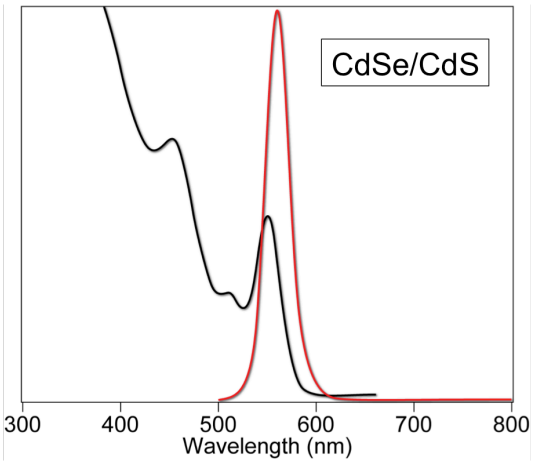

Figure 4.2: Absorption (black) and emission (red) for core/shell CdSe/CdS QDs. Note that trap emission is absent.

exciton emission that is blue-shifted compared to the CdSe exciton emission peak. The second narrow peak at 700 nm is caused by scattered excitation light and is not part of the QD emission spectrum. CdS also has an additional broad peak at longer wavelengths attributed to trap emission. The trap emission is believed to arise from either the electron or hole trapped on the surface.

4.1.1. Nature of Emitting Trap State

When CdS is used as a shell on CdSe QDs, the trap emission peak disappears as

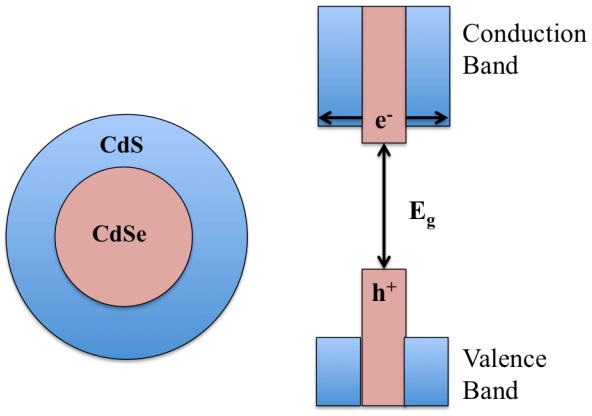

Figure 4.3: Schematic showing core/shell QD (left) and its band structure (right).

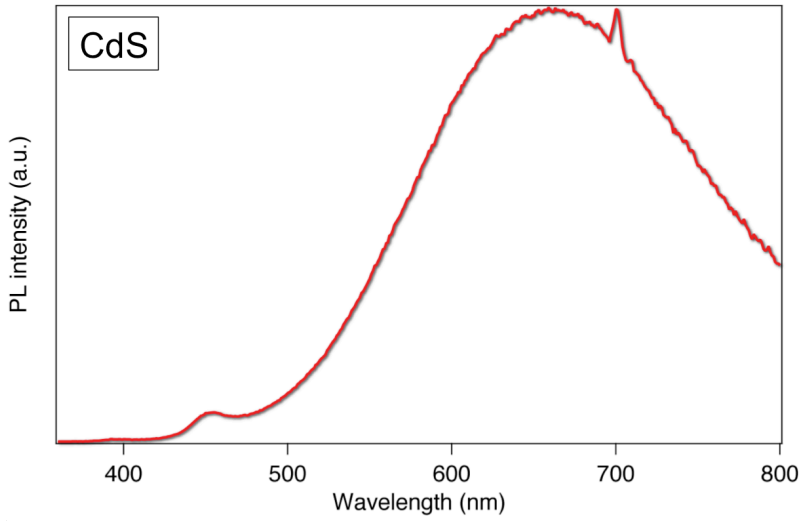

Figure 4.4: CdS emission spectrum for QDs synthesized with excess sulfur. The increase in trap emission is caused by more holes becoming trapped on the QD surface.

shown in Figure 4.2. CdSe/CdS QDs are a type I system, shown schematically in Figure 4.3, where the conduction band offset between the CdSe and CdS is minimal, and the electron is delocalized through both the core and shell. However, the valence band offset is much larger. The CdSe valence band is lower in energy for the hole compared to the CdS valence band, and therefore the hole is energetically confined to the core. Because the hole is confined to the core in CdSe/CdS QDs, it cannot reach the surface and cause trap emission. We also know that the holes are trapped on surface sulfur atoms because when we increase the amount of sulfur on the QD surface, we see an increase in trap emission as shown in Figure 4.4.

4.1.2. Comparing Trap Energetics for CdS and CdSe QDs

Trap emission does occur in CdSe, but only for small sizes. To understand why, we first must look at the relationship between size and the ET parameters, $\Delta G°$ and λ. The free energy curves generated using the procedure discussed in Section 2.3.4 for the exciton and trap state for two different sizes of CdS are shown in Figure 4.5.

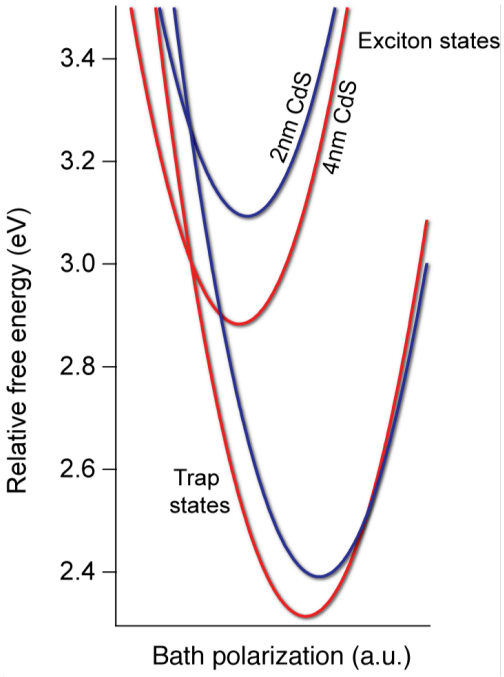

Figure 4.5: Free energy curves for 2 nm CdS (blue) and 4 nm CdS (red). Both the exciton and trap free energy curves are shown for each CdS QD size.

As the size of CdS increases, the exciton free energy curve shifts to lower energy, but the trap free energy curve shows little change. The reorganization energy also shows little change, so changing the QD size mainly impacts $\Delta G°$. Because $\Delta G°$ is much greater than λ, both sizes of CdS are in the inverted region, and electron transfer rates are expected to slow as $-\Delta G°$ increases. However, ET from the exciton state to the trap state is still possible in the inverted region through quantum mechanically tunneling invoking a high frequency vibrational mode within the trap state.

However, CdSe exists in all three regions of ET depending on its size. The free energy curves for small CdSe compared to CdS are shown in Figure 4.6. As Figure 4.6 shows, small CdSe is in the barrierless region so ET can readily occur. When the CdSe QD size increases, the exciton free energy curve shifts to lower energy while the trap free energy surface remains the same. Eventually, CdSe will transition from the barrierless

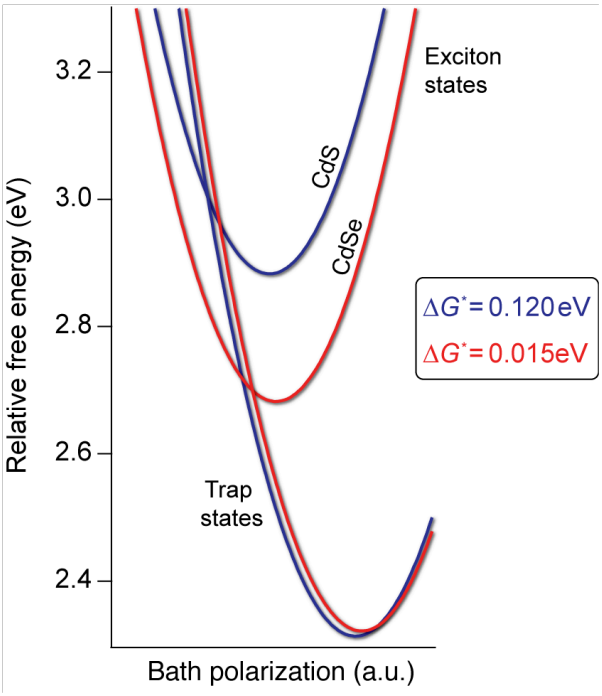

Figure 4.6: Free energy curves for CdS (blue) and CdSe (red). ΔG* refers to the activation barrier for ET from the exciton state to the trap state. CdS is in the inverted region, while CdSe is in the barrierless region.

region to the normal region. The normal region is characterized by an activation barrier, making ET to the trap state less probable. Tunneling to the trap state is also unlikely because the displacement between the exciton and trap state is quite large. Because CdSe transitions from the barrierless region to the normal region as the QD size increases, large CdSe QDs do not exhibit trap emission.

4.1.3. Concluding Remarks

We have determined that CdS QDs, regardless of size, exhibit trap emission because trapping occurs in the inverted region of ET, which is characterized by small reorganization energies. CdSe only manifests trap emission for small sizes because the system transitions from the inverted region to the normal region as the size increases. The normal region is characterized by an activation barrier, preventing trap emission. We also

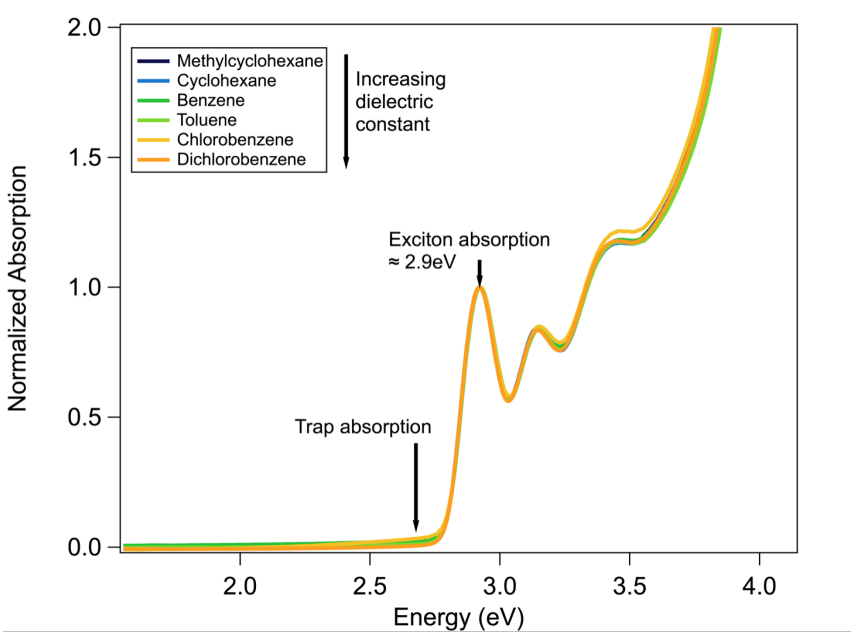

Figure 4.7: CdS UV-Vis absorption spectra in various organic solvents.

have determined that trapped holes cause trap emission by using core/shell structures to confine one charge carrier to the core. Furthermore, we have concluded that holes are primarily trapped on sulfur atoms because of the increase in trap emission when excess sulfur is on the surface.

4.2. Solvent Effects on Trap State Energetics

4.2.1. Absorption Spectra

The UV-Vis spectrum of CdS QDs dispersed in various solvents is shown in Figure 4.7. Each absorption spectrum has been normalized to the intensity of the first exciton peak to make comparisons between the samples easier. All samples clearly show a well-defined exciton peak at approximately 2.9 eV. The peaks at approximately 3.1 eV and 3.4 eV correspond to higher energy exciton states.

It is clear that the solvents do not affect the absorption energy of the exciton state. This is expected because the exciton is formed within the QD core, and therefore has

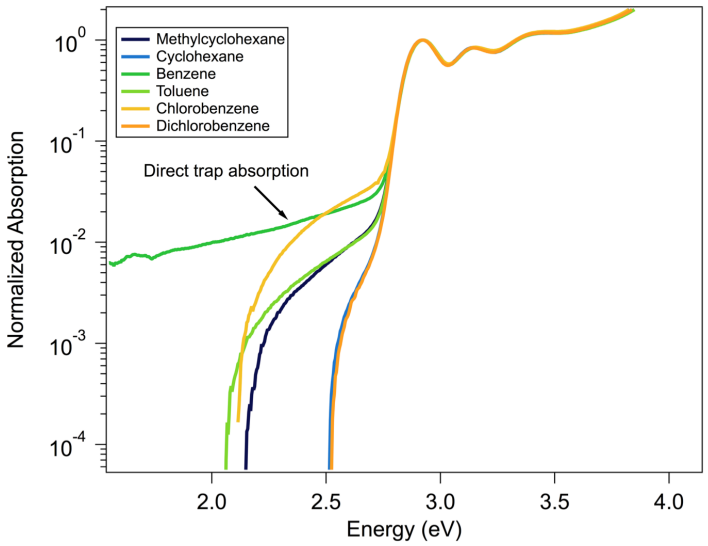

Figure 4.8: Same spectrum as Figure 4.7 plotted on a log scale to make the trap absorption more visible.

little interaction with the solvent. The absorption spectrum also shows a broad low energy peak, which is caused by direct absorption into trap states, which is more clearly seen when plotted on a log scale as in Figure 4.8. It is believed that trap states form near the band-edges and within the band-gap of the QD. Therefore, transitions involving these states would occur at lower energies. Additionally, the trap state absorption is less intense than the exciton, indicating the oscillator strength for this transition is quite small. Since direct trap state absorption is a small fraction of the overall absorption, it is difficult to draw conclusions about how solvent affects this absorption.

4.2.2. Emission Spectra

The emission spectra of CdS QDs are shown in Figure 4.9. The narrow peak at approximately 2.8 eV is caused by exciton radiative recombination, and the broad peak at approximately 1.9eV is caused by trap radiative recombination. The emission spectra in Figure 4.9 have been normalized to the intensity of the exciton emission in a similar manner as the absorption spectra shown in Figure 4.7. As in the case of absorption, the

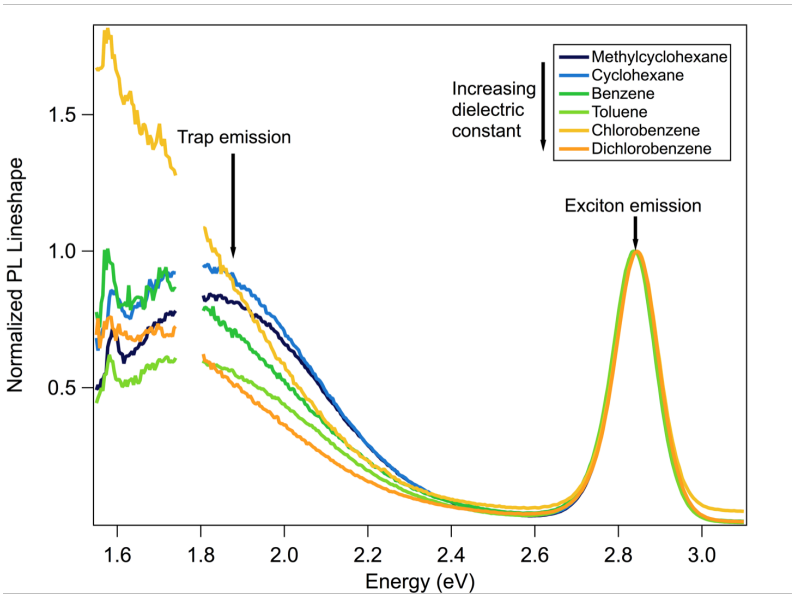

Figure 4.9: CdS PL lineshape spectra in various organic solvents.

exciton emission energy remains unaffected by the solvent because exciton states are formed within the QD core, and they remain in the core when they radiatively recombine.

However, the trap emission is greatly affected by the solvent. The gap in the data at approximately 1.8 eV is caused by scatter from the excitation light. This peak has been removed because it is an artifact from the instrument, and it makes it easier to see the trap emission more clearly. Solvent effects on trap emission are expected because it is believed that trap emission is caused by the hole migrating from the core onto the QD surface where it is localized in an energetically deep trap. Since the hole is located on the surface, it is strongly influenced by the local environment.

The trap emission peak appears to be correlated to the solvent dielectric constant. The dielectric constant refers to the solvent's polarity, and a high dielectric constant indicates a more polar solvent. As the dielectric constant increases, the trap emission peak red-shifts, or shifts to lower energy, in a non-linear fashion as observed in Figure 4.10. As mentioned previously, trap states are formed from a hole trapped on the surface,

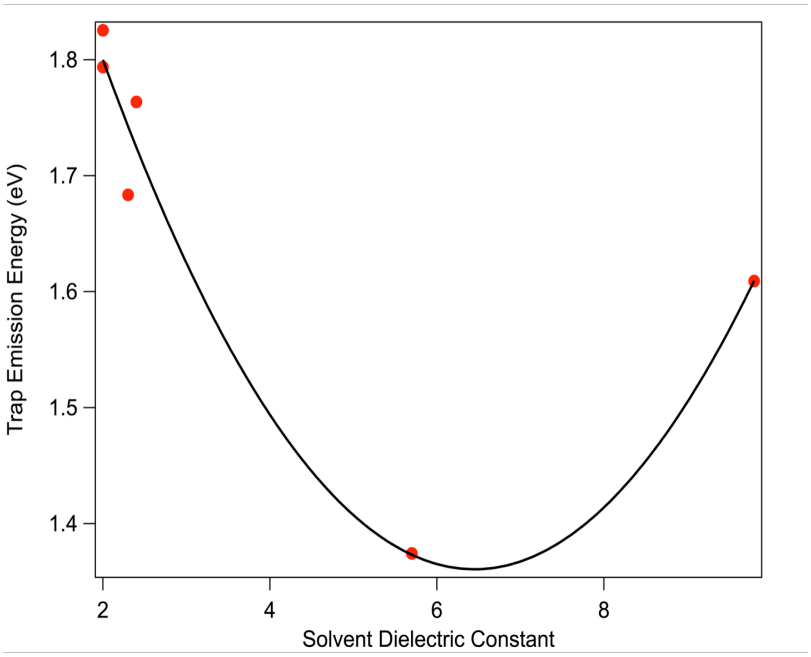

Figure 4.10: CdS trap emission energy for varying solvent dielectric constants. Peak energies were extracted from the emission spectra shown in Figure 4.9.

and hence the surface state is not charge neutral. Therefore, more polar solvents will stabilize this state and lower its energy. As a consequence, the trap emission red-shifts. We observe this trend for all solvents but dichlorobenzene. Dichlorobenzene caused the trap emission to blue-shift compared to the second most polarizable solvent, chlorobenzene, and the reason for the blue-shift is unknown.

4.2.3. Concluding Remarks

The changes in CdS emission observed with various solvents have allowed us to identify the state's location within the QD. Because the solvent did not affect the exciton, we assign this state to the QD core. In contrast, the solvent greatly affected the trap emission, so we assign this state to the QD surface where interactions with the local environment are more likely to occur.

4.3. Exciton and Trap PLE

Representative PLE spectra for the exciton and trap emission are shown in Figure 4.11. The exciton and trap PLE were recorded at the maximum emission wavelength for each state. Each spectrum was normalized to the intensity of the first exciton peak following the procedure from Tonti et al.[74] Both the exciton and trap PLEs have similar features at energies greater than 2.8 eV. These features resemble those found in the absorption spectrum, and represent exciton absorption as well as absorption into higher energy states. The shoulder on the exciton absorption peak in the exciton PLE is caused by the wavelength being the same as the emission wavelength at which the spectrum was recorded. This does not happen in the trap PLE because it was recorded at 600 nm and the excitation spectrum was collected from 300 to 595 nm.

At lower energies, the exciton and trap PLE begin to deviate. The exciton PLE shows very little emission for excitation energies below 2.6 eV. The exciton state is

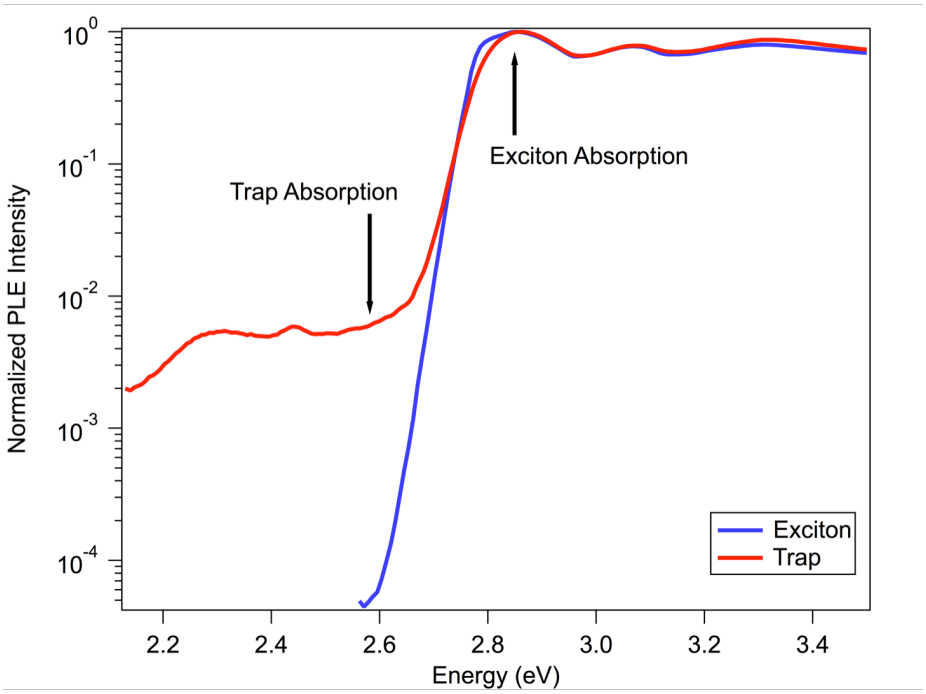

Figure 4.11: Representative PLE spectra for exciton (blue) and trap (red) states.

expected to have less absorption, and hence less emission below 2.9 eV because the band-gap is approximately 2.9 eV. In order for absorption to occur, the exciting light must have energy equal or greater than the band-gap. Some emission is possible with excitation less than 2.9 eV because the QD sample contains a size distribution of absorbing and emitting QDs. Larger QDs will have band-gaps smaller than 2.9 eV, and therefore would be excited at energies less than 2.9 eV. However, large QDs are only a small subset of the QD population, and their contribution to the overall absorption and emission is minimal.

Before discussing the trap PLE spectrum, we first must understand the possible

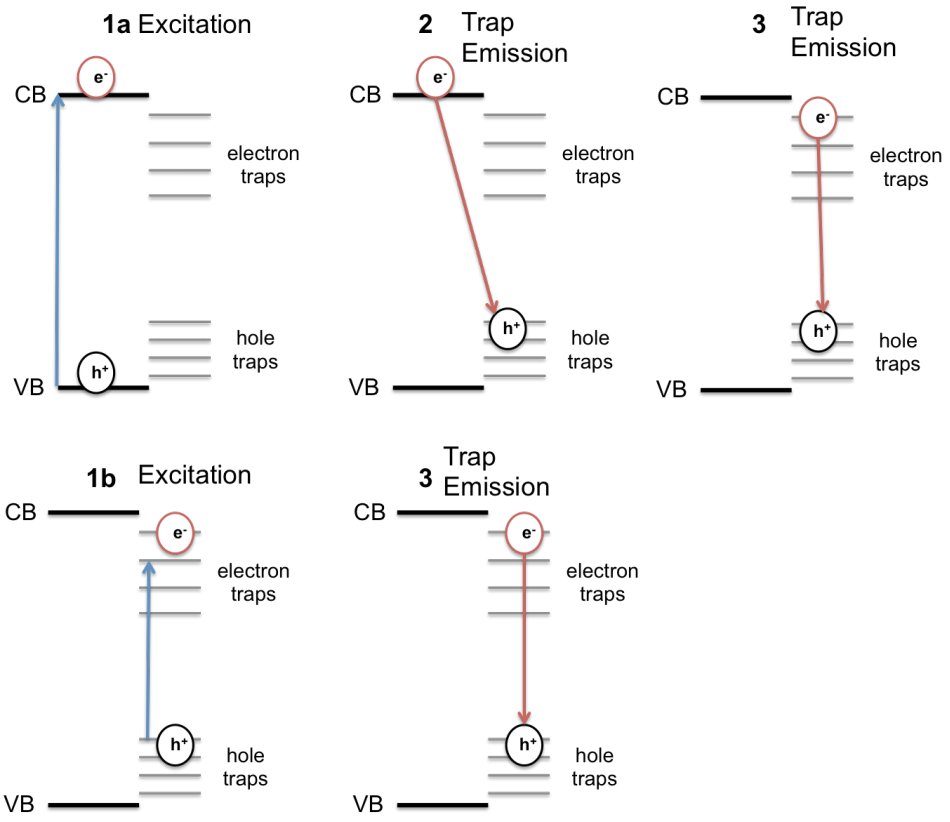

Figure 4.12: Schematic for different ways trap states are formed. Pathway 1a is excitation equal to the QD bandgap, and pathway 1b is excitation below the QD bandgap. Trap emission then occurs from either pathway 2 or pathway 3 for excitation 1a. In contrast, trap emission can only occur from pathway 3 for below bandgap excitations.

ways in which trap states are formed. The mechanism by which trap states are populated depends on the excitation energy. Because trap states are believed to exist within the QD bandgap, they can be formed through either direct or indirect means. Excitation energies above the bandgap would primarily form traps through indirect means, while excitation energies below the QD bandgap form trap states directly. This is shown schematically in Figure 4.12 (top) for excitation energies above the QD bandgap and Figure 4.12(bottom) for excitation energies less than the QD bandgap.

Above bandgap excitations first produces an exciton (1a), which then populates the trap state through two possible ways. In the first mechanism (pathway 2), a hole relaxes into a trap state and the electron remains delocalized. Another possible mechanism is that both the electron and hole relax into traps after an exciton is produced (pathway 3). In pathway 2, trap emission arises from a hole radiatively recombining with a delocalized electron. In pathway 3, trap emission comes from both carriers trapped. Pathway 3 would result in trap emission that is red-shifted compared to pathway 2, and the amount of red-shift depends on the depth of the traps. If the excitation energy is less than the QD bandgap, then only pathway 3 (both carriers trapped) for trap emission is possible.

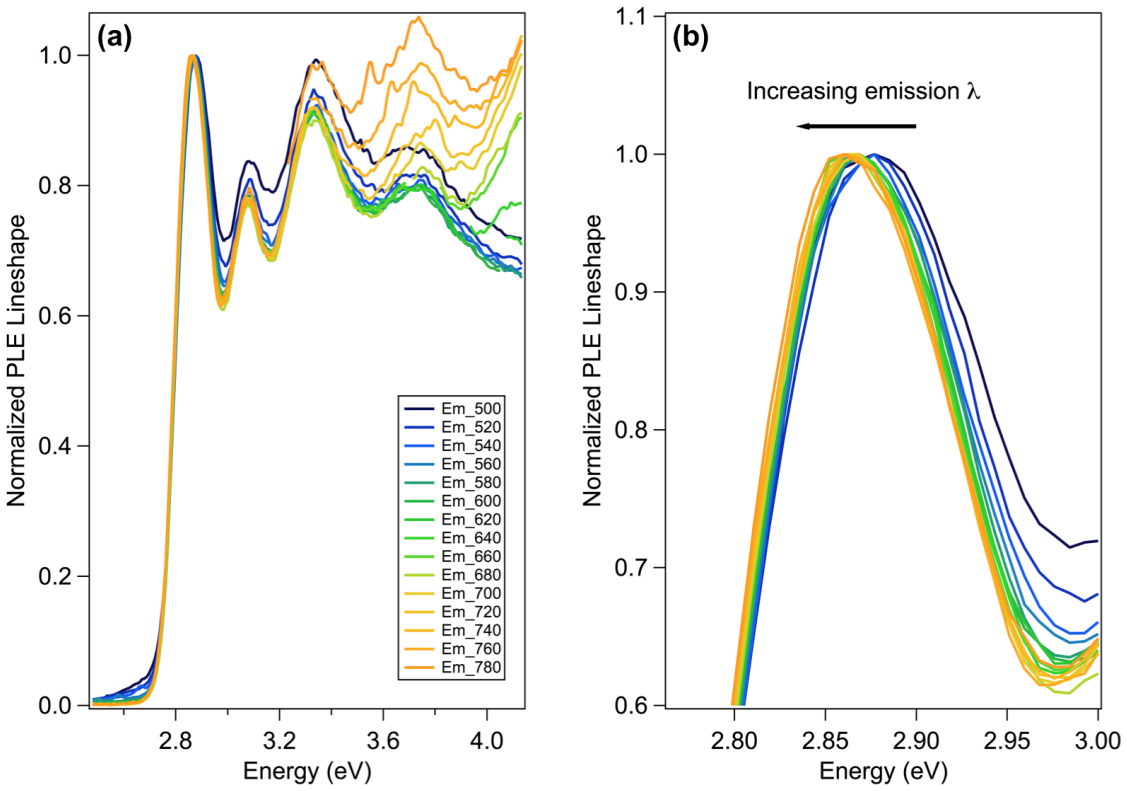

Figure 4.13: Trap PLE collected at different emission wavelengths (a). The first exciton absorption peak redshifts as the trap emission wavelength increases (b).

The trap PLE spectrum in Figure 4.11 looks remarkably similar to the exciton PLE spectrum for excitation energies above 2.6 eV, which is expected because the exciton is influencing the trap state. However, the trap state has an appreciable amount of absorption and hence emission for excitation energies below 2.6 eV in contrast to the exciton state.. For excitation energies below 2.6 eV, it is more likely that trap states are directly excited (pathway 1b) because the excitation energy is approximately 300 meV less than the QD bandgap.

Another interesting observation in the trap PLE is that the exciton absorption peak energy depends on the emission wavelength at which it was recorded. A series of trap PLEs were recorded using emission wavelengths from 500 nm to 780 nm in 20 nm

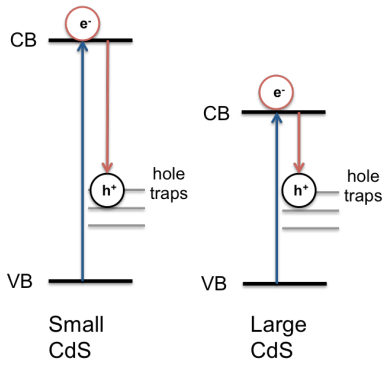

Figure 4.14: Schematic showing how large QDs may exhibit trap emission at longer wavelengths. CB and VB refer to the conduction and valence band respectively. The upwards blue arrow represents absorption into the exciton state, and the downwards red arrow represents emission from the trap state.

intervals, and the results are presented in Figure 4.13(a). Figure 4.13(b) shows the exciton absorption peak red-shifts as the emission wavelength becomes longer. This shift could be caused by the inhomogeneous size distribution as shown schematically in Figure 4.14.

We believe that trap emission is primarily caused by a trapped hole radiatively recombining with an electron located in the conduction band. The hole is assumed to be trapped on the QD surface with an energy within the QD bandgap. As the QD becomes larger, the conduction band lowers in energy, causing a red-shift in the exciton absorption energy. Since the conduction band is now closer in energy to the hole trap state, the trap emission now occurs at longer wavelengths.

The trap state absorption also changes with emission wavelength in addition to a red-shift of the exciton absorption peak. We observe a decrease in the trap absorption regardless of excitation as the emission wavelength lengthens from 500 nm to 640 nm. In contrast, emission wavelengths longer than 640 nm begin to show an increase in trap absorption for excitation energies greater than 3.6 eV. If longer emission wavelengths represent larger QDs, then larger QDs exhibit more trap emission when excited with 3.6 eV or greater excitation energy compared to smaller QDs.

This can be rationalized if we consider how the trap states are populated. In Section 0, I discuss the possibility of a non-emissive trap state that acts as an intermediate state during the charge transfer from the exciton to the deep trap, and this non-emissive state is necessary for ET from the exciton to the deep trap. We theorized that the intermediate state is associated with surface ligands. Further evidence of surface ligands playing a role in trapping dynamics comes from Hoy et al reported who reported that high excitation energies generate charge carriers that are more likely to transfer to ligand states rather than relax to the band-edge.[70] Large QDs have a large surface area, and therefore would have more ligands bound to the surface than smaller QDs. This increases the availability of non-emissive intermediate trap states that are accessible with higher excitation energies. If larger QDs have more non-emissive intermediate trap states, then they would exhibit more absorption and emission at higher excitation energies compared to smaller QDs.

4.4. Spectroscopic Characterization of CdS QDs

Three CdS QD samples of varying sizes were synthesized and redispersed into glass forming solvent. The absorbance and PL line shape for each sample are shown in Figure 4.15. The line shape spectra were fit with a series of Gaussian peaks to determine the exciton absorption and emission energies as well as the trap absorption and emission energies. Only the fitted trap absorption and emission peaks have been included in Figure 4.15. The sizes for each sample are listed in Table 4.1 and were calculated from the first exciton absorption peak following the procedure of Yu et al.[65] Table 4.1 also includes the quantum yields calculated by using rhodamine 6G in ethanol as the standard. The trap

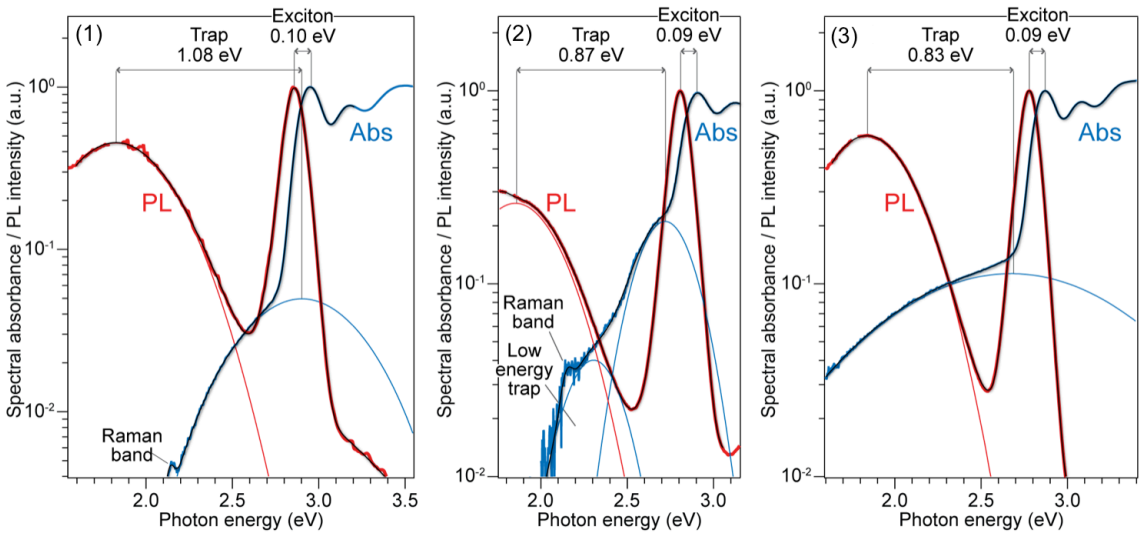

Figure 4.15: Absorption and emission lineshape spectra for three different sized CdS QDs. The numbers listed for the trap and exciton are the Stokes shift for each state.

Table 4.1: Size and quantum yields calculated for the three CdS samples shown in Figure 4.15

Sample	Diameter	Exciton Quantum Yield	Trap Quantum Yield
1	4.0 nm	5.8%	3.6%
2	4.4 nm	10%	4.6%
3	4.5 nm	9.4%	6.8%

absorption is fit with a single peak for samples 1 and 3 indicating one type of trap state. On the other hand, sample 2 required two Gaussian peaks to accurately fit the absorption.

We believe the two Gaussian peaks represent two distinct trap states. The trap emission for all three samples is also well represented with by a single Gaussian peak implying that the absorbing trap state is also the emitting trap state, except in the case of sample II. Sample II may have a second emitting trap state with an energy less than 1.8 eV that is not visible on the recorded PL spectrum. The PL spectra were recorded using a visible light detector that quickly loses efficiency beyond 800 nm. In order to see if a

second trap peak is present, the emission spectra would need to be recorded using a near-IR detector. Figure 4.15 also shows the Stokes shift for the exciton and trap state. The exciton Stokes shift is consistent for all three samples. However, the trap Stokes shift varies considerably across the samples, and decreases as the QD size increases.

4.4.1. Quantum Yield Spectra

The normalized exciton PLE and absorption spectrum are shown in Figure 4.16, and we observe an excitation-dependent QY because the exciton PLE does not match the absorption spectrum. The deviation of the exciton PLE from the absorption spectrum indicates that not all absorbed photons were emitted. This deviation is not constant, especially at higher excitation energies. This means that a smaller fraction of charge carriers generated at higher excitation energies are relaxing to the band-edge for radiative

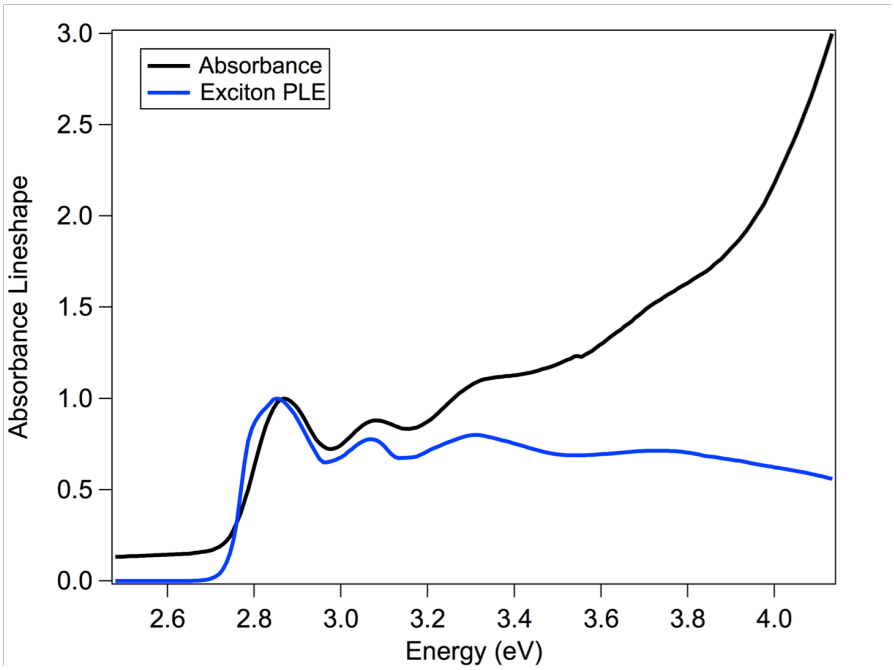

Figure 4.16: Exciton PLE (blue) and absorption spectra (black) for CdS QDs. The low energy shoulder on the exciton PLE is caused by scatter from the excitation light.

recombination, and there is an increase in the proportion of non-radiative relaxation at higher excitation energies.

QY spectra have been shown for InP QDs[72,73] as well as CdSe QDs[70,71]. Two varying mechanisms have been used to explain the excitation-dependence of the QY. The first mechanism relies on the activation of new non-radiative pathways at higher excitation energies. However, femtosecond transient absorption spectroscopy showed no excitation dependence of carriers relaxing to the band-edge.[54,72] Therefore, a second mechanism was developed based on the inhomogeneity of the sample, where smaller QDs are more likely to be non-emissive due to trapping and do not contribute to the PLE at higher excitation energies.[72] Other studies on CdS have found no evidence for a QY spectrum, and state that it may be a sample-dependent phenomenon[54] or a result of scattering caused by aggregates of QDs and other organic molecules that may be present in solution.[74]

The relative QY spectra for all three figures are shown in Figure 4.17. All 3 samples show a changing QY at high excitation energies. If the exciton were responsible for populating the trap state, then changes in the exciton QY would also affect the trap QY at excitation energies above the bandgap. For excitation energies below the bandgap, the relative QY decreases by more than an order of magnitude for all three samples, and then it remains constant below 2.7 eV for samples 1 and 3. In contrast, sample 2 shows a decrease in the relative QY for energies below 2.5 eV.

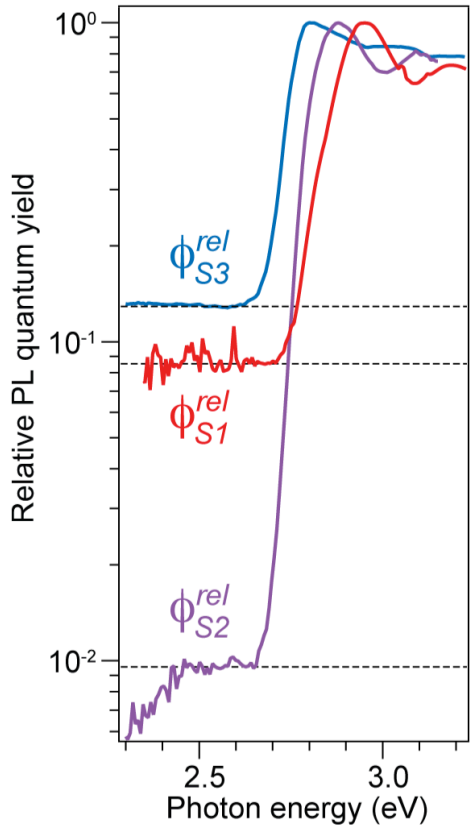

Figure 4.17: Relative QY spectra for three CdS samples shown in Figure 4.15

The sharp decrease in the relative QY is a result of two different types of trap states formed through two different mechanisms as shown in Figure 4.18. Pathway A shows exciton recombination. Trap emission can occur through either pathway B or pathway C. In pathway B, trap emission arises from a trapped hole and bandgap electron, and in pathway C, trap emission occurs from both carriers trapped. When a QD is excited above the bandgap, an exciton is generated (pathway A), and then the hole becomes trapped, leading to trap emission from pathway B. Above bandgap excitation also produces a small fraction of trap emission through pathway C because the electron may also relax into a trap state in addition to the hole. Since the relative QY for pathway B depends on the efficiency at which the exciton is created and then the hole becoming

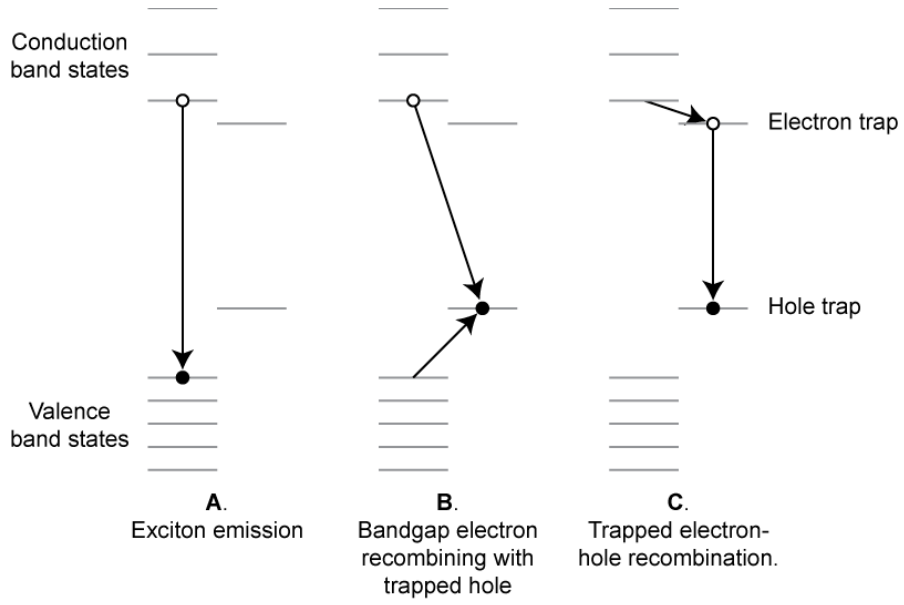

Figure 4.18: Schematic showing the possible recombination pathways (B and C) for trap emission. Pathway A shows exciton recombination.

trapped, we expect pathway B to have a higher relative QY then pathway C because excitation energies greater than 2.8 eV easily produce excitons.

In contrast, excitation energies below 2.8 eV only produce trap emission from pathway C. We propose that pathway C is fast, primarily due to non-radiative recombination, and as a result the relative QY for pathway C is much less compared to pathway B. Furthermore, the relative QY for pathway C remains constant, at least for samples 1 and 3, indicating the excited trap states relax into the emitting trap state with equal efficiency. Sample 2 on the other hand has a changing relative QY for excitation energies below 2.5 eV. This may mean that a second type of trap state is excited, one that does not relax to the emitting state with the same efficiency as the states formed with excitation energies between 2.5 eV and 2.8 eV. A second Gaussian peak was needed to fit the absorption spectrum for sample 2 as shown in Figure 4.15. The changing QY could be related to this peak because the energies for the Gaussian peak and where the QY is changing are similar.

Table 4.2: ET parameters calculated from the multi-peak fits from the absorption and emission lineshape spectra for samples shown in Figure 4.15

Sample	$\Delta G°_{CT}$	λ_{CT}	ΔG^*	Region
1	-698 meV	206 meV	294 meV	inverted
2	-570 meV	194 meV	182 meV	inverted
3	-379 meV	172 meV	62 meV	inverted

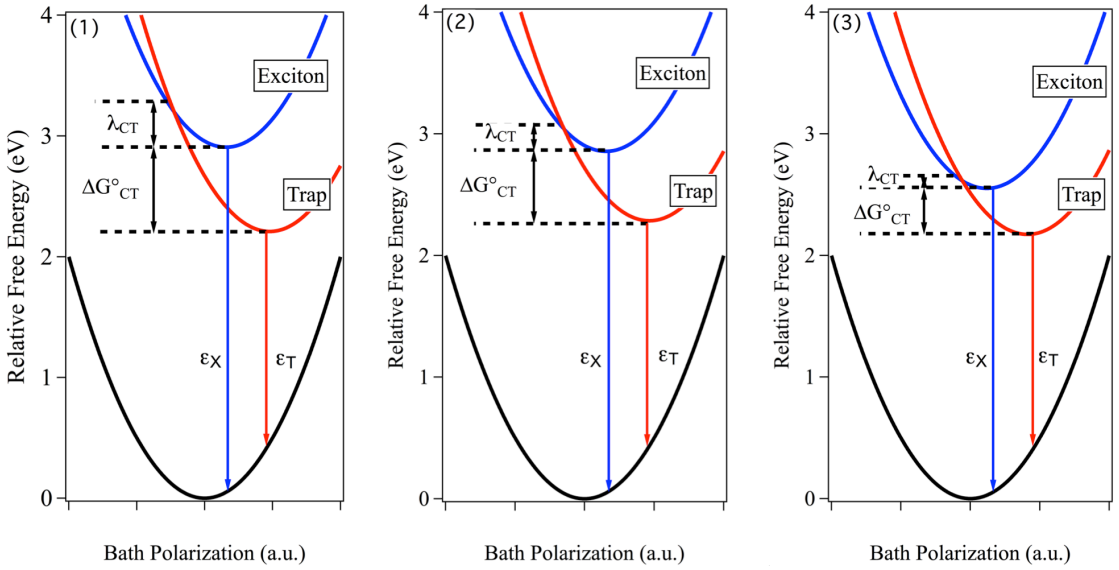

Figure 4.19: Free energy curves constructed using ET parameters in Table 4.2. ε_X and ε_T is the trap emission. λ_{CT} is the reorganization energy for charge transfer, and $\Delta G°$ is the change in free energy for the charge transfer.

4.4.2. ET Parameters for CdS Samples 1, 2, and 3

The classical ET parameters, $\Delta G°_{CT}$, λ_{CT}, and ΔG^* were calculated from the multi-peak fits of the absorption and emission line shape spectra following the procedure outlined in Section 1.3.1, and are listed in Table 4.2. These values are used to generate the free energy curves for the exciton and trap state relative to the ground state for all three samples. The free energy surfaces are plotted in Figure 4.19. Table 4.2 shows that both $\Delta G°_{CT}$ and λ_{CT} decrease as the size of the QD increases. However, the change in $\Delta G°_{CT}$ is more dramatic. In all three samples ET occurs in the inverted region because

$\Delta G°_{CT} > \lambda_{CT}$, and rates are expected to be slow. It also appears the CdS may enter the barrierless region as the size increases because the activation barrier for ET, ΔG^*, is decreasing. Because $\Delta G°_{CT}$ is changing at a much faster rate than λ_{CT}, it is possible that $\Delta G°_{CT}$ will equal λ_{CT} and ET will occur more quickly. If this were true, then larger QDs would exhibit more trap emission than smaller QDs.

As Figure 4.19 shows, each sample is in the inverted region, and an activation barrier exists for ET. Because the activation barrier is larger than room temperature thermal fluctuations (see Table 4.2), ET from the exciton state to the emissive trap state is unlikely to occur in a classical manner. Other possible mechanisms are shown in Figure 4.20. Figure 4.20(a) represents a semi-classical ET process wherein ET occurs from the exciton to a higher excited vibrational state of the trap. This vibrational state is the high frequency vibrational quantum mode used in Marcus-Jortner semi-classical ET theory described in more detail in Section 1.4. The higher excited vibrational state has the same reorganization energy as the emissive trap state, but $-\Delta G°_{CT}$ is smaller. Since $-\Delta G°_{CT}$ is approaching λ_{CT} the system is near the barrierless region and ET from the exciton to the

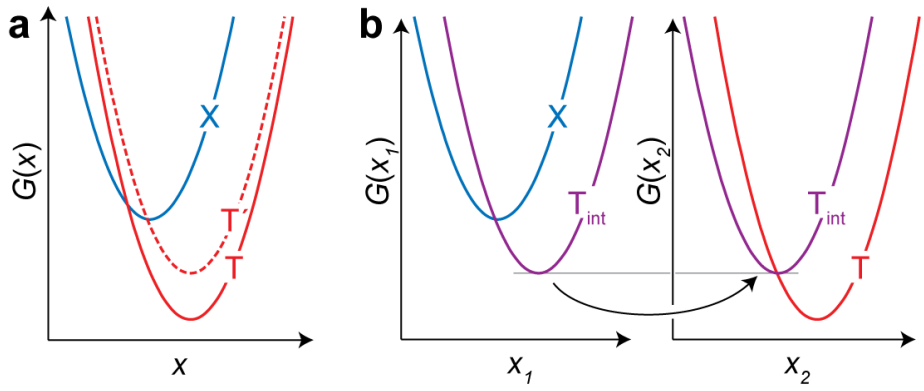

Figure 4.20: Possible mechanisms for ET in the inverted region. X refers to the exciton state and T corresponds to the trap state. ET can either occur through tunneling to an excited vibrational state in the trap (a) or through an intermediate non-emissive state (b).

higher excited vibrational trap state occurs rapidly. Once the ET occurs, the charge immediately relaxes into the lowest excited vibrational state, which is where emission occurs.

A second mechanism shown in Figure x (b) involves an intermediate non-emissive state such as a trap state associated with a ligand. ET occurs more readily from the exciton state because it is in the barrierless region. Then a second ET reaction occurs from the non-emissive trap state to the emissive trap state. The second ET is plotted on a second reaction coordinate because it requires a second set of nuclear coordinates. The $\Delta G°_{CT}$ and λ_{CT} for the second ET must also be equivalent to ensure that ET from the non-emissive trap state to the emissive trap state out competes non-radiative recombination.

4.5. Comparing Temperature-dependent Exciton and Trap TRPL

Temperature-dependent TRPL is an excellent tool for measuring the excited state dynamics of the exciton and trap state because we propose that the exciton populates the trap state through an ET mechanism, and according to the classical Marcus equation (see Section 1.4), ET rates are temperature-dependent. When we control the temperature, we alter the electron transfer rates in a predictable manner. We then analyze each state's temperature-dependent TRPL and construct kinetic schemes based on classical ET theory to reproduce the observed behavior. From these kinetic schemes, we can determine the electron transfer rates.

Exciton and trap PL decays were recorded for a series of temperatures ranging from 80 K to 305 K. The decays for one sample are shown in Figure 4.21. At each temperature, both exciton and trap decays are multi-exponential, indicating a distribution of relaxation processes are occurring. These PL decays are consistent with previous

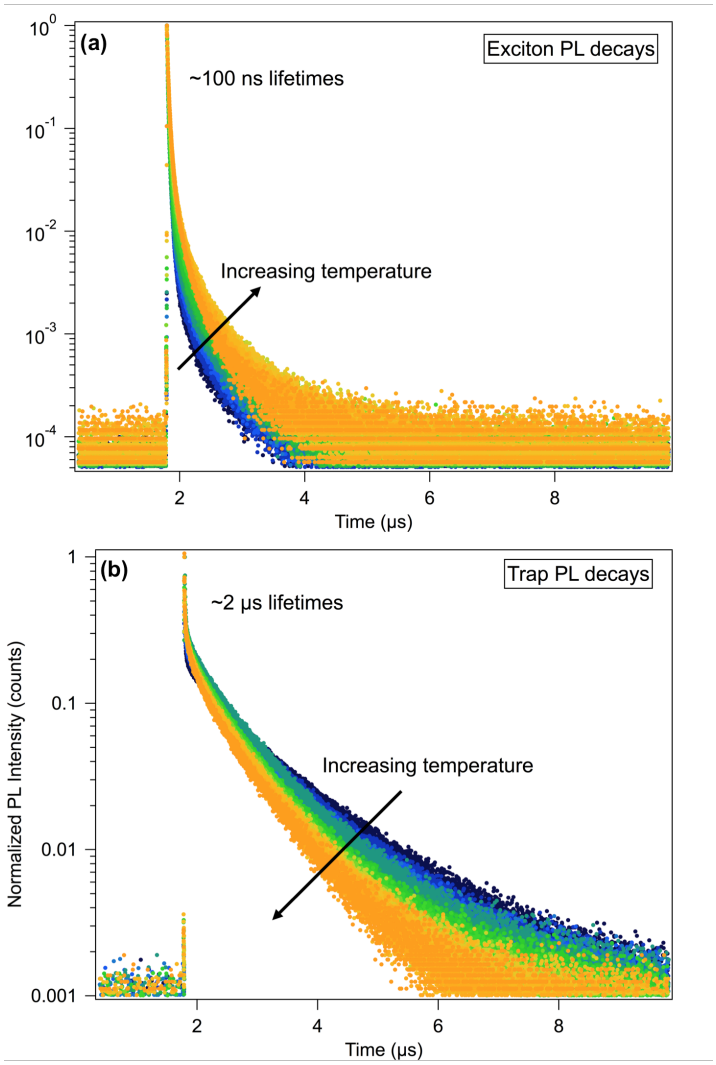

Figure 4.21: Representative PL decays at various temperatures for the exciton state (a) and trap state (b). Each PL decay was recorded using a 10 μs TAC.

studies on CdS colloids.[52,58,59,63,67,84-90] Exciton PL decays are much shorter (~ns) compared to trap PL decays (~μs). Trap decays are expected to be longer because at least one of the charge carriers is localized on the surface resulting in reduced overlap of the electron and hole wavefunctions and decreasing the probability of radiative recombination.

As we have shown earlier, hole traps contribute to the deep trap emission, but whether the electron is also trapped is still under debate. Chestnoy et al proposed the first

model of trap emission in CdS QDs,[67] and suggested that trap emission is caused by a shallowly trapped electron tunneling to radiatively recombine with a deeply trapped hole. The multi-exponential trap PL decays are therefore a result of varying tunneling distances between the trapped carriers. The authors further speculated that a sulfur vacancy or Cd^{2+} edge atom acts as the electron trap, while a cadmium vacancy or S^{2-} acts as a hole trap. Eychmuller et al confirmed this model using CdS QDs that exhibited both exciton and trap emission.[58] The first CdS QDs synthesized by Chestnoy et al only had trap emission. In addition to explaining trap emission, Eychmuller et al proposed that exciton emission is actually a delayed PL. They argue that the electron trapping rates are on the order of picoseconds, which outcompetes radiative recombination. In order for exciton emission to occur, the electron must first be released from the trap state. This also implies that electron traps must be shallow since exciton emission is occurring.

Even though CdS trapping dynamics have been studied since the late 1980's, there is still much debate on trapping rates. Trapping rates have been measured using time resolved PL methods such as transient absorption and fluorescence up-conversion because these techniques provide high resolution on the femtosecond and picosecond time regimes. It is generally believed that hole trapping occurs before electron trapping. Studies have shown that hole trapping occurs on the order of picoseconds,[87,91] and the hole trap state is long lived.[92]

On the other hand, a range of electron trapping times has been reported and differences are primarily due to the nature of the electron traps. Zhang et al showed that traps at the band edge formed in less than 100 fs, and that these traps decayed primarily through electron-hole recombination within 10 ps.[5,93,94] O'Neil et al showed that the rise

time for trap states near the band edge formed in less 10 ps and that deeper traps formed with times greater than 30 ps. They also noted that the rise times for the deeper traps were longer than expected, and suggested that the deep emissive traps were not directly populated from the exciton state.[79] Logunov et al also investigated different electron trap depths and showed that shallow electron traps were formed within hundreds of femtoseconds while deeper traps were formed after 30 ps. More recent work on CdS synthesized in polymer solutions showed that the trap states were populated within 500 fs, and the higher energy trap states rapidly decayed into the lower energy trap states.[60,61]

The shape of the PL decays also differs between the exciton and trap state. The exciton state is dominated by a fast component with the emission intensity dropping by three orders of magnitude within a few hundred ns. The exciton also has a small tail or long component at longer times because the decay does not reach the baseline until after one μs. The trap also has a fast component at early times that accounts for one order of magnitude loss in emission intensity, but this fast component is much shorter compared to the short component in the exciton PL decay. The remaining portion of the trap PL decay is quite long, and in some cases has not fully reached the baseline after 10 μs.

The sharp separation between the short and long components of the trap state PL decay suggests there is two different trap states close in energy with vastly different recombination dynamics. One trap state decays quickly, and the other trap state decays more slowly. Based on the excitation-dependent TRPL discussed later, we tentatively assign the fast component to recombination between a trapped hole and a shallowly trapped electron that are spatially correlated. The long component is assigned to radiative recombination of the trapped hole with a delocalized electron. Finally, the baseline or

background counts are higher for the trap PL decays compared to the exciton PL decays. As shown previously in the steady state spectra, the exciton emission is more intense compared to the trap emission. Therefore, we would expect the exciton to have a higher photon count rate compared to the trap state.

The exciton and trap PL decays also differ in how they change with temperature. The exciton PL decays lengthen as the temperature increases while trap PL decays become shorter as temperature increases. This is discussed in more detail in Section 4.5.1.

4.5.1. Temperature-dependent Exciton and Trap Average PL Lifetimes

These trends become more apparent when looking at the average PL lifetime, or the average time it takes to emit a photon. We fitted each PL decay using a multi-exponential decay function following the procedure discussed in Section 2.4.4. The multi-exponential decay function was then integrated from zero to infinity to calculate the average PL lifetime.

The average exciton and trap PL lifetimes, $\langle\tau\rangle$, for each sample studied are shown in Figure 4.22. The exciton average lifetimes are much shorter than the trap average lifetimes as expected because the exciton PL decays are much shorter. In all samples, the exciton lifetime ($\langle\tau\rangle$) lengthens as the temperature is increased to approximately 200 K. At temperatures greater than 200 K, the exciton $\langle\tau\rangle$ decreases. The temperature at which $\langle\tau\rangle$ begins to decrease is different for each sample and does not appear to be related to the QD size. Additionally, sample 2 shows a much larger increase in $\langle\tau\rangle$ with temperature compared to sample 1 and 3.

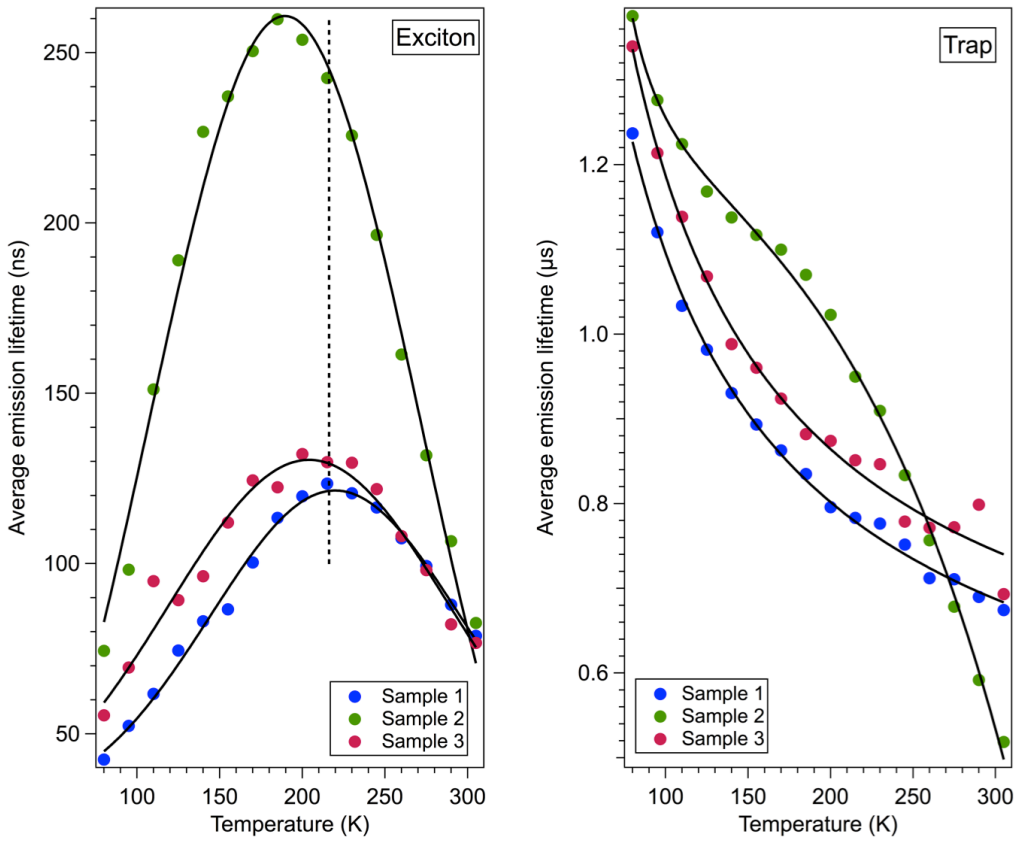

Figure 4.22: Average emission lifetimes for the exciton (left) and trap state (right) in three different CdS samples. The solid black lines are trend lines fitted to the data. For the exciton emission lifetimes, each sample was fitted with a Gaussian function. The trap emission lifetimes were fitted with a power law, except for sample 2, which was fitted with a truncated power law. The dashed line for the exciton state is to show that the average emission lifetimes begin to decrease at different temperatures for different samples.

The trend in the exciton average lifetime with temperature indicates an activated trapping process, which has previously been observed in CdSe[42,43,76] and CdSe/CdTe heterostructures. [95] This is discussed in more detail in Section 4.5.3., and shown schematically in Figure 4.23. At low temperatures, the charge carriers populate non-emissive trap states, and therefore the exciton $\langle\tau\rangle$ is short because non-radiative recombination dominates. As the temperature increases, the charge carriers return to the exciton state, and the exciton $\langle\tau\rangle$ lengthens because more radiative recombination is occurring. As the temperature increases higher than 200 K, trap states higher in energy

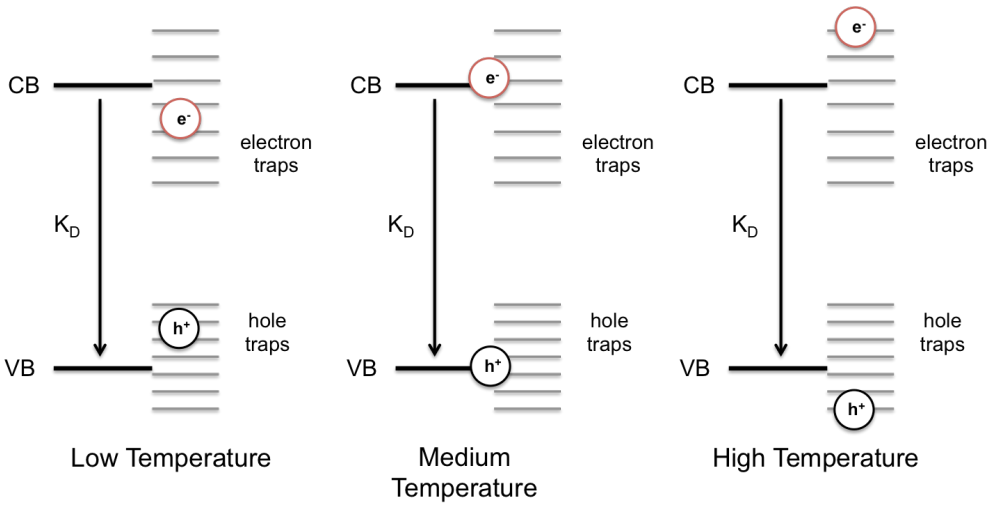

Figure 4.23: Schematic explaining the temperature-dependent average lifetime. K_D refers to the total decay rate.

compared to the exciton are now accessible, and the exciton $\langle\tau\rangle$ decreases because non-radiative recombination outcompetes the detrapping rates.

The temperature at which $\langle\tau\rangle$ is a maximum therefore depends on the energetic relationship between the exciton and the non-emissive trap state distributions. Sample 2 has the maximum $\langle\tau\rangle$ occurring at the lowest temperature, which may indicate it has the shallowest trap state distribution. These samples were made from different QD batches, and the differences in the non-emissive trap state distributions could be caused by changes in synthetic conditions.

The trap $\langle\tau\rangle$ decreases as temperature increases for all three samples. Samples 1 and 3 exhibit power law behavior, while a truncated power law more accurately describes sample 2 shown in Figure 4.22. Power law behavior is quite common in blinking studies on single QDs. Blinking refers to a phenomenon where a QD fluctuates between an on state (high emission intensity) and an off state (low emission intensity). One of the more common mechanisms for blinking is that a QD turns off when a charge migrates to the surface, and the remaining charge non-radiatively recombines. The QD turns back on

when the charge returns to the QD core, and the QD becomes neutral again. If the charge transfer was occurring to a single surface trap with a fixed rate, then the amount of time a QD is either on or off would be described by exponential statistics, which is not observed. Therefore, another mechanism was suggested where charge transfer happens to a static distribution of surface state that results in probabilities with power law statistics.

Average PL lifetimes are calculated by integrating the decay fit function over an infinite time window, but this type of calculation has been shown to bias $\langle\tau\rangle$ to longer times if there are long components in the multi-exponential decay.[43,76] Additionally, $\langle\tau\rangle$ provides no information on how the shape of the decay is changing with temperature. Two PL decays may have similar $\langle\tau\rangle$ values but very different shapes. To address these issues, we calculate $\langle\tau\rangle$ as a function of a time window in addition to temperature using the following equation:

$$\langle\tau\rangle = \sum_n \frac{\int_0^{t_{exp}} A_n\tau_n \exp(-t'/\tau_n)\, dt'}{\sum_m \int_0^{t_{exp}} A_m\tau_m \exp(-t''/\tau_m) dt''}$$

where t_{exp} refers to the time window of the experiment. If the PL decay were single exponential (when plotted on a semi-log scale), then $\langle\tau\rangle$ would be the same regardless of the time window. However, the PL decays shown here deviate quite a bit from single-exponential. Calculating $\langle\tau\rangle$ in terms of a time window allows us to see how the shape of the decay changes with temperature because short components influence $\langle\tau\rangle$ more at short time windows.

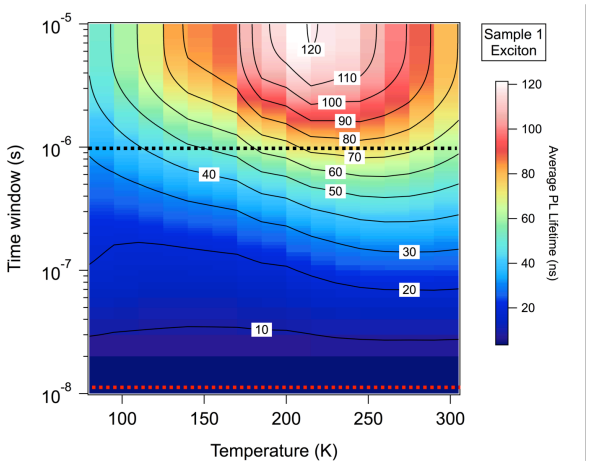

Figure 4.24: Exciton average PL lifetime 2D plot for sample 1. The colors represent the magnitude of the average lifetime. The dashed lines correspond to the average PL lifetimes that were extracted at specific time windows.

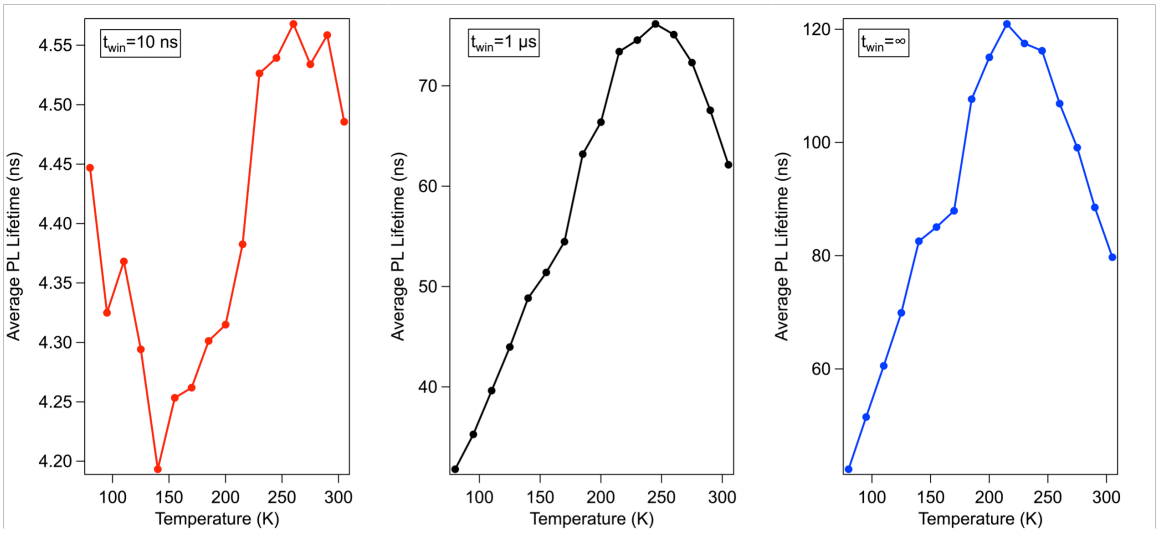

Figure 4.25: Exciton average PL lifetimes within 10 ns (red), 1 µs (black), and infinite time (blue) for sample 1. These graphs were extracted from the 2D plot shown in Figure 4.24.

The exciton $\langle\tau\rangle$ plotted as a function of temperature and time window for sample 1 is shown in Figure 4.24. This is a 2D plot where the abscissa is temperature and the ordinate is the time window. The colors represent the average PL lifetime in nanoseconds. Each horizontal slice shows how the average PL lifetime changes with temperature for a particular time window as seen in Figure 4.25. Figure 4.25 shows a 10

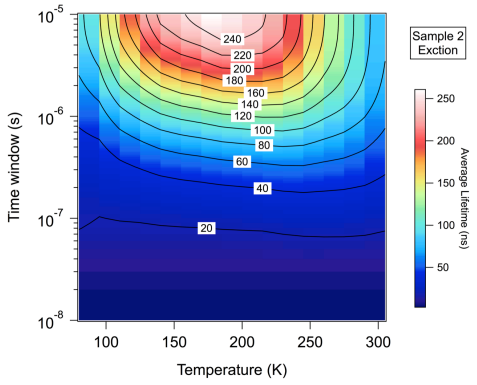

Figure 4.26: Exciton average PL lifetime 2D plot for sample 2.

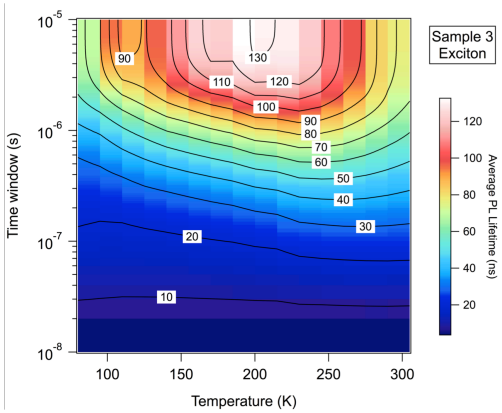

Figure 4.27: Exciton average PL lifetime 2D plot for sample 3.

ns, 1 μs and an infinite time window where the colors correspond to the dashed lines seen in Figure 4.24. The 10 μs time window is assumed to be equivalent to the infinite time window because all the decay components used to fit the exciton PL decays are much less than 10 μs. The exciton $\langle\tau\rangle$ within 10 ns is approximately 4 ns, and it does not show a consistent trend with temperature until the temperature is greater than 150 K. At temperatures greater than 150 K, we see the same increase in $\langle\tau\rangle$ followed by a decrease that is exhibited in the exciton $\langle\tau\rangle$ calculated using an infinite time window. At 1 μs, the exciton $\langle\tau\rangle$ follows the same trend as $t_{win} = \infty$, but the values for $\langle\tau\rangle$ are slightly less, indicating that at least one decay component is longer than 1 μs.

Because the PL decays can be fitted with an infinite number of decay components, we do not assign physical processes to specific decay components or use the number of decay components for analysis. However, we can draw conclusions about the physical processes occurring within the QD by analyzing the PL decays in terms of short and long components. We use the 2D plots to determine which components are changing because short components are emphasized at short time windows and long components dictate $\langle\tau\rangle$ at long time windows. By looking at the 2D plot for sample 1, we see that only the long components (greater than 100 ns) are changing with temperature. Samples 2 and 3 also have long components changing with temperature as seen in Figure 4.26 and Figure 4.27 respectively. The long components are assigned to detrapping and exciton reformation.

The trap $\langle\tau\rangle$ was also analyzed using the 2D plots in a manner similar to the exciton $\langle\tau\rangle$. The trap 2D plot for sample 1 is shown in Figure 4.28, and the trap $\langle\tau\rangle$ for specific time windows are shown in Figure 4.29. At 100 ns, the trap $\langle\tau\rangle$ lengthens as the temperature increases then shortens when the temperature is raised beyond 200 K, similar

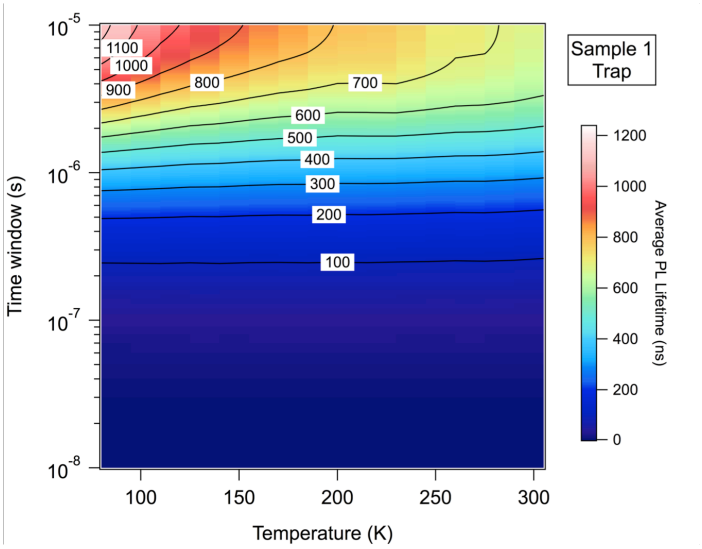

Figure 4.28: Trap average PL lifetime 2D plot for sample 1.

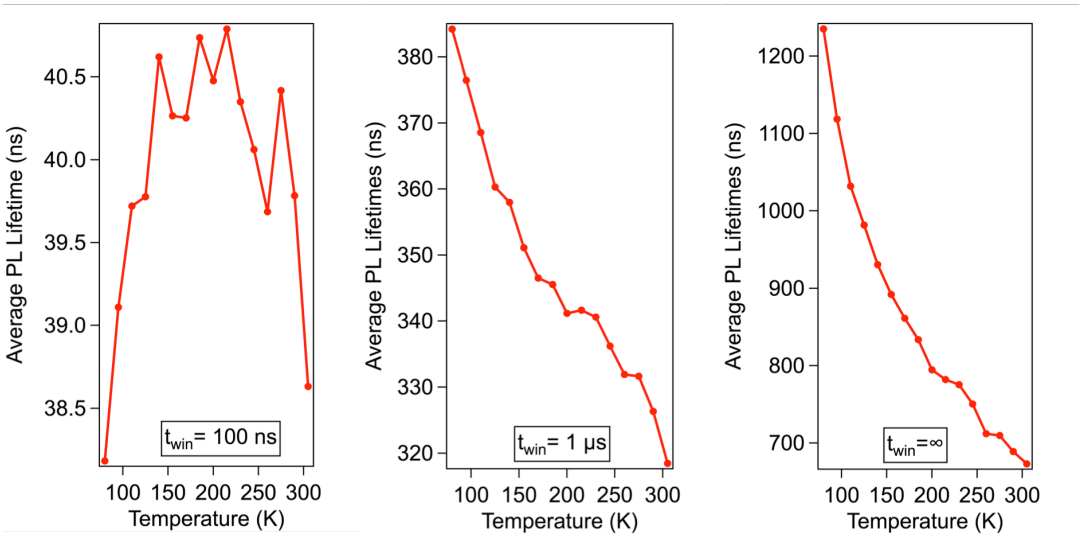

Figure 4.29: Trap average PL lifetimes for sample 1 within specific time windows (t_{win}).

to the exciton behavior for the sample.

Modeling of the exciton dynamics discussed in more detail in Section 4.5.3 suggests there is a Gaussian distribution of non-emissive trap states that is centered slightly higher in energy compared to the exciton. The tail of this distribution lies slightly below the exciton state, and charge transfer occurs from the exciton state to these trap states at low temperatures and back charge transfer to the exciton state is feasible at higher temperatures. This leads to the temperature-dependent exciton $\langle\tau\rangle$ seen in Figure 4.25.

In CdS QDs, the non-emissive trap states are thought to be electron traps, and these shallow electron traps may act as an intermediate step for the formation of the deep emissive trap state. Therefore, how the exciton state populates the shallow electron traps influence the formation and dynamics of the emissive trap state. At low temperatures, both the electron and hole are localized in deep traps and non-radiative recombination is more likely. As the temperature increases, the electrons and holes transition to shallower traps where it may be more likely for them to radiative recombine and the trap $\langle\tau\rangle$ lengthens.

However, at higher temperatures, the electron becomes more delocalized while the hole remains trapped, and the probability for radiative recombination is low resulting in a shortening of the trap $\langle\tau\rangle$. When the time window is increased to 1 μs, we see drastic changes in the trap $\langle\tau\rangle$. First, the trap $\langle\tau\rangle$ increases from 38 ns to 380 ns at 80 K. Second, the trap $\langle\tau\rangle$ decreases by approximately 15% as the temperature increases. This same trend is seen at 10 μs or when $t_{win} = \infty$, but now $\langle\tau\rangle$ is greater than 1 μs at lower temperatures, and decreases by approximately 60% as the temperature is raised. This

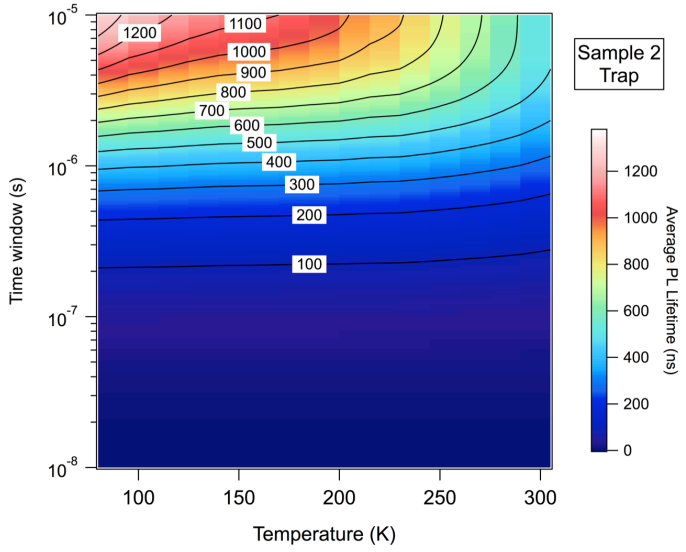

Figure 4.30: Trap average PL lifetime 2D plot for sample 2.

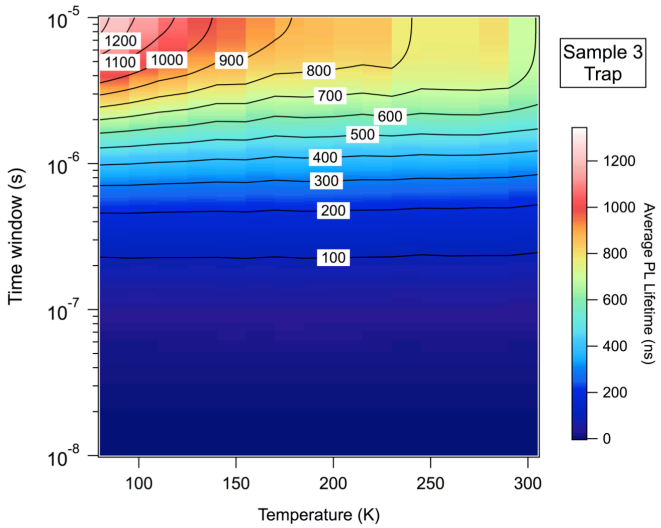

Figure 4.31: Trap average PL lifetime 2D plot for sample 3.

behavior is seen in all CdS samples as shown in Figure 4.30 for sample 2 and Figure 4.31 for sample 3.

These drastic lengthening of the trap $\langle\tau\rangle$ with long time windows indicate the trap PL decays are dominated by decay components longer than 1 µs, and changes in the long

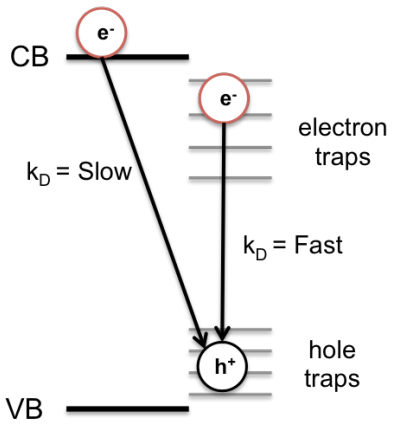

Figure 4.32: Schematic showing a trapped hole recombining with a delocalized electron in the conduction band (CB) or a trapped electron. K_D refers to the total decay rate and includes both the radiative rate and non-radiative rate.

components cause the changes in the trap $\langle\tau\rangle$ seen with temperature, just like the exciton dynamics. As mentioned previously, trap emission is caused by the hole radiatively recombining with either a trapped electron or a delocalized electron. Figure 4.32 depicts both types of recombination. When the electron and hole are trapped, radiative recombination can only occur if the two particles are in close proximity to each other, resulting in fast lifetimes, which are primarily non-radiative. In contrast, if the electron is delocalized, then probability of radiative recombination is minimized and the lifetimes are long. At these long time scales, it is more likely that the electron is delocalized and therefore there is little overlap between the electron and hole wavefunctions. The probability of radiative recombination is low, resulting in a long PL lifetime. As the temperature is increased, non-radiative relaxation pathways are more likely and the trap $\langle\tau\rangle$ shortens.

4.5.2. Calculating Relative Quantum Yields From PL Decays

We previously defined the quantum yield (QY) as the ratio of photons emitted to photons absorbed. If we assume that the number of absorbed photons is constant

regardless of temperature, then a relative QY is determined from the number of photon counts in the PL decay. We know that the oscillator strength or probability of absorption is temperature independent because of previous studies on CdSe QDs.[54]

Because the PL decay is a histogram, the number of emitted photons is easily calculated by totaling the number of counts in each channel that is used to record the PL decay. Each channel also contains noise such as dark counts, and this needs to be accounted for when we calculate the total number of emitted photons. When we collected the PL decay, we always set the delays so the maximum PL intensity or the peak of the decay occurs in a channel number greater than 200. This causes the first 200 channels to only contain noise or background counts, and the fitting software uses those channels to determine an average background count value. The average background count is always calculated from channels before the PL decay because the PL decay may not reach the background level within the time window used to collect the PL decay. We assumed that each channel has the same average number of background counts, and the total number of background counts are calculated by taking the average number of background counts times the number of channels. For all experiments, the number of channels is 4096. Finally, we subtracted the total background count from the total emitted photon count to yield the corrected emitted photon count.

However, the corrected emitted photon count may not accurately reflect the relative QY because of the time taken to collect the PL decay. PL decays that are recorded for longer times will necessarily have larger photon counts. One would expect the average background count to also increase as the recorded time for the PL decay increases, and therefore the corrected emitted photon count remains unaffected. On the

other hand, our hybrid PMT detectors exhibit relatively low dark counts, and the average background count may not increase as the recorded time for the PL decay increases. This is especially true for states with high emission intensities such as the exciton state where background counts are generally low (less than 10), and there is a large separation between the peak number of counts in the decay and the background counts. The total number of counts may increase by hundreds, but the average background count may only change by a few counts if the PL decays are recorded for longer times. Therefore, we divided each corrected emitted photon count by the time it took to record the PL decay to understand how the relative QY changes with temperature.

The exciton relative QYs calculated from the PL decays are shown in Figure 4.33.

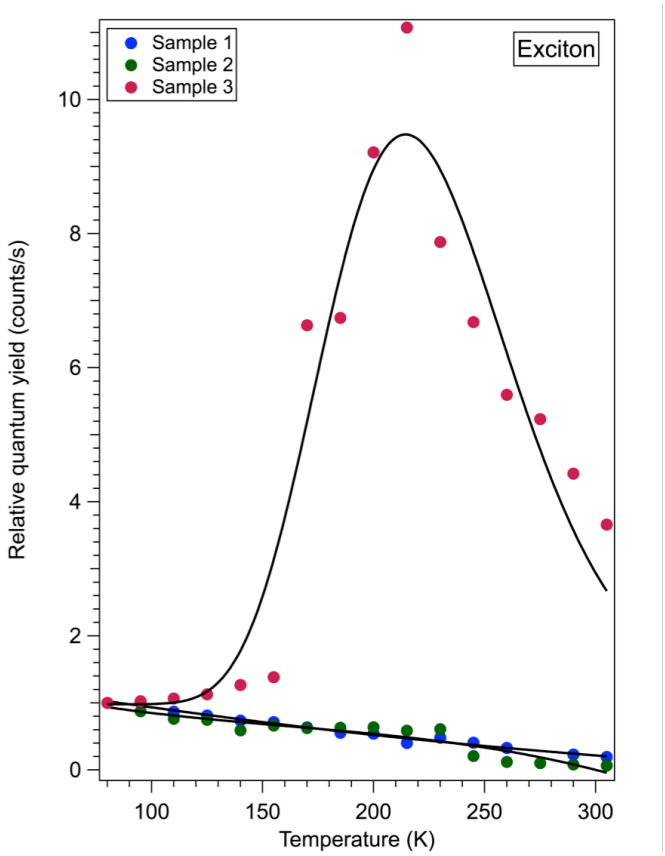

Figure 4.33: Exciton relative QYs calculated from the PL decays. The black lines are trend lines fitted to the data.

As already reported (Table 4.1), the room temperature absolute QYs were also calculated from the steady state PL, sample 1 was the least efficient emitter (QY=5.8%). Sample 2 was the brightest with a QY of 10%, and sample 3 had a QY of 9.4% The exciton relative QY for samples 1 and 2 decreased by approximately 80% as the temperature increased from 80 to 305 K indicating an 80 K absolute QY of 29 and 50%. In contrast, the exciton relative QY increased for sample 3 by one order of magnitude as the temperature was raised to 215 K. Above 215 K, the exciton relative QY decreased, but it still remained three times higher compared to 80 K. The exciton relative QY for sample 3 exhibits similar behavior to the exciton average lifetime, and both quantities peaked at 215 K.

We expect some correlation between the average lifetime and the relative QY because these quantities are defined by the radiative (k_R) and non-radiative (k_{NR}) rates that are occurring within the QD. The relative QY is defined using the following equation:

$$QY = \frac{k_R}{k_R + k_{NR}}$$

and the average PL lifetime, τ, is defined as:

$$\tau = \frac{1}{k_R + k_{NR}}$$

For sample 3, we speculate that changes in k_{NR} are responsible for the temperature-dependent τ and the relative QY. To understand how k_{NR} changes with temperature, we need to know the physical processes that occur within the QD ensemble. We modeled the exciton PL dynamics using a kinetic scheme, and found that an activated trapping process is happening between the exciton and two non-emissive Gaussian trap state distributions. At low temperatures, charge transfer occurs from exciton state to the trap state, and non-

radiative recombination prevails resulting in a high k_{NR}. As the temperature increases, those trapped charges thermally repopulate the exciton state and radiative recombination is more likely, k_{NR} decreases, and we see an increase in the relative QY and exciton average PL lifetime. However, when the temperature increases even more, higher energy trap states are now accessible and k_{NR} increases again, and the relative QY and exciton τ decrease.

This explanation works reasonably well for sample 3, but fails to explain the trend in the relative QY for samples 1 and 2. In order to explain the decrease in the relative QY and the temperature-dependent exciton average PL lifetime, the radiative rate would need to be temperature-dependent as well as the non-radiative rate. However, the radiative rate is generally assumed to be temperature-independent.

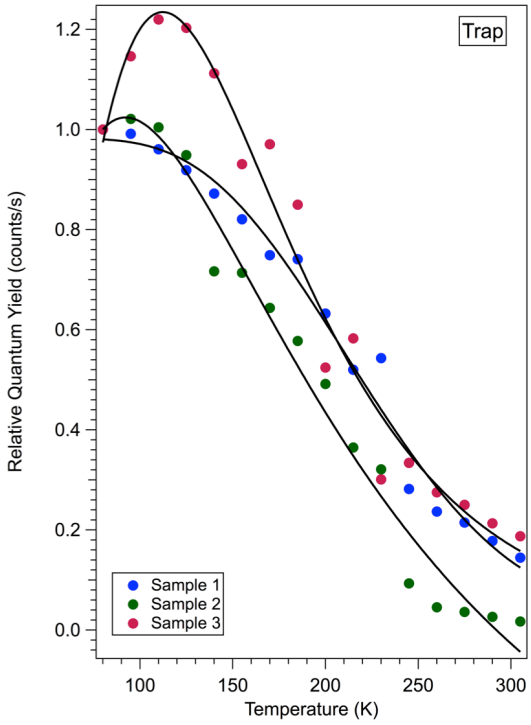

Figure 4.34: Trap relative QYs calculated from the PL decays.

The trap relative QYs for all three samples are shown in Figure 4.34. All samples behave similarly, and the relative QY decreases with an increase in temperature. Samples 2 and 3 exhibit a slight rise in the relative QY for temperatures below 125 K. Because both the trap average PL lifetime and the relative QY drop as the temperature is raised, we speculate that the non-radiative recombination rates are increasing.

We believe that trap emission is caused by a trapped hole radiatively recombining with either a delocalized electron or a trapped electron. At low temperatures, the electron is also trapped, and radiative recombination occurs if the trapped electron is in close proximity to the trapped hole where tunneling may occur. The increase in temperature causes the electron to become more delocalized, and now the overlap of the electron and hole wavefunctions is reduced. The reduction in the overlap integral leads to a higher probability of non-radiative recombination, decreasing the trap average PL lifetime and the relative QY.

The increase in the relative QY at low temperatures for samples 2 and 3 may indicate a higher population in the emissive trap state. We know that the exciton and emissive trap state are correlated because the exciton absorption peak is seen in the trap PLE spectrum. When modeling the exciton PL dynamics, we found that two non-emissive trap state distributions were necessary to adequately reproduce the exciton PL decays. One of these non-emissive trap state distributions had a reorganization energy similar to the reorganization energy calculated for the emissive trap state.

We hypothesize that this non-emissive trap state distribution is involved in the deep trap population mechanism, where charge transfer occurs from the exciton to the non-emissive trap state, and then into the emissive trap state. At low temperatures,

electrons are in the non-emissive trap states rather than delocalized. So we expect to see more trap emission and a higher relative QY at lower temperatures compared to higher temperatures when the electron is delocalized and radiative recombination with the trapped hole is slow.

4.5.3. Modeling Temperature-Dependent Exciton TRPL

Early temperature-dependent TRPL studies were often analyzed using a three state model consisting of a ground state, dark exciton state, and bright exciton state.[96-101] The energy spacing between the dark exciton state and bright exciton state is size dependent and typically a few meV. At low temperatures, only the dark exciton state is populated. Because the transition from the dark exciton to the ground state is spin forbidden, relaxation from this state requires coupling to phonon modes. This results in long lifetimes that are on the order of microseconds.[102-105] As the temperature increases, the bright exciton state becomes thermally populated, and exciton lifetimes begin to shorten. This model describes QD systems reasonably well for temperatures between 10 and 70 K.

However, this simple model fails to describe exciton dynamics at all temperatures, especially those above 100 K and below 20 K. For example, Crooker et al showed that exciton lifetimes in colloidal CdSe QDs below 2 K are temperature independent, and suggested a different relaxation pathway inherent to all dots with a small activation energy.[97] This was further supported by theoretical calculations performed by Califano et al who showed that surface states such as hole traps reduce the splitting between dark and bright exciton states, resulting in a shorter dark exciton decay rate.[106] Above 100 K, exciton PL decays are often multi-exponential, suggesting the

addition of new non-radiative recombination mechanisms based on a decreased quantum yield at higher temperatures.

These multi-exponential decays are apparent in both ensemble,[58] and single particle experiments,[98,107,108] demonstrating that the multitude of recombination pathways are inherent to the QD, and not a result of sample inhomogeneities. Instead, they are attributed to complex interactions between the exciton and non-emissive trap states[20,42,43,95,99,109] that are populated through an activated trapping mechanism. Therefore, exciton average PL lifetimes are a result of competition between the trapping and detrapping rates.

For example, temperature-dependent TRPL on core/shell CdSe/CdZnS showed exciton average PL lifetimes lengthened to a maximum and then shortened as the temperature was increased from 77 to 305 K.[43] At low temperatures, the trapping rate outcompetes the detrapping rate because charge carriers are trapped in states with energies below the exciton state. They are not released from the trap states because there is not enough thermal energy to return to the exciton state. Since most of the charge carriers are in trap states, non-radiative recombination is prominent and the exciton average PL lifetime ($\langle\tau\rangle$) is short. As the temperature increases, more trap states become populated. However, the increase in temperature also allows more charge carriers to overcome the detrapping barrier, resulting in an increased detrapping rate. Because the detrapping rate now competes with the trapping rate, radiative recombination also increases, and the exciton $\langle\tau\rangle$ begins to lengthen. As the temperature increases even more, charge carriers can now enter trap states that are higher in energy compared to the

exciton leading to an increase in the trapping rate where once again non-radiative recombination is prominent. As a consequence, the exciton $\langle\tau\rangle$ begins to shorten again.

Because the temperature-dependent exciton $\langle\tau\rangle$ in CdS shows similar behavior to those seen in core/shell CdSe/CdZnS, we used the previously described activated trapping model as foundation for developing a kinetic scheme to model exciton dynamics in CdS. Our model for carrier trapping is based on electron transfer (ET), and has been described in more detail elsewhere.[42,43] We describe non-emissive trap states using an ensemble probability distribution function ($P_K(\varepsilon)$) because these PL decays were recorded on a QD ensemble, and there is a multitude of possible trap states.

The shape of the non-emissive trap state $P_K(\varepsilon)$ depends on whether the system is described in bulk semiconductor terms or in molecular terms. In organic photoconductors, Gaussian distributions are used to describe trap state energetics,[110] while exponential distribution below the band-edge describe traps in bulk semiconductors. As described in Section 1.2, QDs exhibit properties of both molecular systems and bulk systems, so either type of distribution is applicable to QDs. QDs have discrete electronic transitions such as organic photoconductors so a Gaussian distribution may be suitable. However, trap states in QDs may interact with each other like in bulk semiconductors, so an exponential distribution may also be relevant. Previous modeling on core/shell CdSe/CdZnS used a convolution of a Gaussian and exponential to describe trap state probability distribution functions.[43] For exciton dynamics in CdS we found that a Gaussian distribution adequately reproduced the PL decays, and adding the exponential distribution showed no change in our modeling.

Now that we have defined the trap state distributions for our model, we need to define how the trap states are populated. We modeled trapping rates using classical ET theory, which was described in more detail in Section 1.3. Classical ET rates are governed by the free energy, ΔG_K, the reorganization energy, λ_K, and the electronic coupling parameter, V_K. We assumed that each trap state distribution is symmetrically distributed around the QD in a shell like manner. Each trap within the "shell" would experience the same local environment, and therefore we assigned a single λ_K and V_K to each trap state probability distribution. The trapping rates were then determined using the following equation:

$$k_{iK} = g_K P_K(\varepsilon) \frac{2\pi}{\hbar} |V_K^2| \frac{1}{\sqrt{4\pi\lambda_K k_B T}} exp\left[-\frac{(\lambda_K + \Delta G_{iK})^2}{4\lambda_K k_B T}\right]$$

where g_K represents the average number of trap states in the Kth trap distribution, $P_K(\varepsilon)$ is the probability distribution function that was defined as a Gaussian with a peak energy ε for our modeling efforts. The detrapping rates were then calculated using detailed balance and are defined as:

$$k_{Ki} = \frac{g_i}{g_K P_K(\varepsilon)} k_{iK} \exp\left(\frac{\Delta G_{iK}(\varepsilon)}{k_B T}\right)$$

where g_i represents the degeneracy of the exciton state. After defining the trapping and detrapping rates, we generated a kinetic scheme consisting of *N* states. The dynamics of each state are based on the probability of that state being occupied ($\rho_n(t)$) within a time *t* after the excitation event. The probabilities are calculated from numerical solutions to *N* rate equations defined as:

$$\frac{d\rho_n(t)}{dt} = -\gamma_n^R \rho_n(t) + \sum_{m \neq n} \left(\gamma_{mn}^{NR} \rho_m(t) - \gamma_{nm}^{NR} \rho_n(t)\right)$$

where γ_{mn}^{NR} and γ_{nm}^{NR} are the non-radiative transition rates from state *m* to *n* and from state *n* to *m* respectively. γ_n^R is the radiative transition from state *n*. For our modeling efforts, $N = 2 + \sum_K N_K$ where N_K is the number of trap within the distribution. We used N=2 because our model consists of two distinct states, exciton and ground state, in addition to the states within the trap distribution.

Using software built by Dr. Jones, we constructed kinetic schemes that are solved numerically, and used to globally fir the PL decays for each emitting state at all temperatures as shown in Figure 4.35. Each modeled PL decay is 2 μs long because there is high uncertainty in the experimentally recorded PL decays beyond 2 μs. The modeled PL decays are then compared to the experimentally collected PL decays, and the fitting parameters such as the radiative rates and reorganization energies used within the model are adjusted until the residuals between the model PL decays and experimentally collected PL decays are minimized.

The first iteration of our kinetic scheme consisted of an exciton state, deep emissive trap state, and ground state. The energies for the exciton state and emissive trap state were fixed to the values determined from the multi-peak fit of the PL line shape. The exciton was set to the initial state even though the excitation energy was well above the band-edge because hot carriers relax in ps or less[24,87] and is beyond the resolution of our experiments. Non-radiative decay from either the exciton or emissive trap state to the ground state was excluded to simplify the model. The reorganization energy for the emissive trap was initially set to the reorganization energy extracted from the spectra as discussed in Section 4.5.1.

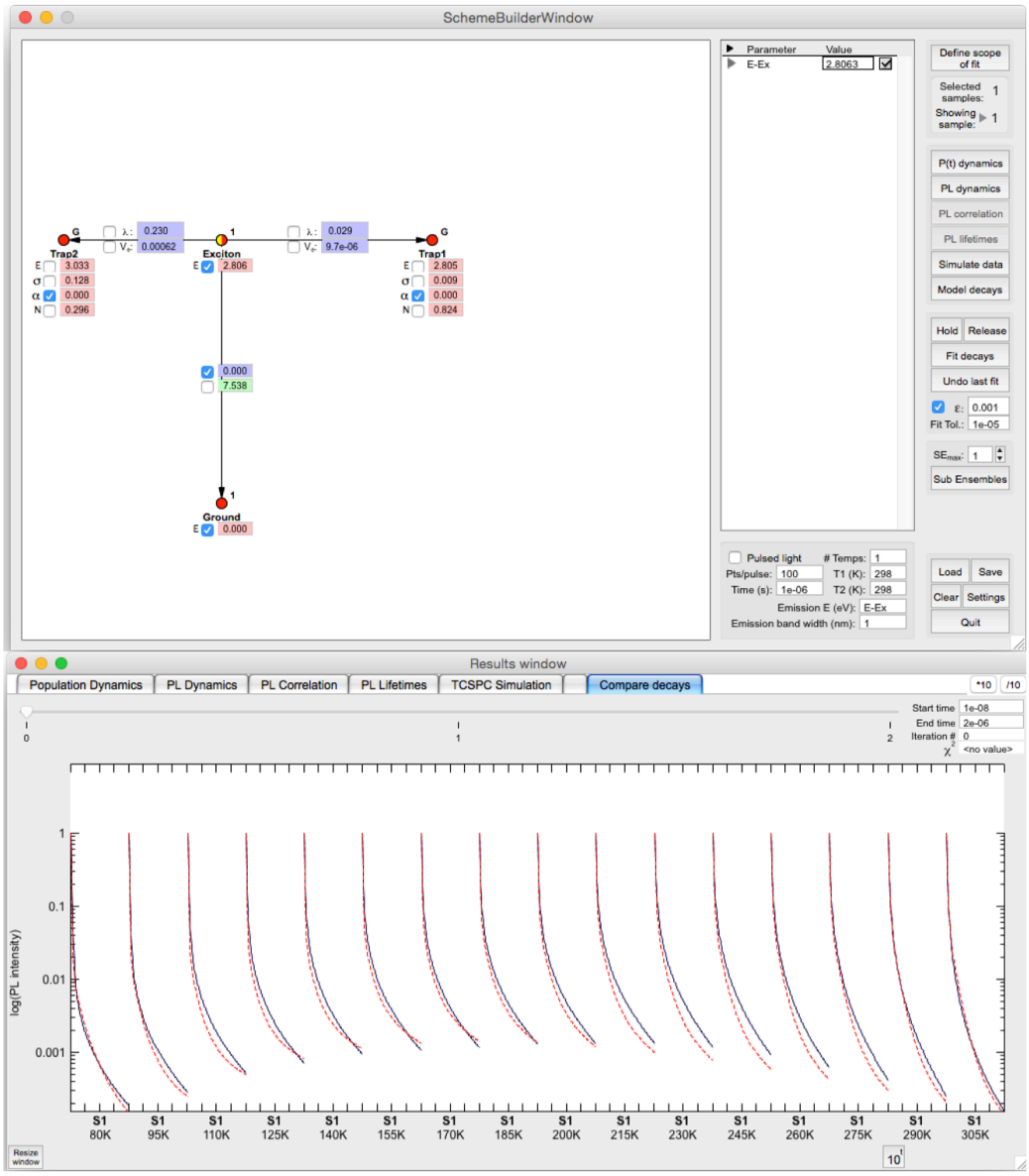

Figure 4.35: Screenshot of the software used to construct the kinetic schemes for TRPL analysis. The upper window shows a kinetic scheme consisting of an exciton state, two trap states and a ground state. The bottom panel shows how the model PL decays (red) produced by the scheme shown above compare to the experimental decays (black).

However, this model was unsuccessful in reproducing either the exciton PL decays or trap PL decays. One possible reason could be the different time scales for the exciton and trap PL decays because the exciton decays on the order of nanoseconds while the trap decays in microseconds. It is challenging to construct one single model to

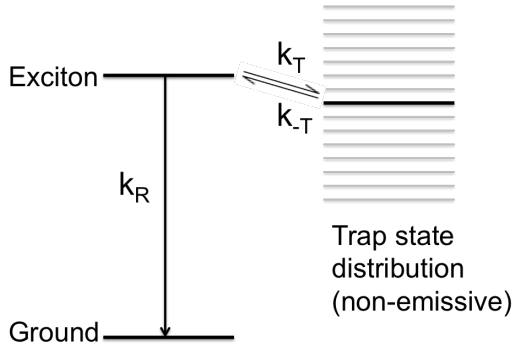

Figure 4.36: General three state model consisting of an exciton state, a distribution of non-emissive trap states, and a ground state used to build the kintetic scheme. K_R is the exciton radiative rate. $K_{(T)}$ and $K_{(-T)}$ refer to the non-radiative trapping and detrapping rates respectively.

represent dynamics on such a wide time scale. Another challenge is the energy difference between the exciton state and the emissive trap state. The deep trap is located approximately 1 eV below the exciton state. Once a charge transfers from the exciton state to the trap state, it will not be able to return to the exciton state for radiative recombination. Furthermore, ET from the exciton to the emissive trap state is heavily in the inverted region, and the barriers for ET are quite large. Therefore, we do not expect the exciton to populate the emissive trap directly, and we focused our efforts on modeling only the exciton dynamics.

To successfully model the exciton PL decays, our kinetic scheme required a single exciton state and two distinct non-emissive trap state distributions. A generalized schematic of the model showing the exciton state and a trap distribution is presented in Figure 4.36. We used a single exciton state instead of a manifold of bright and dark exciton states because the temperature range for this experiment ensured that the majority of the exciton PL signal arises from the bright exciton state. The results of our modeling for one sample are shown in Figure 4.37 where the experimentally recorded PL decays

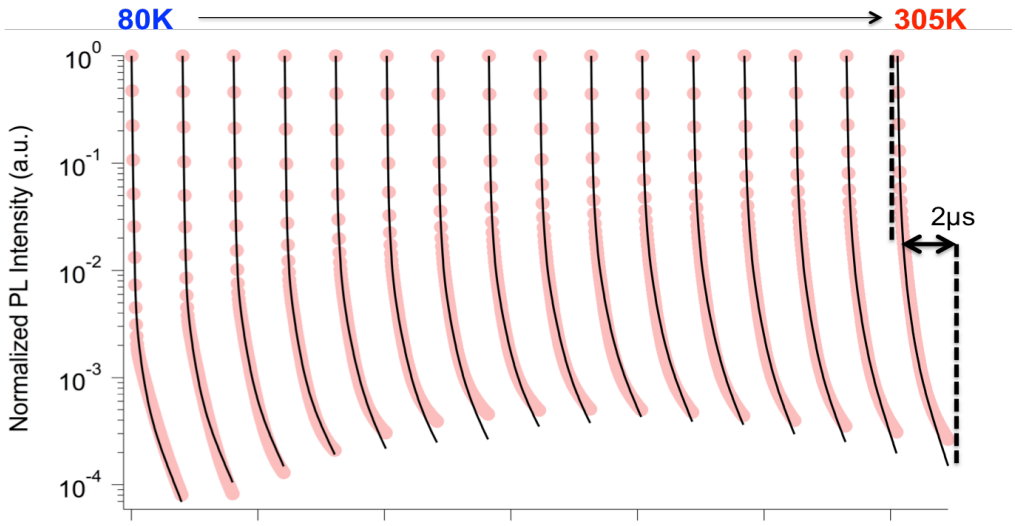

Figure 4.37: Comparison of model exciton PL decays (black) with experimental exciton PL decays (red) for temperatures ranging from 80 K to 305 K. Both model and experimental PL decays are 2 μs.

are shown in red and the model decays are shown in black. Our model fits the recorded PL decays reasonably well for three orders of magnitude change in intensity. The kinetic model allows us to estimate radiative rates for the exciton state, and we found the exciton radiative rate ranged from 29 to 36 ns, which is consistent with values reported for CdS QDs in heptane,[111] but slightly longer than CdS nanorods.

The kinetic model required two trap state populations to reproduce the temperature dependent exciton PL decays, and their probability distribution functions for one sample is presented in Figure 4.38. The parameters used for each trap distribution from the fitting software are listed in Table 4.3 where ε_i is the peak energy of the distribution, λ_i is the reorganization energy, V_i is the electronic coupling parameter, and σ_i is the width of the Gaussian probability distribution function. The trap state distributions used in the model apply to the QD ensemble and are specific to a single QD.

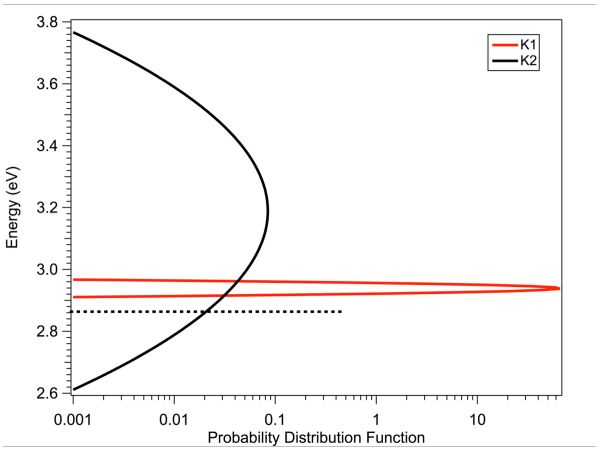

Figure 4.38: Non-emissive trap state distributions needed to adequately model the exciton PL decays. The exciton emission is 2.86 eV and is represented by the horizontal dashed line. K_1 and K_2 are described in the text.

Table 4.3: ET parameters extracted from the modeling with the kinetic scheme for K_1 (above) and K_2 (below). The column headings are defined in the text.

Trap	ε (eV)	λ (meV)	σ (meV)
1	2.939	77	6
2	3.189	213	194

Sample	ε_{K2} (eV)	λ_{K2} (meV)	σ_{K2} (meV)
1	3.189	213	194
2	3.033	230	128

One distribution (K_1) is narrow with a width of a few meV and a peak energy within a few meV of the exciton state. K_1 is also characterized by small reorganization values. This narrow distribution is similar to the narrow distribution seen in other core/shell QD samples[42,43] and was attributed to trap states caused by the interface between the core and shell of the QD. The QDs used in our experiments are core only so interfacial trap states are unlikely to cause K_1. The second distribution (K_2) is much broader than K_1 and, it is centered more than 150 meV higher in energy compared to the exciton. This means that only the tail of K_2 is interacting with the exciton because trap

states at the peak of the distribution are not accessible at room temperature. K_2 is also characterized by large reorganization energies on the order of hundreds of meV. We assign K_2 to traps located on the QD surface because the reorganization energies are so large, and surface states are expected to have high reorganization energies.

One interesting thing to note is the reorganization energies generated in the kinetic scheme for the non-emissive trap state distributions are quite similar to the reorganization energies calculated from the steady state PL and PLE for the emissive trap state. We previously discussed how ET in CdS might occur through an intermediate state that would have similar reorganization energies as the deep trap but a smaller change in free energy. We propose that K_2 acts as this intermediate trap state, and the deep emissive trap is populated through a sequential trapping mechanism. The concept of a sequential trapping process in CdS has been proposed before. O'Neil first showed that shallow traps near the band-edge formed more quickly than deeper traps. Other experiments using time-resolved emission spectroscopy on CdS QDs synthesized or embedded in polymers showed that high-energy trap states of the broad deep trap decayed quickly into low energy trap states resulting in a time-dependent Stokes shift.[60,61] However, these CdS samples did not exhibit exciton emission, so it is unclear how those high-energy trap states were originally populated. More recent work using pulsed optically magnetic resonance (pODMR) on CdS nanorods showed that both the exciton and deep trap interact with the same species of shallow trap, but the nature of the shallow trap was not discussed.[112]

4.6. Understanding Trap Dynamics with Excitation-Dependent TRPL

The previous experiments used an excitation energy that was well above the QD band-edge, and therefore excited both the exciton state and the deep trap state. We know that the exciton influences the steady-state PL because the trap PLE shows more trap

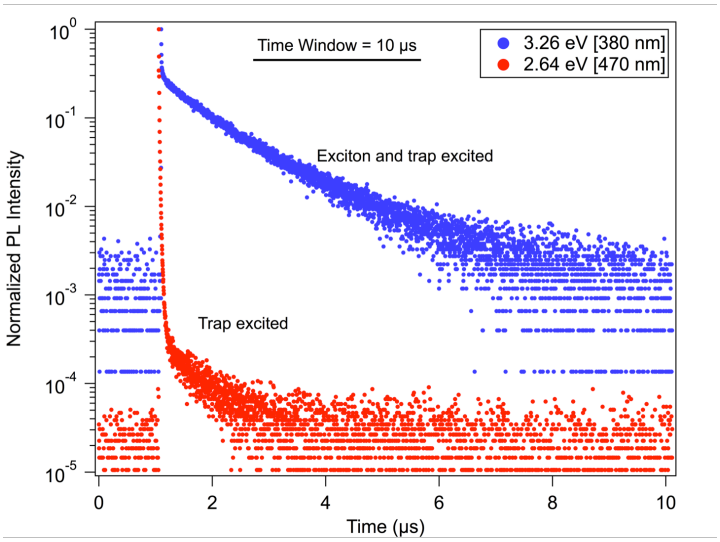

Figure 4.39: Trap PL decays at 110 K collected with 3.26 eV excitation (blue) and 2.64 eV excitation (red). Both trap PL decays were recorded at the same emission wavelength using a 10 µs TAC.

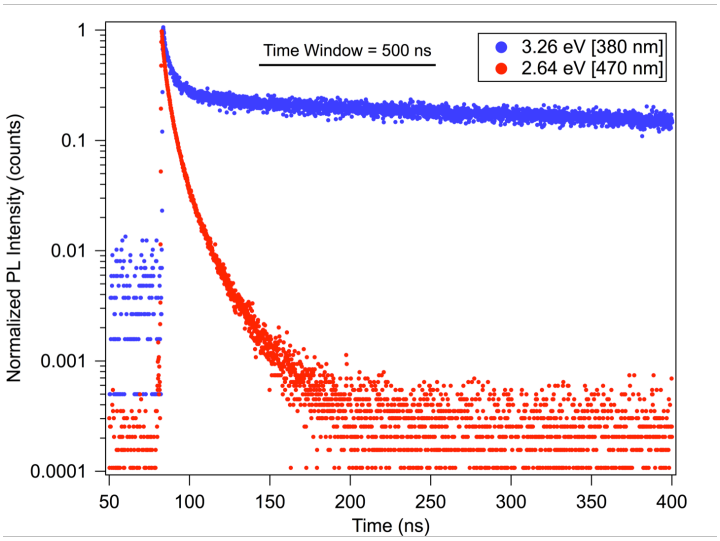

Figure 4.40: Trap PL decays at 110 K collected with 3.26 eV excitation (blue) and 2.64 eV excitation (red). Both PL decays were recorded at the same emission wavelength using a 500 ns TAC.

emission at the exciton absorbance energy, but does the exciton also influence the trap state recombination dynamics? To answer this question, we changed the excitation energy to 2.64 eV. The exciton absorbs at 2.87 eV, so this excitation energy will only excite the deep trap states. We collected a series of trap PL decays at varying temperatures in the same manner as the previous experiments.

The results were quite unexpected. The trap PL decay at 110 K for 3.26 eV excitation energy and for 2.64 eV excitation energy are presented in Figure 4.39. The trap PL decay drastically changes in both shape and length when excited directly. The fast component seen as a small fraction of the trap PL decay using 3.26 eV exciton, now dominates the PL decay when using 2.64 eV excitation, which is more easily seen in Figure 4.40 where the PL decays were collected using a 500 ns TAC. At 3.26 eV excitation, approximately 3% of the PL decay has decay components less than 100 ns. However, at 2.64 eV excitation, 95% of the PL decay has decay components less than 50 ns.

At first we were concerned the fast component was caused by scatter from the laser, but there are several reasons why this is not the case. First, the trap PL decays were recorded using a 484 nm dichroic where light with wavelengths shorter than 484 nm is reflected onto the sample, and light with wavelengths longer than 484 nm is transmitted onto the detector. However, the transition at which light is reflected or transmitted is not sharp, and some excitation light still passes through to the detector. Second, the trap PL decays are recorded at 2.07 eV using a monochromator, so it is unlikely that light at 2.64 eV would also be collected. Finally, the fast component is much longer than our instrument response function (IRF) as seen in Figure 4.42. If the laser caused the fast

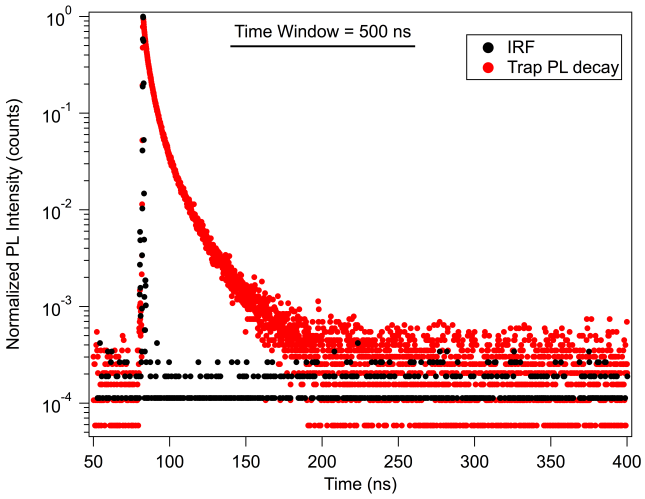

Figure 4.42: Trap PL decay (red) at 110 K and IRF (black) recorded using a 500 ns TAC. The IRF width is one channel, which is approximately 122 ps.

component, then the fast component would have the same width as the IRF. Since it does not, we attribute the fast component to the trap state recombination dynamics, and not to an artifact from the laser system.

Figure 4.40 also shows the trap PL decay at 2.64 eV excitation decreases by four orders of magnitude within the first 200 ns, while the trap PL decay at higher excitation energies decreases by less than an order of magnitude within the same time window. The

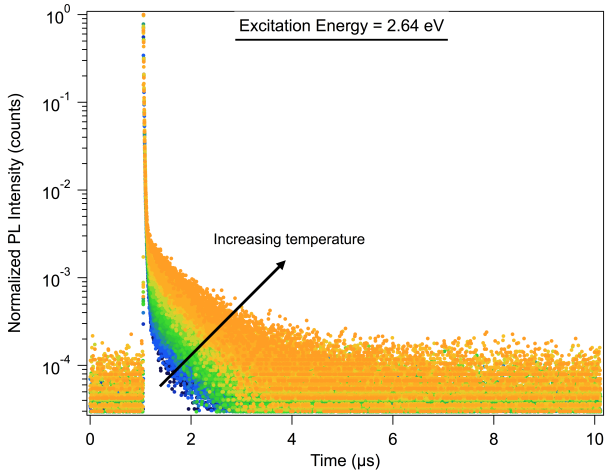

Figure 4.41: Trap PL decays recorded using 2.64 eV excitation for temperatures ranging from 80 K to 305 K.

trap PL shape and length when directly excited remains the same at all temperatures as shown in Figure 4.41.

The trap average lifetime, $\langle\tau\rangle$, is also remarkably different with different excitations as shown in Figure 4.43. First, the trap $\langle\tau\rangle$ is much shorter when excited with 2.64 eV light as compared to 3.26 eV excitation, which is expected because the PL decays are much shorter. Second, the change in trap $\langle\tau\rangle$ with temperature is also different with different excitation energies. The trap $\langle\tau\rangle$ when excited with 3.26 eV excitation decreases by approximately 50% as the temperature is increased. In contrast, the trap $\langle\tau\rangle$ when excited with 2.64 eV excitation increases by 500% as the temperature is increased.

The change in trap PL decays, and therefore the trap $\langle\tau\rangle$ with excitation energy is unusual because it appears that the trap state emission violates Kasha's rule. Kasha's rule states that emission is independent of excitation,[113] so we would expect the trap dynamics

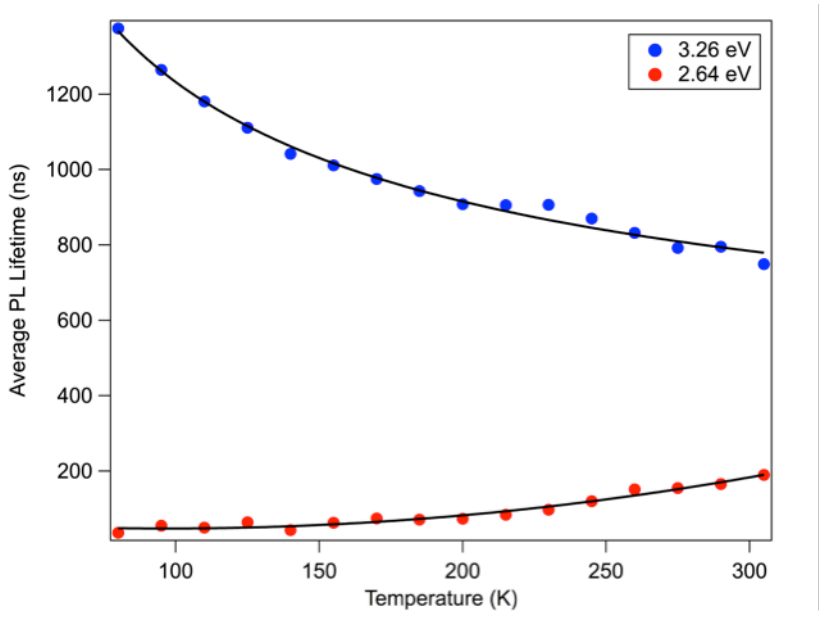

Figure 4.43: Temperature-dependent trap average PL lifetimes for 3.26 eV excitation energy (blue) and 2.64 eV excitation energy (red). The solid black lines are trend lines fitted to the data.

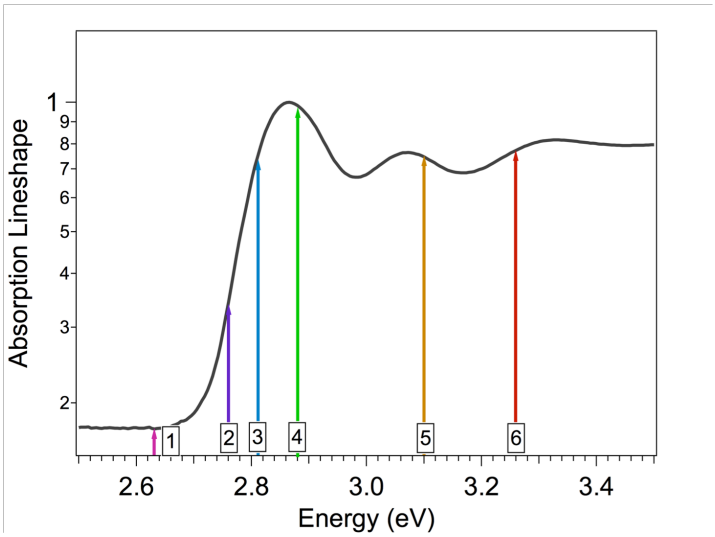

Figure 4.44: Absorption lineshape spectrum for CdS QDs. Each arrow represents a different excitation energy used in the experiment. The values for the excitation energies are listed in Table 4.3. Excitations 1-3 are below the band-gap and 4-6 are above the band-gap.

to be the same regardless of excitation. Obviously this is not the case, and we suggest that the different excitation energies are actually creating fundamentally different trap states with similar emission energies. For example, the trap state formed with the 2.64 eV excitation is both the electron and hole trapped, while the trap state formed with 3.26 eV excitation is the electron delocalized and only the hole trapped. Because the electron traps are expected to be shallow,[52,58,79,114] the energy difference between the hole recombining with a trapped electron or a delocalized electron would be small.

To test this hypothesis, we performed the same temperature-dependent TRPL with six different excitation energies ranging from well above the QD band-gap to well below the QD band-gap. The different excitation energies were chosen based on the absorption spectrum of the sample as seen in Figure 4.44 These energies and their equivalent wavelengths are listed in Table 4.4. The exciton absorption energy is 2.87 eV, so excitation energies equal or greater than 2.87 eV would excite mainly the exciton state,

Table 4.4: Excitation energies and wavelengths used for excitation-dependent TRPL study. The exciton absorption energy is 2.87 eV.

	Excitation Energy (eV)	Excitation Wavelength (nm)	Relation to Band-edge
(1)	2.64	470	Below
(2)	2.76	450	Below
(3)	2.82	440	Below
(4)	2.88	430	At
(5)	3.10	400	Above
(6)	3.26	380	Above

and only a small fraction of the QDs would have deep trap directly excited. For excitation energies below 2.87 eV, only the deep trap state is excited.

It is important to note that these experiments were performed on the same sample with the different excitation energies in no particular order. Furthermore, the trap PL decays were recorded at the same emission wavelength regardless of excitation. Additionally, the excitation power at the sample was kept to a minimum using neutral density filters to prevent photobleaching of the sample. We saw no change in the PL intensity at room temperature throughout the course of the experiment, indicating photobleaching has not occurred. However, we cannot confirm this by steady state PL because the sample volume within in the cryostat is too low for the PL measurement, and once a sample has been removed from the cryostat, it cannot be used again.

4.6.1. Excitation Energies Above the Band-edge

The trap PL decays using excitation energies greater than the band-edge (>2.87 eV) show the same temperature-dependence regardless of the excitation energy. The trap average PL lifetime, $\langle\tau\rangle$, 2D plot constructed from the PL decays for the three excitation energies above the band-edge are shown in Figure 4.45. All three excitation energies cause the trap $\langle\tau\rangle$ to be constant with temperature at short time windows. At long time windows, the trap $\langle\tau\rangle$ decreases as temperature increases. These trends are more clearly seen in Figure 4.46, where the temperature-dependent trap $\langle\tau\rangle$ are plotted for 100 ns, 1 µs, and 10 µs time windows. The 10 µs time window is assumed to be equivalent to the infinite time window because none of the decay components used to fit the decays are longer than 10 µs. Time windows less than 100 ns have not be shown because the trap $\langle\tau\rangle$ changes by tenths of a nanosecond, and it is difficult to draw conclusions on such a small change.

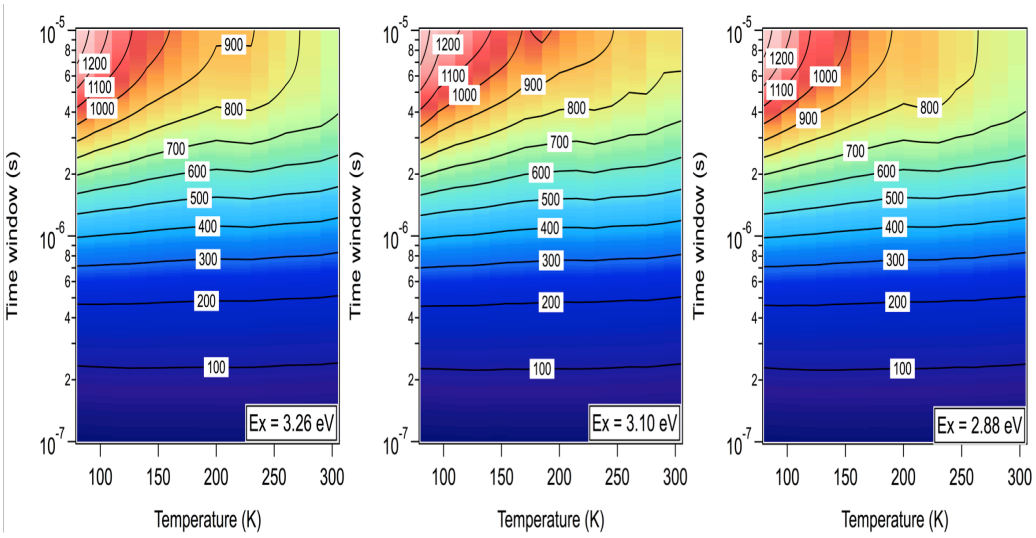

Figure 4.45: Trap average PL lifetime 2D plots for three different excitation energies above the QD band-edge. From left to right: 3.26 eV (380 nm), 3.10 eV (400 nm), and 2.88 eV (430 nm). The exciton absorption occurs at 2.87 eV.

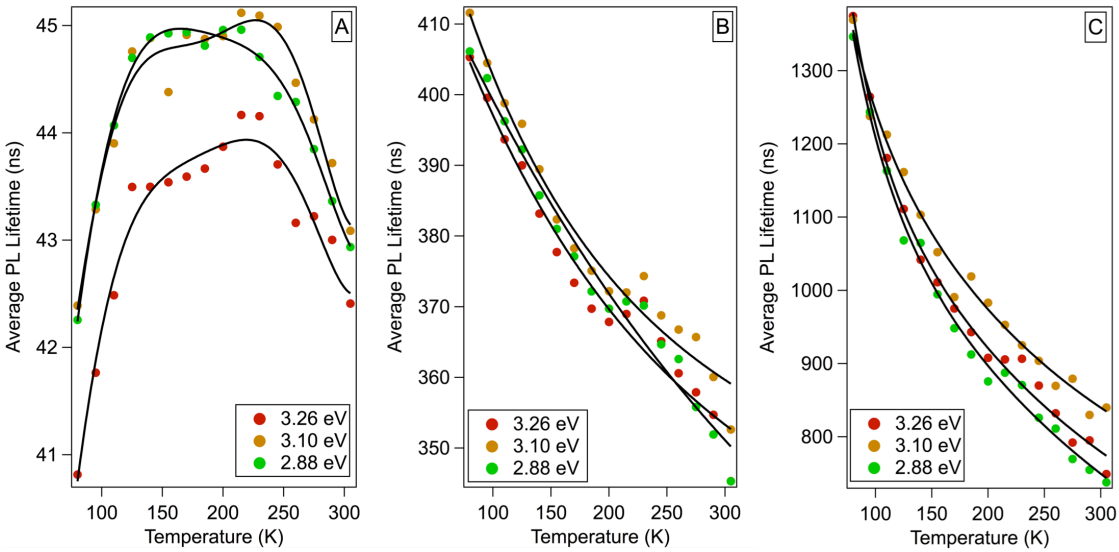

Figure 4.46: Excitation and temperature-dependent trap average PL lifetimes extracted from Figure 4.45 at specific time windows. (A) 100 ns (B) 1 µs (C) 10 µs

The trap $\langle\tau\rangle$ within 100 ns exhibits a trend with temperature similar to the exciton $\langle\tau\rangle$ that was discussed previously. At 80 K, the trap $\langle\tau\rangle$ is approximately 40 ns. As the temperature increases, the trap $\langle\tau\rangle$ lengthens and then reaches a maximum. Once the temperature increases beyond 200 K, the trap $\langle\tau\rangle$ begins to shorten again. We previously discussed the same temperature-dependence seen in the exciton $\langle\tau\rangle$ in terms of an activated trapping process where the exciton $\langle\tau\rangle$ is a result of competition between the trapping and detrapping rates occurring between the exciton state and a non-emissive trap state distribution.

However, an activated trapping mechanism is not applicable in this case, because one of the carriers, the hole, is already deeply trapped. We know that the trapped carrier is a hole because of the discussions in Section 4.1.1. We assume that the electron remains delocalized when using these excitation energies. The hole trap state is more than likely a narrow distribution of trap states, where thermal population exchange occurs between the

states. It is possible that there is an optimal trap state configuration for radiative recombination with the delocalized electron that occurs at temperatures ranging from 125 K to 230 K. Below these temperatures, the hole may be too deeply trapped, and the overlap with the electron wavefunction is too low to allow radiative recombination. Above 230 K, the hole interacts with higher energy states, and non-radiative recombination increases, leading to a decrease in the trap $\langle\tau\rangle$.

When the time window is increased to 1 μs or longer, we see a slightly different trend with temperature. Now, the trap $\langle\tau\rangle$ increases dramatically to over 400 ns at 1 μs and over 1300 ns for 10 μs. Furthermore, the trap $\langle\tau\rangle$ continuously decreases by approximately 20% for the 1 μs time window and by approximately 40% for the 10 μs time window as the temperature is raised. The decrease in the trap $\langle\tau\rangle$ accompanied by a decrease in the relative QY (see Figure 4.50 (left)) with an increase in temperature suggests that the non-radiative recombination is increasing at longer time windows. The exact nature of the non-radiative relaxation pathways is unknown. Because we see no change in the trap recombination dynamics with excitation energies above the band-edge, we speculate that the deep emissive trap is formed after the carriers have relaxed to the band-edge and hot carrier trapping does not play a role.

4.6.2. Excitation Energies Below the Band-Edge

The trap recombination dynamics vary with different excitation energies that are below the band-edge in contrast to the dynamics when excited with above band-gap energies. The trap $\langle\tau\rangle$ 2D plots for the three different excitations below the band-edge are shown in Figure 4.47. For 2.82 eV (440 nm) excitation, the trap $\langle\tau\rangle$ 2D plot looks remarkably similar to those shown in Figure 4.45. This is expected because this QD sample has an absorption spectrum that is inhomogenously broadened because of a size distribution. Even though the first exciton absorption occurs at 2.87 eV for the majority of QDs, there exists a sub population of larger QDs with a slightly smaller band-gap. The 2.82 eV excitation would generate excitons within these larger QDs. Since excitons are still produced in the larger QDs, we expect similar trap dynamics using 2.82 eV excitation energy compared to excitation energies well above the band-edge. However, the 2.76 eV (450 nm), and 2.64 eV (470 nm) excitation energies are well below the band-gap, so excitons should not be produced with these excitation energies. Therefore, we should only observe trap dynamics at these excitation energies.

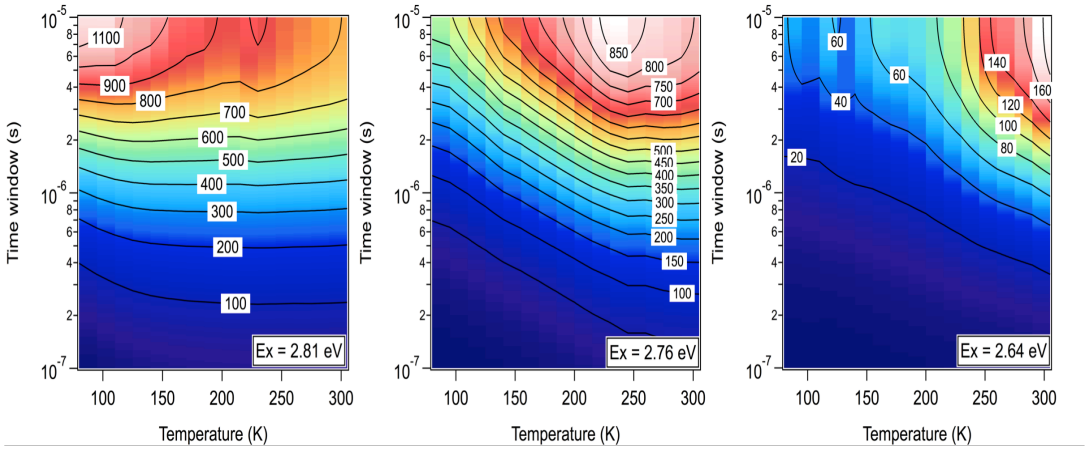

Figure 4.47: Trap average PL lifetime 2D plots for three different excitation energies below the QD band-edge. From left to right: 2.81 eV (440 nm), 2.76 eV (450 nm), and 2.64 eV (470 nm).

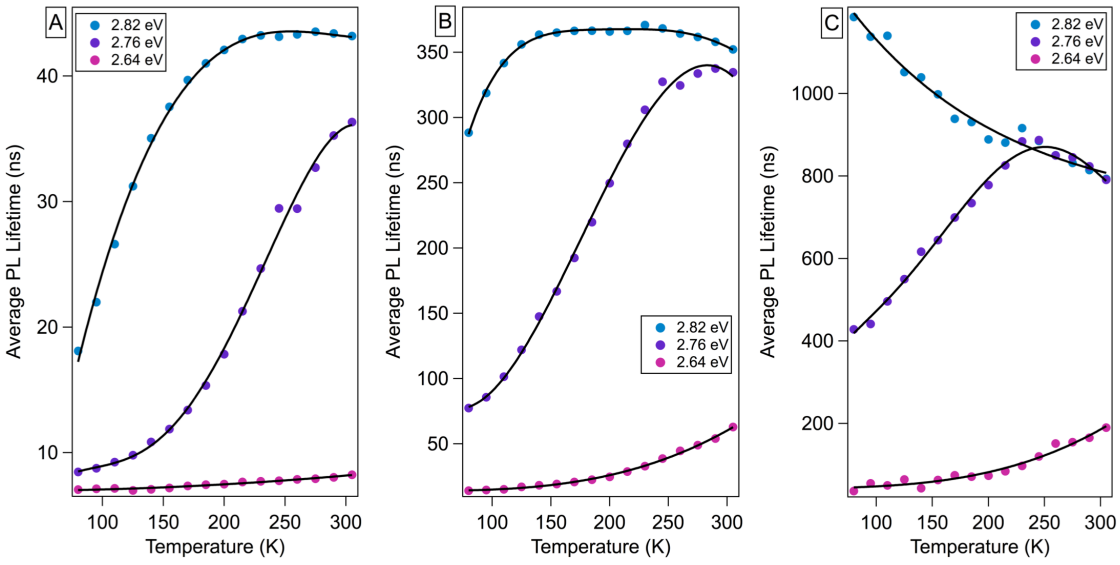

Figure 4.48: Excitation and temperature-dependent trap average PL lifetimes extracted from Figure 4.47 at specific time windows. (A) 100 ns (B) 1 µs (C) 10 µs

When we excite the deep trap state directly, we start to detect a fast component at low temperatures, as indicated by the lower (bluer) trap $\langle\tau\rangle$ at time windows greater than 1 µs. This fast component becomes more dominant when using 2.64 eV excitation energy compared to 2.76 eV. The fast component is unusual because we expect dynamics to slow down at lower temperatures. Another noteworthy observation is the trap $\langle\tau\rangle$ temperature-dependence with below band-edge excitation energies. Instead of the trap $\langle\tau\rangle$ shortening with increasing temperature as seen in Figure 4.45, we see a lengthening of the trap $\langle\tau\rangle$ with increasing temperature. This lengthening is greater for 2.76 eV excitation compared to 2.64 eV excitation. The temperature-dependent trap $\langle\tau\rangle$ are more clearly seen in Figure 4.48, where the trap $\langle\tau\rangle$ is plotted for specific time windows.

Before discussing the temperature trends observed in the trap state $\langle\tau\rangle$, we first must consider the nature of the trap state we are forming with the different excitation energies. A general schematic showing possible trap state configurations formed with different excitation energies is presented in Figure 4.49.. When the QDs are excited using

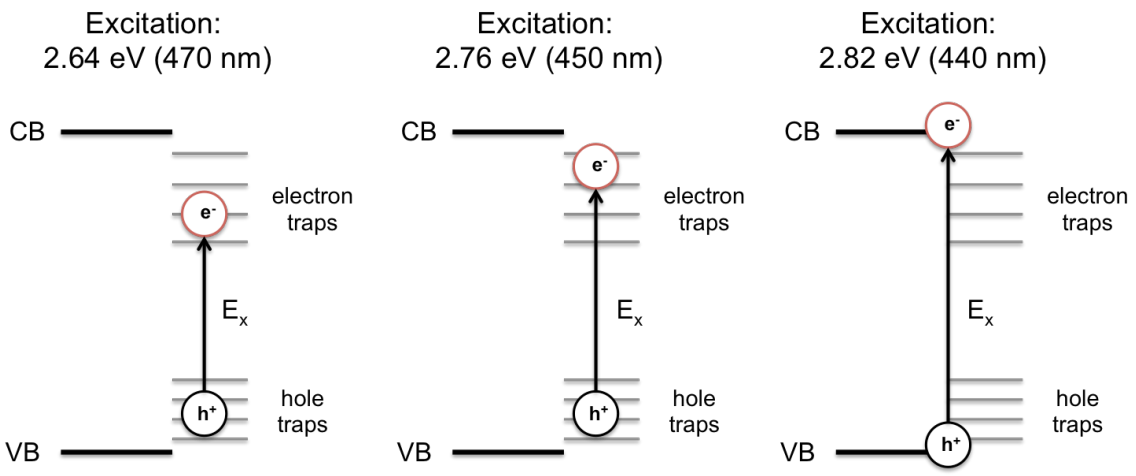

Figure 4.49: Cartoon showing how trap states are formed with different excitation energies. CB and VB refer to the conduction band and valence band respectively. E_X is the excitation energy.

2.64 eV, only states deep within the band-gap are excited, and no interactions with the conduction or valence band is possible. Electrons are excited from states within the band-gap to shallow electron traps below the conduction band. The holes remain in traps, which are lower in energy than the valence band. When the excitation energy is increased to 2.76 eV, the electrons are still excited into electron trap states, but these trap states are closer in energy to the conduction band, and it is feasible for an electron to enter the conduction band. As discussed previously, 2.82 eV excitation energy is high enough to excite an electron into the conduction band for the larger QDs. The remaining hole then relaxes into a hole trap state, and it radiatively recombines with the electron in the conduction band.

Now that we know what states are formed with the different excitation wavelengths, we can start discussing the temperature-dependent trap recombination dynamics seen in Figure 4.48. For 2.64 eV excitation, we observe for all time windows that the trap $\langle\tau\rangle$ are magnitudes are less than the other excitations, and they are mainly temperature-independent. Because the low excitation energy only excites the trap states,

we assign the fast component seen in the trap PL decays and the 2D plot for 2.64 eV excitation energy to radiative recombination to between a trapped electron and a trapped hole.

In order for radiative recombination to occur, the trapped electron and hole must be spatially correlated. When a charge carrier becomes trapped, their wavefunction becomes localized, and the overlap between the electron and hole wavefunctions is reduced. However, if the electron and hole are localized in close proximity to each other than wavefunctions may overlap enough to permit radiative recombination. Furthermore, if the charge carriers are in nearby, then it is possible for one carrier to tunnel and recombine with the other carrier.

Since the probability of both carriers being trapped in the same area is relatively low, we would expect non-radiative recombination to strongly influence the PL decays, resulting in fast PL decays and short average lifetimes, which is what we observe. Tunneling would also explain the near temperature independence because tunneling is a distance-dependent phenomenon and not temperature-dependent.

The slight increase in the trap $\langle\tau\rangle$ with temperature for 2.64 eV excitation at long time windows can perhaps be explained by QD surface reconstruction. We recognize that trap states are formed on the particle surface, and higher temperatures may cause fluctuations in the surface environment. These fluctuations may shift the electron and hole trap states into a configuration that increases the likelihood of radiative recombination. This increases in the trap $\langle\tau\rangle$ with increasing temperature is more likely to be detected at longer time windows because of the time scales at which surface reorganizations occur.

The 2.76 eV excitation is a rather unique case because this excitation energy produces trap dynamics that contain elements of both above band-edge and below band-edge excitations. At low temperatures (below 200 K), the trap state recombination dynamics behaves as if it was excited directly, and at higher temperatures (greater than 200 K) the trap behaves as if it was influenced by the exciton state. For example the trap $\langle\tau\rangle$ using 2.76 eV excitation is only a few nanoseconds longer than 2.64 eV excitation at 80 K within the first 100 ns of the PL decay. The difference in the trap $\langle\tau\rangle$ at low temperatures between 2.76 eV and 2.64 eV excitation energies becomes greater with longer time windows, but the trap $\langle\tau\rangle$ for 2.76 eV excitation always remains closer to the 2.64 eV rather than the 2.82 eV excitation.

However, as the temperature is increased, the trap $\langle\tau\rangle$ using 2.76 eV shows a more dramatic increase compared to the 2.64 eV excitation, and the 2.76 eV excitation begins to behave as the 2.82 eV excitation, especially at longer time windows. Both the 2.82 eV and 2.76 eV excitations show the trap $\langle\tau\rangle$ increasing with temperature for the 100 ns and 1 μs time windows, but the maximum trap $\langle\tau\rangle$ occurs at different temperatures and the amount of increase varies for the two excitation energies. For example, the trap $\langle\tau\rangle$ using 2.82 eV has reached a maximum at 200 K for the 100 ns time window and a maximum at 125 K for the 1 μs time window. However, the 2.76 eV excitation produces a maximum trap $\langle\tau\rangle$ at 305 K for the 100 ns time window and 245 K for the 1 μs time window.

The difference in the temperatures at which the maximum trap $\langle\tau\rangle$ for the two different excitation energies can be attributed to different electron trap depths. From previous discussions, we theorize that the trap $\langle\tau\rangle$ becomes longer when the electron is delocalized, based on the lengthening of the trap $\langle\tau\rangle$ for above band-gap excitations.

Therefore, a lengthening in the trap $\langle\tau\rangle$ for below band-gap excitations would indicate that the electron transitioned from a trap state into a delocalized state or conduction band. Because thermal energy would be required for the transition, the temperature at which the trap $\langle\tau\rangle$ begins to length would provide insights into the trap depths. If the electron is localized in a deep trap, then more thermal energy is needed to make the electron delocalized, and this causes the trap $\langle\tau\rangle$ to lengthen at a higher temperature. If the electron is in a shallow trap, then the trap $\langle\tau\rangle$ would lengthen at a lower temperature, since less energy is involved in the transition to the conduction band.

Based on this argument, we speculate that the 2.64 eV excitation only excites electrons into the deepest traps. The 2.64 eV excitation showed no transition to long lifetimes that would occur if the electron were delocalized. We believe that 2.64 eV is too low to generate electrons into traps shallow enough to thermally interact with the conduction band. Thermal energy is approximately 25 meV at room temperature, which is not high enough to overcome the 200 meV difference between the excitation energy and the exciton absorption energy.

On the other hand, the trap $\langle\tau\rangle$ for the 2.76 eV excitation does show a transition from short to long lifetimes, indicating the electron becomes delocalized at some point. Therefore, the 2.76 eV excitation energy creates electron traps, which are shallow enough for thermal energy to delocalize the electron. Even though the 2.76 eV is still over 100 meV lower than the exciton absorption energy, it may be high enough to generate shallow traps in the larger QDs, which would have a slightly smaller band-gap and lower exciton absorption energy. Finally, the 2.82 eV excitation energy generates the shallowest electron traps because the trap $\langle\tau\rangle$ show similar trends to the above band-gap excitations.

This is expected because the 2.82 eV excitation energy is close enough to the exciton absorption energy that little thermal energy is needed to delocalize the electron, and the 2.82 eV excitation energy is also high enough to generate exciton states for the largest QDs.

4.6.3. Relative Quantum Yields

The relative QYs also vary with excitation energies in addition to the trap $\langle\tau\rangle$. We previously showed that the trap recombination dynamics are similar for excitation energies above the QD band-edge, and this is also true for the relative QYs as shown in Figure 4.50 (left). The relative QY decreases with increasing temperature for all excitation energies above the band-gap. Because the trap $\langle\tau\rangle$ also decreases with temperature, at least for long time windows, we attribute the change in the relative QY to

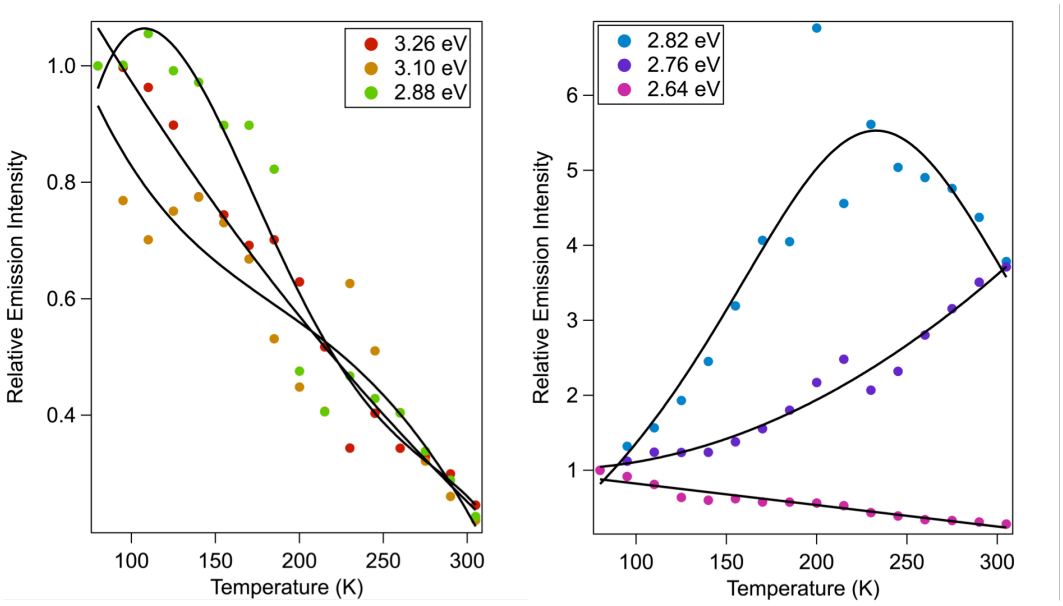

Figure 4.50: Trap state relative QY calculated from the PL decays for above band-gap excitation (left) and below band-gap excitation (right) energies. The relative QY has been normalized to the QY at 80 K. The black lines are included to help visualize the trends in the data.

an increase in the non-radiative recombination processes. This is reasonable because the electron is delocalized while the hole remains trapped with these excitation energies, and the probability for radiative recombination is low. Therefore, it is more likely for non-radiative processes to outcompete the radiative ones.

In contrast, the below band-gap excitation energies show different trends in the relative QY with excitation energy as observed in Figure 4.50 (right). The lowest excitation energy, 2.64 eV, results in a temperature-dependent relative QY that is similar to the above band-gap excitation energies. However, this excitation energy only generates trapped electrons in addition to the trapped holes. Since both carriers are localized, the overlap of their wavefunctions is reduced. Radiative recombination can only occur if the carriers are trapped in close proximity to each other, and the probability of this happening is relatively low. Therefore, we expect non-radiative recombination to be more prevalent and increase as the temperature increases in a similar manner as the above band-gap excitation energies.

The 2.76 eV and 2.82 eV excitation energies are the only excitation energies that show an increase in the relative QY with an increase in temperature. However, the relative QY for the 2.82 eV excitation energy differs from the 2.76 eV excitation energy because it begins to decrease for temperatures greater than 230 K, although the relative QY at 305 K is still three times greater than 80 K. The trend in the relative QY for 2.82 eV excitation shows the same characteristics as the exciton relative QY for sample 3 (see Figure 4.33). Sample 3 used in the experiments discussed in Section 4.5 is the same sample that was used for the excitation-dependent TRPL studies.

The exciton PL decays used to generate the relative QY were collected using 3.1 eV excitation energy, yet the similarity in the temperature-dependent relative QY for the trap only occurs for the 2.82 eV excitation. The temperature-dependent relative QY for the exciton state was explained as a competition between trapping and detrapping rates between the exciton and a distribution of non-emissive trap states. At low temperatures, charge transfer occurs from the exciton state to the non-emissive trap state, but back charge transfer is unlikely. As the temperature increases, the possibility of back charge transfer to the exciton state also increases. As a result, the exciton relative QY also increases. Eventually, the increasing temperature makes higher energy trap states more accessible, and the trapping rate becomes faster than the detrapping rate, causing the exciton relative QY to decrease.

4.7. Controlling Trap Emission with Oleic Acid

The final component of this project is to determine the cause of trap emission because once we understand the nature of trap emission, we can develop new methods to control trap emission or to eliminate it completely. The most prevailing theory for trap emission is incomplete ligand coverage.[21,52,57,58,61,67,77,85,87,115,116] Colloidal QDs are generally synthesized using wet chemical procedures that utilize a variety of organic stabilizing ligands to promote particle growth and prevent aggregation.[31,117-120] However, their primary function is to passivate the QD surface, thereby preventing trap states. The ligands passivate the surface either by binding to defects in the crystal lattice[67,121] or to unbound surface sites, removing any surface dangling bonds. As a result of binding to the QD surface, ligands have been shown to strongly affect the QD optical properties.[21,122-125]

QDs may lose ligands through the purification process or by the dilutions necessary for spectroscopic measurements. During the purification processes, QDs are precipitated by the addition of non-solvent followed by centrifugation to remove unreacted precursors and other impurities. However, this process has been shown to also remove weakly bound ligands.[126-128] Dilution may also remove ligands based on the theory of chemical equilibrium. During synthesis, there is an excess of free ligands in solution, and ligands are more likely to remain adsorbed to the QD surface. After purification, QDs are redispersed into clean solvents containing no ligands, and the ligands will desorb from the QD to maintain chemical equilibrium based on Le Chatelier's principle. Le Chatelier's principle states that the equilibrium of a system will shift in order to counteract the change in conditions.[129] In this case, there is a lack of ligands in solution, so ligands desorb from the QD surface in order to establish dqual concentrations of ligands in solution and on the QD. NMR studies on oleic acid bound to CdSe QDs have confirmed that an equilibrium exists between bound ligands and free ligands in solution.[130,131]

If incomplete ligand coverage causes trap emission, then adding more ligands to the QD solution after purification should prevent trap emission. By adding ligands to the clean solvent, the chemical equilibrium will favor more ligands bound to the QD surface rather than in solution. To test our hypothesis, we synthesized CdS QDs using oleic acid as the stabilizing ligand. After we purified the QDs and diluted them to the concentrations necessary for spectroscopic measurements, we added varying amounts of oleic acid to each QD sample in order to determine the oleic acid concentration needed to promote ligand adsorption onto the QD. The full experimental details are discussed in

Section 3.5. Once the samples are prepared, we monitored the change in the trap emission using steady state and time-resolved PL.

4.7.1. Changes in Trap Emission Using 90% Oleic Acid

The first set of samples was prepared using CdS QDs synthesized with technical grade (90%) oleic acid. Each sample contained the same concentration of QDs and varying amounts of 90% oleic acid. The changes seen in the PL behavior is discussed in terms of volumes added oleic acid rather than concentrations of oleic acid because we do not know the starting amount of oleic acid that may already be present on the QD surface.

The UV-Vis absorption spectra for the first series is presented in Figure 4.51, and we see that adding oleic acid causes little change in the first exciton absorption peak at 385 nm. We do not expect the oleic acid to affect the absorption because excitons are primarily generated in the QD core, and therefore would not be affected by the QD

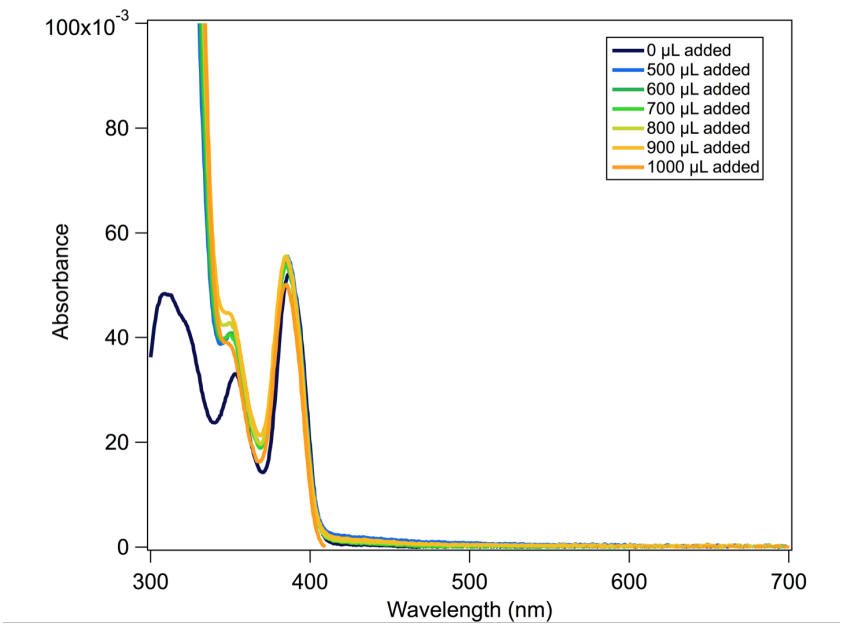

Figure 4.51: CdS absorption spectra with varying amounts of 90% oleic acid added.

surface. However, we do observe an increase in the absorption at shorter wavelengths for all samples compared to the control (no oleic acid added). We primarily use UV-Vis absorption to confirm the concentration of QDs in solution and to ensure that aggregates have not formed. If oleic acid is affecting the trap states, then changes are more likely to be seen in the emission spectra rather than the absorption spectra because the trap emission signal is more intense than its absorption signal.

The steady state emission spectra for the CdS-oleic acid samples are shown in Figure 4.52 (left). Each emission spectrum has been normalized to the absorptance at the excitation wavelength. This normalization ensures that the changes seen in the PL is caused by changes in oleic acid and not because a sample had more absorption. An

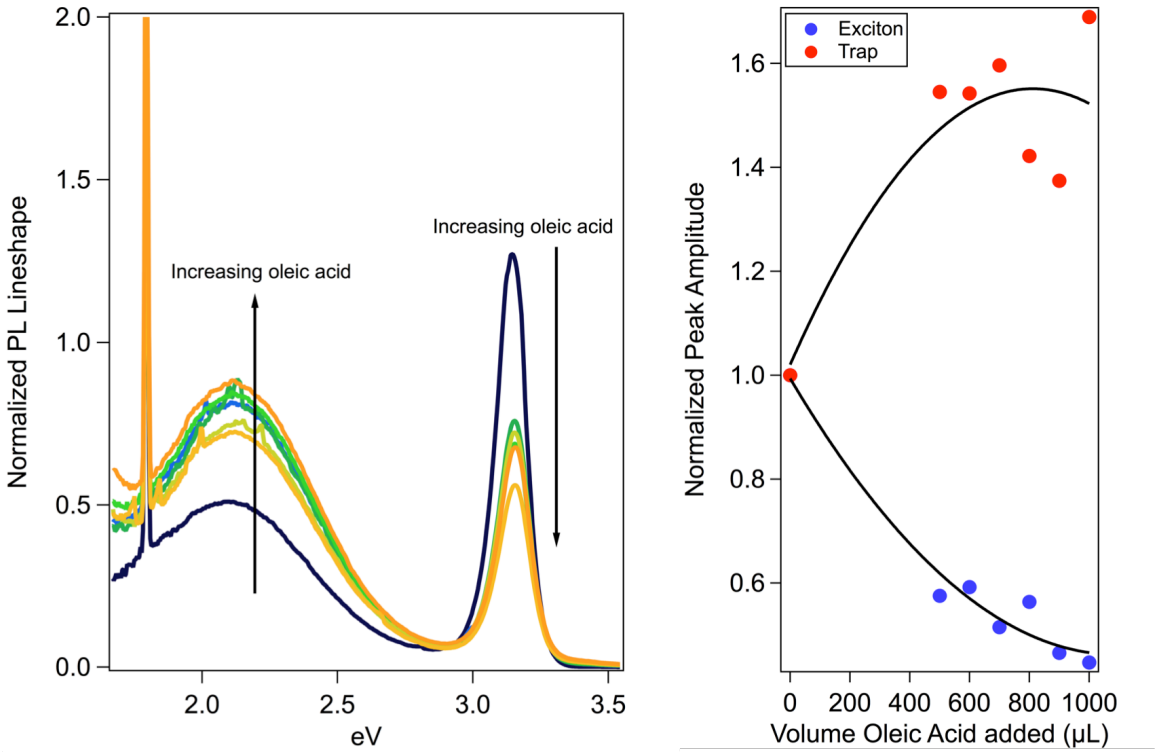

Figure 4.52: Normalized CdS PL spectra with increasing amounts of 90% oleic acid (left). The sharp feature at 1.8 eV is scatter from the excitation light. On the right is the relative change in emission intensity for the exciton (blue) and trap (red).

increase in added oleic acid caused the exciton emission to decrease and the trap emission to increase, contrary to our predictions.

If more ligands were binding to the QD surface and passivating the trap states, then the exciton emission would increase while trap emission would lessen. Each PL spectrum was converted into a lineshape spectrum and fitted with a series of Gaussian peaks to determine the change in signal intensity for both the exciton and the trap. The results are presented in, Figure 4.52 (right) where the exciton and trap peak amplitudes have been normalized to the control sample.

For the exciton, we see that exciton emission decreased by approximately 40% with additional amounts of oleic acid, and trap emission increased by a similar amount. Another interesting observation in Figure 4.52 (left) is the exciton appears to slightly blue-shift (shifts to higher energy) as the amount of added oleic acid is increased. The blue-shift is less than 10 meV for the largest amount of added oleic acid, but it does appear to consistently increase as more oleic acid is added as shown in Figure 4.53.

Because the exciton emission energy is indicative of the QD size, a blue-shift implies that the band-gap is becoming larger, and hence the QD size is shrinking. Ligand adsorption should not affect the QD size because ligands bind to empty surface sites and would not extend beyond the length of ligands already present on the surface. So the blue-shift in the exciton emission is unusual. However, it may provide insight into the mechanism that causes the decrease in exciton emission and an increase in trap emission.

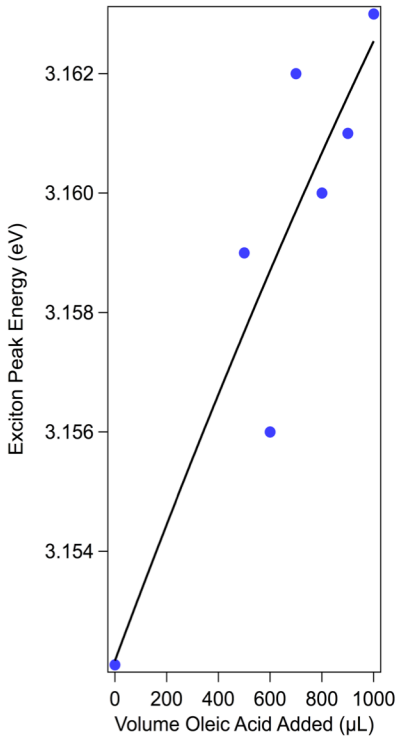

Figure 4.53: Change in exciton emission energy with additional oleic acid.

NMR studies have shown that ligands desorb from the QD surface as either ligands or metal-ligand complexes.[130,132] In the case of CdS, oleic acid may desorb from QD surface as cadmium oleate, removing cadmium from the QD surface. This would cause the QD to become smaller, shifting the exciton emission to higher energies. The removal of cadmium also creates unpassivated surface states such as charged sulfur atoms, increasing the probability of trap emission. Additionally, the samples are exposed to oxygen during spectroscopic measurements, and oxidation may affect the ligand chemical equilibrium. For example, oxidation of PbSe QDs caused the oleic acid to desorb from the surface as lead oleate.[132]

4.7.2. Effects of Purified Oleic Acid on Trap Emission

Since the oleic acid used previously is only 90% pure, it is possible that the impurities in the oleic acid are causing the changes observed in the exciton and trap

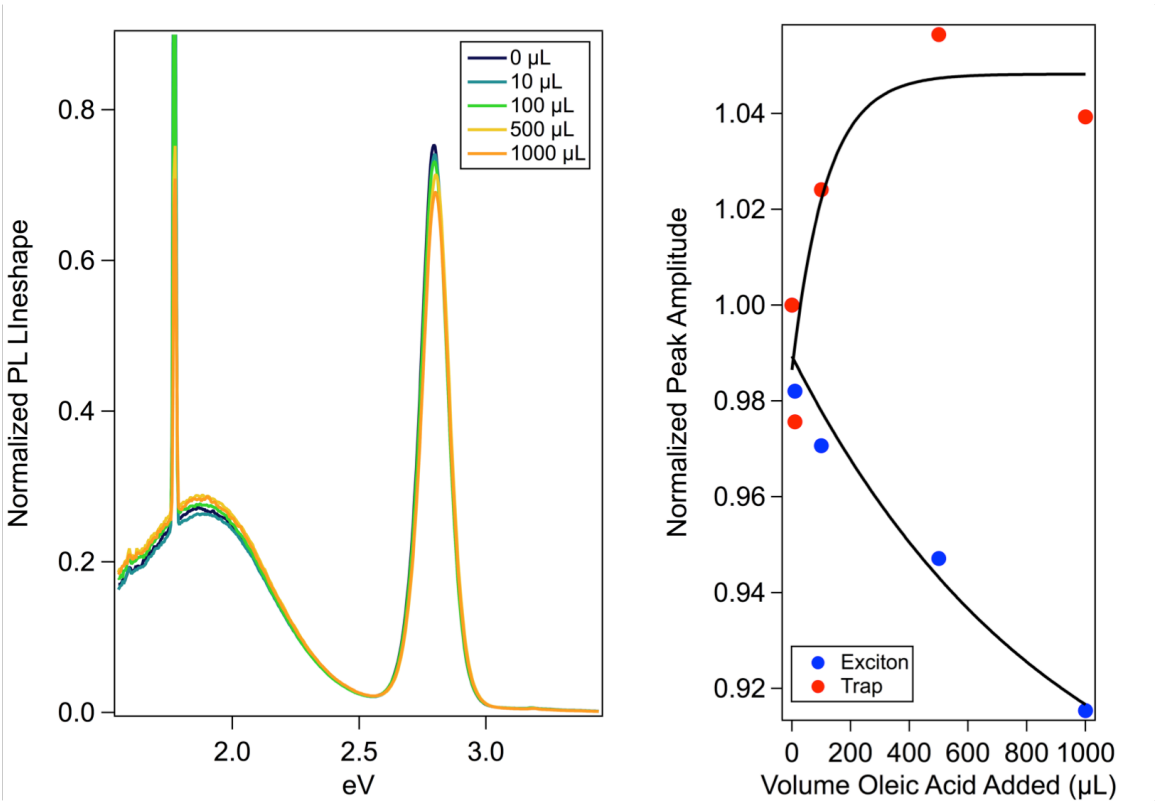

Figure 4.54: Normalized CdS PL spectra with increasing amounts of purified oleic acid (left). The sharp feature at 1.8 eV is scatter from the excitation light. On the right is the relative change in emission intensity for the exciton (blue) and trap (red).

emission. In order to ensure that only oleic acid is binding to the QD, and not the impurities, we purified the oleic acid using the procedure described in Section 3.5.1. We attempted to synthesize CdS QDs using the purified oleic acid, but were unsuccessful. Therefore, we synthesized a new batch of CdS QDs using the 90% oleic acid, and used purified oleic acid for the additional amounts added after synthesis and purification.

When we add increasing amounts of purified oleic acid to the samples, we still observe changes in the exciton emission, but the trap emission is hardly affected as seen in Figure 4.54 (left). Previously, the exciton emission decreased by 40%, but when using purified oleic acid, the exciton emission decreased by less than 6% as shown in Figure 4.54 (right). The trap emission is affected in a similarly affected. When using 90% oleic

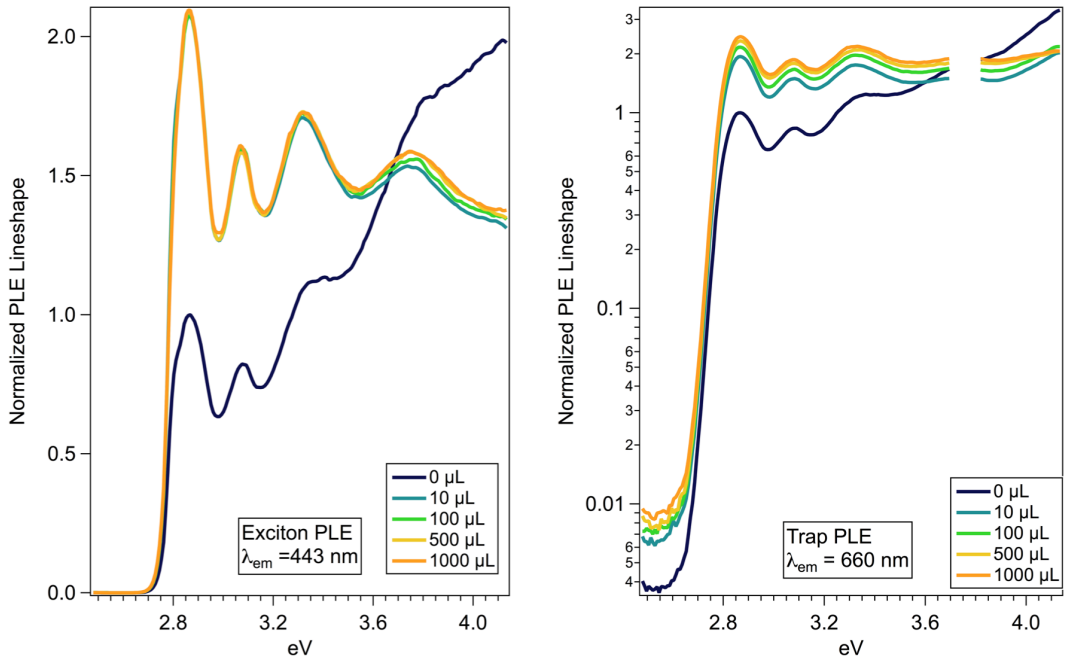

Figure 4.55: Normalized PLE spectra recorded at the exciton emission (left) and maximum trap emission (right). The gap in the trap PLE is from removing scatter from the excitation light.

acid, the trap emission increased by 40%, but the purified oleic acid causes an increase that is less than 0.4%, which is too small to definitively attribute to changes in the purified oleic acid.

Even though the PL spectrum is not changing, we can still draw conclusions about oleic acid affecting the emission by using the PLE spectrum. When collecting a PLE spectrum, the emission wavelength remains constant while the excitation wavelengths are changing. Therefore, any changes seen in the emission are caused by changes in the absorption.

PLE spectra were collected for both the exciton and trap state in addition to the emission spectra shown in Figure 4.55. Each PLE spectrum has been normalized to the first exciton absorption peak of the control. For the exciton PLE, the exciton absorption at

2.86 eV initially doubles, and then remains constant with increasing oleic acid. This indicates that the exciton state in the samples with additional oleic acid emits with over twice as much intensity as the control. The trap PLE shows a similar trend in the exciton absorption as the exciton PLE. Additional amounts of oleic acid cause a doubling of the trap emission at 2.86 eV excitation energy for the first addition of oleic acid. Subsequent additions of oleic acid cause an even greater rise in the trap emission. Furthermore, additional oleic acid results in an increase in trap emission when the trap states are excited directly with excitation energies below 2.8 eV.

Even though there is over twice as much exciton and trap emission at the exciton absorption energy (2.86 eV), we do not observe large changes in the PL spectrum. One possible reason for this could be due to the chosen excitation light. All CdS-oleic acid samples were excited well above the band-edge and Figure 4.55 shows that the emission

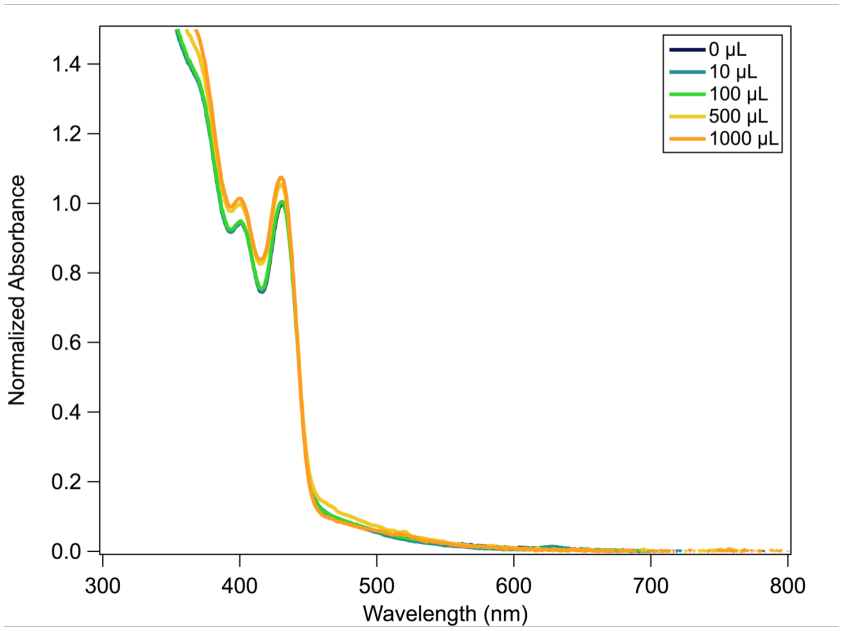

Figure 4.56: Normalized CdS absorption spectra for varying additions of purified oleic acid. Each absorption spectra has been normalized to the exciton absorption of the control (0 µL added).

is approximately equal at 3.6 eV, near where the samples were excited. A future experiment would be to excite the samples at the band-edge where the most change in absorption (according to the PLE) is occurring.

Another interesting observation is the UV-Vis absorption also shows little change in the exciton absorption as observed in Figure 4.56. By comparing the PLE spectrum to the absorption spectrum, we can get a sense of how the quantum yield for the exciton state is changing with additional oleic acid. Since exciton absorption hardly changes in the UV-Vis spectra, we theorize that additional oleic acid enhances the quantum yield for the exciton state because the emission has more than doubled in the PLE spectrum.

We realize that the PL spectra do not support this claim, and we argue that PL spectra does not tell the whole story because of the excitation energy is well above the band-edge. We previously showed that high excitation energies reduce the QY because of either activating new non-radiative recombination pathways at higher excitation energies or by exciting smaller QDs that are non-emissive. If the exciton QY is indeed increasing, then additional oleic acid is either changing the recombination rates or passivating more QD surfaces, and thereby increasing the number of emitting QDs. Time-resolved PL would be capable of differentiating between the two mechanisms. If the recombination rates were changing such as a reduction in the non-radiative recombination or an enhancement in the radiative recombination, then the shape of the PL decay, and hence its average lifetime would also be affected. If the number of emitting QDs increased, then only the PL signal intensity would be changed and the shape of the PL decay remains the same.

4.7.3. Concluding Remarks

In summary, we have shown that oleic acid, the primary ligand for CdS synthesis, does affect emission behavior, and these changes depend on the oleic acid purity. When 90% oleic acid is used, the exciton emission is diminished and the trap emission is enhanced. We speculated that adding additional oleic acid caused oleic acid to desorb from the QD surface as cadmium oleate, etching the QD, and thereby reducing its size in addition to creating more unpassivated surface states. However, purified oleic acid produced different results, and caused an increase in both exciton and trap emission when exciting at the QD band-edge. The increase in exciton emission was explained by either a change in the recombination rates or an increase in the number of emitting particles. Further work is needed in order to confirm the trends observed in the emission behavior as well as to determine the cause of either the enhancement or decline in emission intensity.

CHAPTER 5: FINAL REMARKS

At a first glance, QDs are promising candidates for a variety of applications because of their size tunable optical properties. However, as we probe these systems more deeply, we begin to understand that QDs are inherently complex, and controlling their optical properties is not simply a matter of controlling their size. QDs are even more challenging because the relationship between their surface chemistry and resultant optical properties is not always apparent or straightforward. For example, the ligands necessary for QD synthesis can either enhance QD emission or diminish it. Furthermore, surface effects on photogenerated charge carrier recombination dynamics in QDs are still not well defined, especially for systems with multiple emissive states.

The overlaying theme of this dissertation is to understand how the QD surface impacts charge carrier recombination dynamics. In particular, we have focused our efforts on trapping because trapping is often stated as a reason for explaining exciton recombination dynamics, low photoluminescent quantum yields, and low device efficiencies. However, the mechanism by which trapping occurs is not well defined, nor is the exact nature of trap states known. Therefore, we concentrated on comprehending trap states and trap recombination dynamics in CdS QDs, where the trap state is emissive.

We have learned that trap states are surface states that are strongly influenced by the surrounding medium, and trap emission in CdS QDs is caused by a positive hole trapped on a negatively charged sulfur atom. Additionally, we described the probability of trap emission within the framework of electron transfer (ET) theory, allowing us to

make predictions concerning trap emission in other QD systems. For example, CdS always exhibits trap emission because this type of QD occurs in either the barrierless or inverted region of (ET) based on the Gibb's free energy and reorganization energies calculated from the absorption and emission spectra. In contrast, CdSe is in the normal region for all but the smallest sizes, where trapping is unlikely to compete with radiative recombination due to an activated barrier for trapping.

We also have determined that exciton dynamics in CdS are similar to those reported for CdSe using temperature-dependent TRPL. Both systems exhibit temperature-dependent exciton average lifetimes indicative of an activated trapping process. We successfully modeled these dynamics in CdS using a three state model where the exciton interacts with a distribution of non-emissive trap states through an electron transfer mechanism. Our previous attempts to model the exciton dynamics using ET from the exciton state to the emissive trap state were unsuccessful, and we proposed that the emissive trap state is formed through an intermediate state rather than direct ET.

Furthermore, we learned that trap state recombination dynamics are heavily influenced by the exciton state. For the first time, we demonstrated that trap average lifetimes depend on the nature of the trap state using excitation-dependent TRPL. For example, trap average lifetimes are four times longer at room temperature using above bandgap excitation (exciton formed) compared to direct excitation (only traps formed). We discussed these differences in terms of two distinct trap states, where above bandgap excitation produces trap emission from a trapped hole and delocalized electron and direct excitation causes trap emission from a trapped hole and trapped electron.

Finally, we attempted to control trap emission by changing the ligand coverage on the QD surface, and learned that ligand interactions affect both exciton and trap emission in complex ways. Adding more ligands to the QD solution after synthesis did not remove trap emission, but actually increased it and concurrently decreased the exciton emission when using 90% pure oleic acid. Purified oleic acid caused different behavior in which both the exciton and trap emission increased. We explained these findings with two different mechanisms. In the first mechanism, oleic acid desorbs from the QD surface as cadmium oleate when oxygen is present, etching the QD surface and creating more trap states. The second mechanism relies on oleic acid influencing the exciton state rather than the trap state, and we proposed further experiments to help elucidate this mechanism.

The work highlighted in this dissertation emphasizes the importance of understanding the correlation between exciton recombination dynamics and trap recombination dynamics. When trap states were first discussed in QDs, they were seen as a detriment, and therefore should be removed rather than studied. I propose our perception of trap states needs to change, and these states may actually be beneficial. For example, we can design white light emitting diodes by tuning the broad trap emission to encompass all wavelengths. I can also see trap states being advantageous for applications that require long-lived charge separated states because trap states under certain conditions are charge separated states with lifetimes on the order of microseconds. But before we can start using trap states, we must first understand them, and this work has laid the foundation for further investigation into trap states.

REFERENCES

(1) SunShot Initiative: DOE Pursues SunShot Initiative to Achieve Cost Competitive Solar Energy by 2020 http://www1.eere.energy.gov/solar/sunshot/news_detail.html?news_id=16701 (accessed Nov 19, 2014).

(2) Hillhouse, H. W.; Beard, M. C. Solar Cells From Colloidal Nanocrystals: Fundamentals, Materials, Devices, and Economics. *Current Opinion in Colloid & Interface Science* **2009**, *14*, 245–259.

(3) Alivisatos, A. P. Semiconductor Clusters, Nanocrystals, and Quantum Dots. *Science* **1996**, *271*, 933–937.

(4) Alivisatos, A. P. Perspectives on the Physical Chemistry of Semiconductor Nanocrystals. *J. Phys. Chem.* **1996**, *100*, 13226–13239.

(5) Zhang, J. Z. Ultrafast Studies of Electron Dynamics in Semiconductor and Metal Colloidal Nanoparticles: Effects of Size and Surface. *Accounts of Chemical Research* **1997**, *30*, 423–429.

(6) El-Sayed, M. A. Small Is Different: Shape-, Size-, and Composition-Dependent Properties of Some Colloidal Semiconductor Nanocrystals. *Accounts of Chemical Research* **2004**, *37*, 326–333.

(7) Kamat, P. V. Quantum Dot Solar Cells. the Next Big Thingin Photovoltaics. *J. Phys. Chem. Lett.* **2013**, *4*, 908–918.

(8) Semonin, O. E.; Luther, J. M.; Choi, S.; Chen, H. Y.; Gao, J.; Nozik, A. J.; Beard, M. C. Peak External Photocurrent Quantum Efficiency Exceeding 100% via MEG in a Quantum Dot Solar Cell. *Science* **2011**, *334*, 1530–1533.

(9) McGuire, J. A.; Joo, J.; Pietryga, J. M.; Schaller, R. D.; Klimov, V. I. New Aspects of Carrier Multiplication in Semiconductor Nanocrystals. *Accounts of Chemical Research* **2008**, *41*, 1810–1819.

(10) Midgett, A. G.; Hillhouse, H. W.; Hughes, B. K.; Nozik, A. J.; Beard, M. C. Flowing Versus Static Conditions for Measuring Multiple Exciton Generation in PbSe Quantum Dots. *J. Phys. Chem. C* **2010**, *114*, 17486–17500.

(11) Nozik, A. J.; Beard, M. C.; Luther, J. M.; Law, M.; Ellingson, R. J.; Johnson, J. C. Semiconductor Quantum Dots and Quantum Dot Arrays and Applications of Multiple Exciton Generation to Third-Generation Photovoltaic Solar Cells. *Chemical Reviews* **2010**, *110*, 6873–6890.

(12) Sambur, J. B.; Novet, T.; Parkinson, B. A. Multiple Exciton Collection in a Sensitized Photovoltaic System. *Science* **2010**, *330*, 63–66.

(13) Ip, A. H.; Thon, S. M.; Hoogland, S.; Voznyy, O.; Zhitomirsky, D.; Debnath, R.; Levina, L.; Rollny, L. R.; Carey, G. H.; Fischer, A.; et al. Hybrid Passivated Colloidal Quantum Dot Solids. *Nature Nanotech* **2012**, *7*, 577–582.

(14) Kim, H.-S.; Lee, C.-R.; Im, J.-H.; Lee, K.-B.; Moehl, T.; Marchioro, A.; Moon, S.-J.; Humphry-Baker, R.; Yum, J.-H.; Moser, J. E.; et al. Lead Iodide Perovskite Sensitized All-Solid-State Submicron Thin Film Mesoscopic Solar Cell with Efficiency Exceeding 9%. *Sci Rep* **2012**, *2*, 591.

(15) Lee, M. M.; Teuscher, J.; Miyasaka, T.; Murakami, T. N.; Snaith, H. J. Efficient Hybrid Solar Cells Based on Meso-Superstructured Organometal Halide Perovskites. *Science* **2012**, *338*, 643–647.

(16) Tang, J.; Kemp, K. W.; Hoogland, S.; Jeong, K. S.; Liu, H.; Levina, L.; Furukawa, M.; Wang, X.; Debnath, R.; Cha, D.; et al. Colloidal-Quantum-Dot Photovoltaics Using Atomic-Ligand Passivation. *Nat Mater* **2011**, *10*, 765–771.

(17) Elbaum, R.; Vega, S.; Hodes, G. Preparation and Surface Structure of Nanocrystalline Cadmium Sulfide (Sulfoselenide) Precipitated From Dimethyl Sulfoxide Solutions. *J. Phys. Chem. C* **2001**, *13*, 2272–2280.

(18) Berrettini, M. G.; Braun, G.; Hu, J. G.; Strouse, G. F. NMR Analysis of Surfaces and Interfaces in 2-Nm CdSe. *J. Phys. Chem. C* **2004**, *126*, 7063–7070.

(19) Bawendi, M.; Wilson, W.; Rothberg, L.; Carroll, P.; Jedju, T.; Steigerwald, M.; Brus, L. Electronic Structure and Photoexcited-Carrier Dynamics in Nanometer-Size CdSe Clusters. *Phys. Rev. Lett.* **1990**, *65*, 1623–1626.

(20) Morello, G.; Anni, M.; Cozzoli, P. D.; Manna, L.; Cingolani, R.; DeGiorgi, M. Picosecond Photoluminescence Decay Time in Colloidal Nanocrystals: the Role of Intrinsic and Surface States. *J. Phys. Chem. C* **2007**, *111*, 10541–10545.

(21) Kalyuzhny, G.; Murray, R. W. Ligand Effects on Optical Properties of CdSe Nanocrystals. *J. Phys. Chem. B* **2005**, *109*, 7012–7021.

(22) Blumling, D. E.; Tokumoto, T.; McGill, S.; Knappenberger, K. L. Temperature- and Field-Dependent Energy Transfer in CdSe Nanocrystal Aggregates Studied by Magneto-Photoluminescence Spectroscopy. *Phys. Chem. Chem. Phys.* **2012**, *14*, 11053.

(23) Gaponenko, S. V. Optical Properties of Semiconductor Nanocrystals;

Cambridge University Press, 1998.

(24) Kambhampati, P. Hot Exciton Relaxation Dynamics in Semiconductor Quantum Dots: Radiationless Transitions on the Nanoscale. *J. Phys. Chem. C* **2011**, *115*, 22089–22109.

(25) Martinez-Ferrero, E.; Sero, I. M.; Albero, J.; Gimenez, S.; Bisquert, J.; Palomares, E. Charge Transfer Kinetics in CdSe Quantum Dot Sensitized Solar Cells. *Phys. Chem. Chem. Phys.* **2010**, *12*, 2819–2821.

(26) Mlinar, V. Engineered Nanomaterials for Solar Energy Conversion. *J. Phys.: Condens. Matter* **2013**, *24*, 042001.

(27) Bakulin, A. A.; Neutzner, S.; Bakker, H. J.; Ottaviani, L.; Barakel, D.; Chen, Z. Charge Trapping Dynamics in PbS Colloidal Quantum Dot Photovoltaic Devices. *ACS Nano* **2013**, *7*, 8771–8779.

(28) Leschkies, K. S.; Divakar, R.; Basu, J.; Enache-Pommer, E.; Boercker, J. E.; Carter, C. B.; Kortshagen, U. R.; Norris, D. J.; Aydil, E. S. Photosensitization of ZnO Nanowires with CdSe Quantum Dots for Photovoltaic Devices. *J. Phys. Chem. C* **2007**, *7*, 1793–1798.

(29) Wanger, D. D.; Correa, R. E.; Dauler, E. A.; Bawendi, M. G. The Dominant Role of Exciton Quenching in PbS Quantum-Dot-Based Photovoltaic Devices. *Nano Letters* **2013**, *13*, 5907–5912.

(30) Sukhovatkin, V.; Hinds, S.; Brzozowski, L.; Sargent, E. H. Colloidal Quantum-Dot Photodetectors Exploiting Multiexciton Generation. *Science* **2009**, *324*, 1542–1544.

(31) Talapin, D. V.; Lee, J.-S.; Kovalenko, M. V.; Shevchenko, E. V. Prospects of Colloidal Nanocrystals for Electronic and Optoelectronic Applications. *Chemical Reviews* **2010**, *110*, 389–458.

(32) Coe, S.; Woo, W.-K.; Bawendi, M.; Bulović, V. Electroluminescence From Single Monolayers of Nanocrystals in Molecular Organic Devices. *Nature* **2002**, *420*, 800–803.

(33) Jang, E.-P.; Song, W.-S.; Lee, K.-H.; Yang, H. Preparation of a Photo-Degradation- Resistant Quantum Dot–Polymer Composite Plate for Use in the Fabrication of a High-Stability White-Light-Emitting Diode. *J. Phys.: Condens. Matter* **2013**, *24*, 045607.

(34) Kim, J. Y.; Voznyy, O.; Zhitomirsky, D.; Sargent, E. H. 25th Anniversary Article: Colloidal Quantum Dot Materials and Devices: a Quarter-Century of Advances. *Adv. Mater.* **2013**, *25*, 4986–5010.

(35) Michalet, X.; Pinaud, F. F.; Bentolila, L. A.; Tsay, J. M.; Doose, S.; Li, J. J.; Sundaresan, G.; Wu, A. M.; Gambhir, S. S.; Weiss, S. Quantum Dots for Live Cells, in Vivo Imaging, and Diagnostics. *Science* **2005**, *307*, 538–544.

(36) Bruchez, M.; Moronne, M.; Gin, P.; Weiss, S.; Alivisatos, A. P. Semiconductor Nanocrystals as Fluorescent Biological Labels. *Science* **1998**, *281*, 2013–2016.

(37) Dubertret, B.; Skourides, P.; Norris, D. J.; Noireaux, V.; Brivanlou, A. H.; Libchaber, A. In Vivo Imaging of Quantum Dots Encapsulated in Phospholipid Micelles. *Science* **2002**, *298*, 1759–1762.

(38) Cai, W.; Shin, D.-W.; Chen, K.; Gheysens, O.; Cao, Q.; Wang, S. X.; Gambhir, S. S.; Chen, X. Peptide-Labeled Near-Infrared Quantum Dots for Imaging Tumor Vasculature in Living Subjects. *J. Phys. Chem. C* **2006**, *6*, 669–676.

(39) Marcus, R. A.; Sutin, N. Electron Transfers in Chemistry and Biology. *Biochimica Et Biophysica Acta* **1985**, *811*, 265–322.

(40) Tvrdy, K.; Frantsuzov, P. A.; Kamat, P. V. Photoinduced Electron Transfer From Semiconductor Quantum Dots to Metal Oxide Nanoparticles. *Proc. Natl. Acad. Sci. U. S. A.* **2011**, *108*, 29–34.

(41) Chuang, C.-H.; Lo, S. S.; Scholes, G. D.; Burda, C. Charge Separation and Recombination in CdTe/CdSe Core/Shell Nanocrystals as a Function of Shell Coverage: Probing the Onset of the Quasi Type-II Regime. *J. Phys. Chem. Lett.* **2010**, *1*, 2530–2535.

(42) Jones, M.; Lo, S. S.; Scholes, G. D. Quantitative Modeling of the Role of Surface Traps in CdSe/CdS/ZnS Nanocrystal Photoluminescence Decay Dynamics. *Proc. Natl. Acad. Sci. U. S. A.* **2009**, *106*, 3011–3016.

(43) Jones, M.; Lo, S. S.; Scholes, G. D. Signatures of Exciton Dynamics and Carrier Trapping in the Time-Resolved Photoluminescence of Colloidal CdSe Nanocrystals. *J. Phys. Chem. C* **2009**, *113*, 18632–18642.

(44) Jones, M.; Kumar, S.; Lo, S. S.; Scholes, G. D. Exciton Trapping and Recombination in Type II CdSe/CdTe Nanorod Heterostructures. *J. Phys. Chem. C* **2008**, *112*, 5423–5431.

(45) Scholes, G. D.; Jones, M.; Kumar, S. Energetics of Photoinduced Electron-Transfer Reactions Decided by Quantum Confinement. *J. Phys. Chem. C* **2007**, *111*, 13777–13785.

(46) Bolton, J. R.; Mataga, N.; McLendon, G. Electron Transfer in Inorganic, Organic, and Biological Systems; An American Chemical Society Publication, 1991.

(47) Turro, N. J.; Ramamurthy, V.; Scaiano, J. C. Principles of Molecular Photochemistry; University Science Books, 2009.

(48) Barbara, P. F.; Meyer, T. J.; Ratner, M. A. Contemporary Issues in Electron Transfer Research. *J. Phys. Chem.* **1996**, *100*, 13148–13168.

(49) Jortner, J. Temperature Dependent Activation Energy for Electron Transfer Between Biological Molecules. *J. Chem. Phys.* **1976**, *64*, 4860.

(50) Mooney, J.; Krause, M. M.; Saari, J. I.; Kambhampati, P. A Microscopic Picture of Surface Charge Trapping in Semiconductor Nanocrystals. *J. Chem. Phys.* **2013**, *138*, 204705.

(51) Mooney, J.; Krause, M. M.; Saari, J. I.; Kambhampati, P. Challenge to the Deep-Trap Model of the Surface in Semiconductor Nanocrystals. *Phys. Rev. B* **2013**, *87*, 081201.

(52) Hässelbarth, A.; Eychmüller, A.; Weller, H. Detection of Shallow Electron Traps in Quantum Sized CdS by Fluorescence Quenching Experiments. *Chem. Phys. Lett.* **1993**, *203*, 271–276.

(53) Jones, M.; Nedeljkovic, J.; Ellingson, R. J.; Nozik, A. J.; Rumbles, G. Photoenhancement of Luminescence in Colloidal CdSe Quantum Dot Solutions. *J. Phys. Chem. B* **2003**, *107*, 11346–11352.

(54) Mooney, J.; Krause, M. M.; Kambhampati, P. Connecting the Dots: the Kinetics and Thermodynamics of Hot, Cold, and Surface-Trapped Excitons in Semiconductor Nanocrystals. *J. Phys. Chem. C* **2014**, *118*, 7730–7739.

(55) Reiss, P.; Bleuse, J.; Pron, A. Highly Luminescent CdSe/ZnSe Core/Shell Nanocrystals of Low Size Dispersion. *Nano Letters* **2002**, *2*, 781–784.

(56) Mekis, I.; Talapin, D. V.; Kornowski, A.; Haase, M.; Weller, H. One-Pot Synthesis of Highly Luminescent CdSe/CdS Core−Shell Nanocrystals via Organometallic and "Greener" Chemical Approaches †. *J. Phys. Chem. B* **2003**, *107*, 7454–7462.

(57) Resch, U.; Eychmueller, A.; Haase, M.; Weller, H. Absorption and Fluorescence Behavior of Redispersible Cadmium Sulfide Colloids in Various Organic Solvents. *Langmuir* **1992**, *8*, 2215–2218.

(58) Eychmüller, A.; Hässelbarth, A.; Katsikas, L.; Weller, H. Photochemistry of Semiconductor Colloids. 36. Fluorescence Investigations on the Nature of Electron and Hole Traps in Q-Sized Colloidal CdS Particles. *Berichte der Bunsengesellschaft für physikalische Chemie* **1991**, *95*, 79–84.

(59) Wu, F.; Zhang, J. Z.; Kho, R.; Mehra, R. K. Radiative and Nonradiative Lifetimes of Band Edge States and Deep Trap States of CdS Nanoparticles Determined by Time-Correlated Single Photon Counting. *Chem. Phys. Lett.* **2000**, *330*, 237–242.

(60) Mandal, D.; Chatterjee, U. Synthesis and Spectroscopy of CdS Nanoparticles in Amphiphilic Diblock Copolymer Micelles. *The Journal of Chemical Physics* **2007**, *126*.

(61) Mandal, D.; Hosoi, H.; Chatterjee, U.; Tahara, T. Direct Observation of Time-Dependent Photoluminescence Spectral Shift in CdS Nanoparticles Synthesized in Polymer Solutions. *J. Chem. Phys.* **2009**, *130*, 034902.

(62) Lü, W.; Tokuhiro, Y.; Umezu, I.; Sugimura, A.; Nagasaki, Y. Trap State Emission of Water-Soluble CdS Nanocrystals. *Angewandte Chemie International Edition* **2009**, *6*, 346–349.

(63) Lakowicz, J. R.; Gryczynski, I.; Gryczynski, Z.; Nowaczyk, K.; Murphy, C. J. Time-Resolved Spectral Observations of Cadmium-Enriched Cadmium Sulfide Nanoparticles and the Effects of DNA Oligomer Binding. *Analytical Biochemistry* **2000**, *280*, 128–136.

(64) Yu, W. W.; Peng, X. Formation of High-Quality CdS and Other II–VI Semiconductor Nanocrystals in Noncoordinating Solvents: Tunable Reactivity of Monomers. *Angewandte Chemie International Edition* **2002**, *41*, 2368–2371.

(65) Yu, W. W.; Qu, L. H.; Guo, W. Z.; Peng, X. G. Experimental Determination of the Extinction Coefficient of CdTe, CdSe, and CdS Nanocrystals. *Chem. Mater.* **2003**, *15*, 2854–2860.

(66) Clapp, A. R.; Goldman, E. R.; Mattoussi, H. Capping of CdSe–ZnS Quantum Dots with DHLA and Subsequent Conjugation with Proteins. *Nat Protoc* **2006**, *1*, 1258–1266.

(67) Chestnoy, N.; Harris, T. D.; Hull, R.; Brus, L. E. Luminescence and Photophysics of Cadmium Sulfide Semiconductor Clusters: the Nature of the Emitting Electronic State. *J. Phys. Chem.* **1986**, *90*, 3393–3399.

(68) Valeur, B.; Berberan-Santos, M. N. Molecular Fluorescence; John Wiley & Sons, 2012.

(69) Mooney, J.; Kambhampati, P. Get the Basics Right: Jacobian Conversion of Wavelength and Energy Scales for Quantitative Analysis of Emission Spectra. *J. Phys. Chem. Lett.* **2013**, *4*, 3316–3318.

(70) Hoy, J.; Morrison, P. J.; Steinberg, L. K.; Buhro, W. E.; Loomis, R. A.

Excitation Energy Dependence of the Photoluminescence Quantum Yields of Core and Core/Shell Quantum Dots. *J. Phys. Chem. Lett.* **2013**, *4*, 2053–2060.

(71) Hoheisel, W.; Colvin, V. L.; Johnson, C. S.; Alivisatos, A. P. Threshold for Quasicontinuum Absorption and Reduced Luminescence Efficiency in CdSe Nanocrystals. *J. Chem. Phys.* **1994**, *101*, 8455.

(72) Rumbles, G.; Selmarten, D. C.; Ellingson, R. J.; Blackburn, J. L.; Yu, P.; Smith, B. B.; Mićić, O. I.; Nozik, A. J. Anomalies in the Linear Absorption, Transient Absorption, Photoluminescence and Photoluminescence Excitation Spectroscopies of Colloidal InP Quantum Dots. *Journal of Photochemistry and Photobiology A: Chemistry* **2001**, *142*, 187–195.

(73) Ellingson, R. J.; Blackburn, J. L.; Yu, P.; Rumbles, G.; Mićić, O. I.; Nozik, A. J. Excitation Energy Dependent Efficiency of Charge Carrier Relaxation and Photoluminescence in Colloidal InP Quantum Dots. *J. Phys. Chem. B* **2002**, *106*, 7758–7765.

(74) Tonti, D.; van Mourik, F.; Chergui, M. On the Excitation Wavelength Dependence of the Luminescence Yield of Colloidal CdSe Quantum Dots. *Nano Lett.* **2004**, *4*, 2483–2487.

(75) Burda, C.; Chen, X. B.; Narayanan, R.; El-Sayed, M. A. Chemistry and Properties of Nanocrystals of Different Shapes. *Chemical Reviews* **2005**, *105*, 1025–1102.

(76) Jones, M.; Scholes, G. D. On the Use of Time-Resolved Photoluminescence as a Probe of Nanocrystal Photoexcitation Dynamics. *J. Mater. Chem.* **2010**, *20*, 3533–3538.

(77) Gómez-Campos, F. M.; Califano, M. Hole Surface Trapping in CdSe Nanocrystals: Dynamics, Rate Fluctuations, and Implications for Blinking. *Nano Letters* **2012**, *12*, 4508–4517.

(78) Jiang, Z. J.; Kelley, D. F. Role of Surface States in the Exciton Dynamics in CdSe Core and Core/Shell Nanorods. *J. Phys. Chem. C* **2010**, *114*, 17519–17528.

(79) O'Neil, M.; Marohn, J.; McLendon, G. Picosecond Measurements of Exciton Trapping in Semiconductor Clusters. *Chemical Physics* **1990**, *168*, 208–210.

(80) Saari, J. I.; Dias, E. A.; Reifsnyder, D.; Krause, M. M.; Walsh, B. R.; Murray, C. B.; Kambhampati, P. Ultrafast Electron Trapping at the Surface of Semiconductor Nanocrystals: Excitonic and Biexcitonic Processes. *J. Phys. Chem. B* **2013**, *117*, 4412–4421.

(81) O'Connor, D. Time-Correlated Single Photon Counting; Academic Press, 1984.

(82) Battaglia, D.; Li, J. J.; Wang, Y.; Peng, X. Colloidal Two-Dimensional Systems: CdSe Quantum Shells and Wells. *Angewandte Chemie International Edition* **2003**, *42*, 5035–5039.

(83) Arudi, R. L.; Sutherland, M. W.; Bielski, B. H. Purification of Oleic Acid and Linoleic Acid. *Journal of Lipid Research* **1983**, *24*, 485–488.

(84) Chandler, R. R.; Coffer, J. L.; Atherton, S. J.; Snowden, P. T. Addition of Ferrocene Derivatives to the Surface of Quantum-Confined Cadmium Sulfide Clusters: Steady-State and Time-Resolved Photophysical Effects. *J. Phys. Chem.* **1991**, *96*, 2713–2717.

(85) Garrett, M. D.; Dukes, A. D.; McBride, J. R.; Smith, N. J.; Pennycook, S. J.; Rosenthal, S. J. Band Edge Recombination in CdSe, CdS and CdSxSe1-X Alloy Nanocrystals Observed by Ultrafast Fluorescence Upconversion: the Effect of Surface Trap States. *J. Phys. Chem. C* **2008**, *112*, 12736–12746.

(86) Lakowicz, J. R.; Gryczynski, I.; Gryczynski, Z.; Murphy, C. J. Luminescence Spectral Properties of CdS Nanoparticles. *J. Phys. Chem. B* **1999**, *103*, 7613–7620.

(87) Logunov, S.; Green, T.; Marguet, S.; El-Sayed, M. A. Interfacial Carriers Dynamics of CdS Nanoparticles. *J. Phys. Chem. C* **1998**, *102*, 5652–5658.

(88) Mandal, A.; Saha, J.; De, G. Stable CdS QDs with Intense Broadband Photoluminescence and High Quantum Yields. *Optical Materials* **2011**, *34*, 6–11.

(89) Misawa, K.; Yao, H.; Hayashi, T.; Kobayashi, T. Size Effects on Luminescence Dynamics of CdS Microcrystallites Embedded in Polymer Films. *Chem. Phys. Lett.* **1991**, *183*, 113–118.

(90) O'Neil, M.; Marohn, J.; McLendon, G. Dynamics of Electron-Hole Pair Recombination in Semiconductor Clusters. *J. Phys. Chem.* **1990**, *94*, 4356–4363.

(91) Klimov, V.; Bolivar, P.; Kurz, H. Ultrafast Carrier Dynamics in Semiconductor Quantum Dots. *Phys. Rev. B* **1996**, *53*, 1463–1467.

(92) Klimov, V. I.; Haring-Bolivar, P.; Kurz, H.; Karavanskii, V. A. Optical Nonlinearities and Carrier Trapping Dynamics in CdS and CuxS Nanocrystals. *Superlattices and Microstructures* **1996**, *20*, 395–404.

(93) Zhang, J. Z. Interfacial Charge Carrier Dynamics of Colloidal Semiconductor

Nanoparticles; American Chemical Society, 2000; Vol. 104, pp. 7239–7253.

(94) Zhang, J. Z.; Oneil, R. H.; Roberti, T. W.; McGowen, J. L.; Evans, J. E. Femtosecond Studies of Trapped Electrons at the Liquid—Solid Interface of Aqueous CdS Colloids. *Chem. Phys. Lett.* **1994**, *218*, 479–484.

(95) Lo, S. S.; Khan, Y.; Jones, M.; Scholes, G. D. Temperature and Solvent Dependence of CdSe/CdTe Heterostructure Nanorod Spectra. *J. Chem. Phys.* **2009**, *131*, 084714.

(96) de Mello Donegá, C.; Bode, M.; Meijerink, A. Size- and Temperature-Dependence of Exciton Lifetimes in CdSe Quantum Dots. *Phys. Rev. B* **2006**, *74*, 085320.

(97) Crooker, S. A.; Barrick, T.; Hollingsworth, J. A.; Klimov, V. I. Multiple Temperature Regimes of Radiative Decay in CdSe Nanocrystal Quantum Dots: Intrinsic Limits to the Dark-Exciton Lifetime. *Appl. Phys. Lett.* **2003**, *82*, 2793–2795.

(98) Labeau, O.; Tamarat, P.; Lounis, B. Temperature Dependence of the Luminescence Lifetime of Single CdSe/ZnS Quantum Dots. *Phys. Rev. Lett.* **2003**, *90*, 257404.

(99) Gaponenko, M.; Lutich, A.; Tolstik, N.; Onushchenko, A.; Malyarevich, A.; Petrov, E.; Yumashev, K. Temperature-Dependent Photoluminescence of PbS Quantum Dots in Glass: Evidence of Exciton State Splitting and Carrier Trapping. *Phys. Rev. B* **2010**, *82*, 125320.

(100) Wuister, S. F.; van Houselt, A.; de Mello Donegá, C.; Vanmaekelbergh, D.; Meijerink, A. Temperature Antiquenching of the Luminescence From Capped CdSe Quantum Dots. *Angewandte Chemie International Edition* **2004**, *43*, 3029–3033.

(101) Califano, M.; Franceschetti, A.; Zunger, A. Lifetime and Polarization of the Radiative Decay of Excitons, Biexcitons, and Trions in CdSe Nanocrystal Quantum Dots. *Phys. Rev. B* **2007**, *75*, 115401.

(102) Efros, A. Luminescence Polarization of CdSe Microcrystals. *Phys. Rev. B* **1992**, *46*, 7448–7458.

(103) Nirmal, M.; Norris, D.; Kuno, M.; Bawendi, M.; Efros, A.; Rosen, M. Observation of the “Dark Exciton” in CdSe Quantum Dots. *Phys. Rev. Lett.* **1995**, *75*, 3728–3731.

(104) Andreakou, P.; Brossard, M.; Li, C.; Bernechea, M.; Konstantatos, G.; Lagoudakis, P. G. Size- and Temperature-Dependent Carrier Dynamics in Oleic Acid Capped PbS Quantum Dots. *J. Phys. Chem. C* **2013**, *117*, 1887–

1892.

(105) Efros, A. L.; Rosen, M.; Kuno, M.; Nirmal, M.; Norris, D. J.; Bawendi, M. Band-Edge Exciton in Quantum Dots of Semiconductors with a Degenerate Valence Band: Dark and Bright Exciton States. *Phys. Rev. B* **1996**, *54*, 4843.

(106) Califano, M.; Franceschetti, A.; Zunger, A. Temperature Dependence of Excitonic Radiative Decay in CdSe Quantum Dots: the Role of Surface Hole Traps. *Nano Letters* **2005**, *5*, 2360–2364.

(107) Schlegel, G.; Bohnenberger, J.; Potapova, I.; Mews, A. Fluorescence Decay Time of Single Semiconductor Nanocrystals. *Phys. Rev. Lett.* **2002**, *88*, 137401.

(108) Fisher, B. R.; Eisler, H.-J.; Stott, N. E.; Bawendi, M. G. Emission Intensity Dependence and Single-Exponential Behavior in Single Colloidal Quantum Dot Fluorescence Lifetimes. *J. Phys. Chem. B* **2003**, *108*, 143–148.

(109) Valerini, D.; Cretí, A.; Lomascolo, M.; Manna, L.; Cingolani, R.; Anni, M. Temperature Dependence of the Photoluminescence Properties of Colloidal CdSe⁄ZnS Core/Shell Quantum Dots Embedded in a Polystyrene Matrix. *Phys. Rev. B* **2005**, *71*, 235409.

(110) Bässler, H. Charge Transport in Disordered Organic Photoconductors a Monte Carlo Simulation Study. *physica status solidi (b)* **1993**, *175*, 15–56.

(111) Boulesbaa, A.; Huang, Z. Q.; Wu, D.; Lian, T. Q. Competition Between Energy and Electron Transfer From CdSe QDs to Adsorbed Rhodamine B. *J. Phys. Chem. C* **2010**, *114*, 962–969.

(112) van Schooten, K. J.; Huang, J.; Talapin, D. V.; Boehme, C.; Lupton, J. M. Spin-Dependent Electronic Processes and Long-Lived Spin Coherence of Deep-Level Trap Sites in CdS Nanocrystals. *Phys. Rev. B* **2013**, *87*, 125412.

(113) Kasha, M. Characterization of Electronic Transitions in Complex Molecules. *Discuss. Faraday Soc.* **1950**, *9*, 14–19.

(114) Skinner, D. E.; Colombo, D. P., Jr; Cavaleri, J. J.; Bowman, R. M. Femtosecond Investigation of Electron Trapping in Semiconductor Nanoclusters. *J. Phys. Chem.* **1995**, *99*, 7853–7856.

(115) Underwood, D. F.; Kippeny, T.; Rosenthal, S. J. Ultrafast Carrier Dynamics in CdSe Nanocrystals Determined by Femtosecond Fluorescence Upconversion Spectroscopy. *Journal of Physical Chemistry B* **2001**, *105*, 436–443.

(116) Kern, S. J.; Sahu, K.; Berg, M. A. Heterogeneity of the Electron-Trapping

Kinetics in CdSe Nanoparticles. *Nano Letters* **2011**, *11*, 3493–3498.

(117) and, C. B. M.; Kagan, C. R.; Bawendi, M. G. Synthesis and Characterization of Monodisperse Nanocrystals and Close-Packed Nanocrystal Assemblies. *Annual Review of Material Research* **2003**, *30*, 545–610.

(118) Trindade, T.; Paul O'Brien, A.; Pickett, N. L. Nanocrystalline Semiconductors: Synthesis, Properties, and Perspectives. *Chem. Mater.* **2001**, *13*, 3843–3858.

(119) Yin, Y.; Alivisatos, A. P. Colloidal Nanocrystal Synthesis and the Organic–Inorganic Interface. *Nature* **2005**, *437*, 664–670.

(120) Green, M. The Nature of Quantum Dot Capping Ligands. *J. Mater. Chem.* **2010**, *20*, 5797–5809.

(121) Bavykin, D. V.; Savinov, E. N.; Parmon, V. N. Surface Effects on Regularities of Electron Transfer in CdS and CdS/Cu xS Colloids as Studied by Photoluminescence Quenching. *Langmuir* **1999**, *15*, 4722–4727.

(122) Knowles, K. E.; Tice, D. B.; McArthur, E. A.; Solomon, G. C.; Weiss, E. A. Chemical Control of the Photoluminescence of CdSe Quantum Dot-Organic Complexes with a Series of Para-Substituted Aniline Ligands. *J. Am. Chem. Soc.* **2010**, *132*, 1041–1050.

(123) Hines, D. A.; Kamat, P. V. Recent Advances in Quantum Dot Surface Chemistry. *ACS Appl Mater Interfaces* **2014**, *6*, 3041–3057.

(124) Li, J. J.; Wang, Y. A.; Guo, W. Z.; Keay, J. C.; Mishima, T. D.; Johnson, M. B.; Peng, X. G. Large-Scale Synthesis of Nearly Monodisperse CdSe/CdS Core/Shell Nanocrystals Using Air-Stable Reagents via Successive Ion Layer Adsorption and Reaction. *J. Am. Chem. Soc.* **2003**, *125*, 12567–12575.

(125) Knowles, K. E.; Frederick, M. T.; Tice, D. B.; Morris-Cohen, A. J.; Weiss, E. A. Colloidal Quantum Dots: Think Outside the (Particle-in-a-)Box. *J. Phys. Chem. Lett.* **2011**, *3*, 18–26.

(126) Morris-Cohen, A. J.; Donakowski, M. D.; Knowles, K. E.; Weiss, E. A. The Effect of a Common Purification Procedure on the Chemical Composition of the Surfaces of CdSe Quantum Dots Synthesized with Trioctylphosphine Oxide. *J. Phys. Chem. C* **2010**, *114*, 897–906.

(127) Munro, A. M.; Jen-LaPlante, I.; Ng, M. S.; Ginger, D. S. Quantitative Study of the Effects of Surface Ligand Concentration on CdSe Nanocrystal Photoluminescence. *J. Phys. Chem. C* **2007**, *111*, 6220–6227.

(128) Morris-Cohen, A. J.; Vasilenko, V.; Amin, V. A.; Reuter, M. G.; Weiss, E. A.

Model for Adsorption of Ligands to Colloidal Quantum Dots with Concentration-Dependent Surface Structure. *ACS Nano* **2012**, *6*, 557–565.

(129) Jenkins, H. D. B. Chemical Thermodynamics at a Glance; John Wiley & Sons, 2008.

(130) Knittel, F.; Gravel, E.; Cassette, E.; Pons, T.; Pillon, F.; Dubertret, B.; Doris, E. On the Characterization of the Surface Chemistry of Quantum Dots. *Nano Letters* **2013**, *13*, 5075–5078.

(131) Fritzinger, B.; Capek, R. K.; Lambert, K.; Martins, J. C.; Hens, Z. Utilizing Self-Exchange to Address the Binding of Carboxylic Acid Ligands to CdSe Quantum Dots. *J. Am. Chem. Soc.* **2010**, *132*, 10195–10201.

(132) Moreels, I.; Fritzinger, B.; Martins, J. C.; Hens, Z. Surface Chemistry of Colloidal PbSe Nanocrystals. *J. Am. Chem. Soc.* **2008**, *130*, 15081–15086.